Received August 19, 2015, accepted September 1, 2015, date of publication September 15, 2015, date of current version October 15, 2015.

Digital Object Identifier 10.1109/ACCESS.2015.2477307

Bridging the Social and Wireless Networking Divide: Information Dissemination in Integrated Cellular and Opportunistic Networks

JIE HU[1], (Student Member, IEEE), LIE-LIANG YANG[1], (Senior Member, IEEE), H. VINCENT POOR[2], (Fellow, IEEE), AND LAJOS HANZO[1], (Fellow, IEEE)

[1]School of Electronics and Computer Science, University of Southampton, Southampton SO17 1BJ, U.K.
[2]Department of Electrical Engineering, Princeton University, Princeton, NJ 08544, USA

Corresponding author: L. Hanzo (lh@ecs.soton.ac.uk)

This work was supported in part by the RC–U.K.'s India–U.K. Advanced Technology Centre, in part by the European Union's Concerto Project, and in part by the China Scholarship Council. The work of L. Hanzo was supported by the European Research Council under its Advanced Fellow Award.

ABSTRACT An increasing number of mobile users (MUs) share common interests in general information, such as traffic information, weather forecast, and domestic/international news. However, the centralized infrastructure-based system has not been designed for efficiently disseminating the information of common interest (IoCI) to numerous requesters. Thanks to the rapid development of mobile devices equipped with large storage and multiple communication modes, opportunistic communication between a pair of MUs can be readily realized. With the aid of opportunistic networks formed by MUs, we can improve the connectivity of cellular networks in the rural areas, we can offload the tele-traffic from the overloaded cellular networks, and we can efficiently disseminate the IoCI in the densely populated areas. We commence with a detailed survey on the cross-disciplinary research area of social network analysis aided telecommunication networking. We continue by focusing our attention on the family of integrated cellular and large-scale opportunistic networks, whose performance is dominated by the inter-contact duration as well as the contact duration between any pairs of MUs. A continuous-time-pure-birth Markov chain is invoked for analyzing the relevant performance. We demonstrate that the delivery ratio of the IoCI before it expires becomes higher than 90% with the aid of opportunistic networks consisting of 20 MUs. Moreover, our experiments based on the InfoCom 2006 mobility trace show that the opportunistic networks are capable of offloading 58% of the tele-traffic from the cellular networks. Thereafter, we propose a hybrid information dissemination scheme for the integrated cellular and small-scale opportunistic networks, which is comprised of two main stages: 1) the base station-aided single-hop multicast (BSSHM) stage and 2) the cooperative multicast aided spontaneous dissemination stage. In contrast to their large-scale counterparts, in small-scale opportunistic networks, the information dissemination is mainly affected by the mobility of the MUs, by the wireless channel attenuation and by the resource scheduling, where a discrete-time-pure-birth Markov chain is utilized for characterizing the relevant performance. We demonstrate that our hybrid information dissemination scheme outperforms the traditional BSSHM in terms of various delay metrics, despite consuming less energy.

INDEX TERMS Cellular networks, large-scale/small-scale opportunistic networks, information dissemination, pure-birth Markov chain, social network analysis.

NOMENCLATURE

ACK	Acknowledgement
ana	Analytical
BF	BeamForming
BS	Base Station
BSSHM	Base Station aided Single-Hop Multicast
CCDF	Complementary Cumulative Distribution Function
CDF	Cumulative Distribution Function
CI	Centralised Infrastructure
CMM	Community-based Mobility Model
Co-multicast	Cooperative Multicast
CT-PBMC	Continuous-Time-Pure-Birth Markov Chain

DTN	Delay-Tolerant Network
DT-PBMC	Discrete-Time-Pure-Birth Markov Chain
HCMM	Home-cell-Community-based Mobility Model
ICI	Inter-Cell Interference
IM	Information Multicaster
IO	Information Owner
IoCI	Information of Common Interest
LTE-A	Long-Term-Evolution-Advanced
MAC	Medium-Access-Control
MANET	Mobile Ad Hoc Network
MU	Mobile User
PDF	Probability Density Function
PL	Path Loss
PHY	PHYsical
PSD	Power Spectrum Density
QoS	Quality of Service
RD	Random Direction
RR	Round-Robin
RU	Road Unit
RW	Random Walk
RWP	Random Way-Point
sim	Simulation
SNA	Social Network Analysis
SNR	Signal-to-Noise-Ratio
SPM	Social Pressure Metric
TCN	Telephone Call Network
TDMA	Time-Division-Multiple-Access
TS	Time Slot
uMU	unserved Mobile User

I. INTRODUCTION

At the time of writing, we are witnessing a dramatic increase of the number of mobile devices and connections. The white paper published by Cisco in 2014 [1] predicted that by the end of 2014, the number of mobile-connected devices would exceed the number of people on earth and this number would break through the 10 billion limit by 2018. Accommodating the huge amount of tele-traffic generated by billions of mobile devices is a 'mission impossible' for the conventional centralised infrastructure (CI) based communication system. However, most of the mobile devices are equipped with multiple communication modes, which makes device-to-device communication [2] and the Internet of things [3] become attractive solutions. Furthermore, since mobile devices are held by people, communication between mobile devices is featured by the social behaviours of people, which stimulates the cross-disciplinary research area of *mobile social networks* [4] based on the combination of social science and wireless communication networking. The growing interest can be observed in Fig.1. In Section I-A, the tools of social network analysis will be introduced first.

A. SOCIAL NETWORK ANALYSIS (SNA)

To most people, the phrase 'social network' refers to online social networking services such as *Facebook* and *Twitter*. However, the research of social networks goes back farther than the emergence of the Internet. The true foundation of this field is attributed to Moreno, who studied social interactions within groups of people and published his research entitled *Who Shall Survive* [21] in 1934. Unfortunately, traditional data collection methods such as interviews and questionnaires [22] as well as observations [23] are extremely inefficient. Hence, research on Social Network Analysis (SNA) progressed slowly in the early decades of the 20th century, until the invention of computer technology and online social networking services. Since then, the research community became more prosperous than ever before. In the rest of section I-A, we will characterise the structure of social networks and introduce the new research trends in terms of nodes' importance evaluation (centralities), communities and topologies, as summarised in Fig.2.

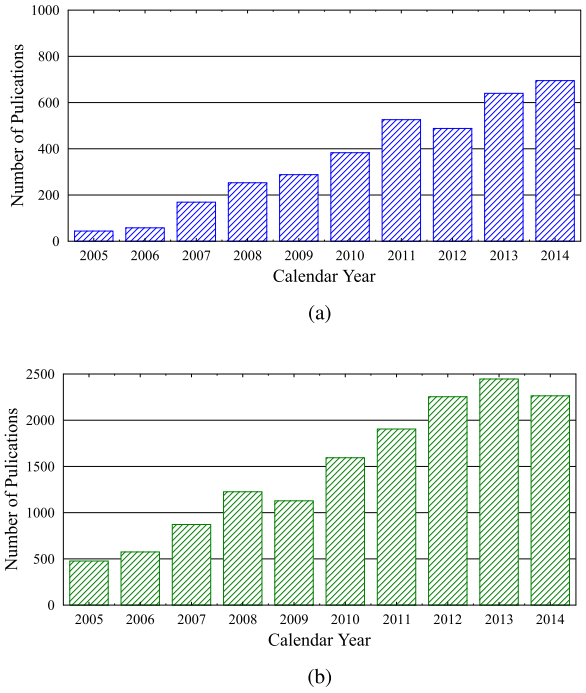

FIGURE 1. The number of publications including the searching term 'mobile social network' in both the IEEE digital library and the ACM digital library from the calendar year 2005 to 2014. (a) IEEE digital library. (b) ACM digital library.

1) STRUCTURE OF SOCIAL NETWORKS

A social network is comprised of social users (represented by nodes) and social links (represented by edges). A pair of social network users is said to be connected by a social link, if they share friendship, as portrayed in Fig.3(a). Mathematically, the structure of a generic social network having N nodes can be characterised by an adjacency matrix $A = [a_{ij}]_{N\times N}$, where $a_{ij} = 1$ if there is a social link spanning from node i to node j and $a_{ij} = 0$, otherwise. The social network of Fig.3(a) characterises the friendships amongst the members of a karate club at an American university [24]. An edge represents that a pair of individuals consistently were observed to interact also outside the normal activities of the

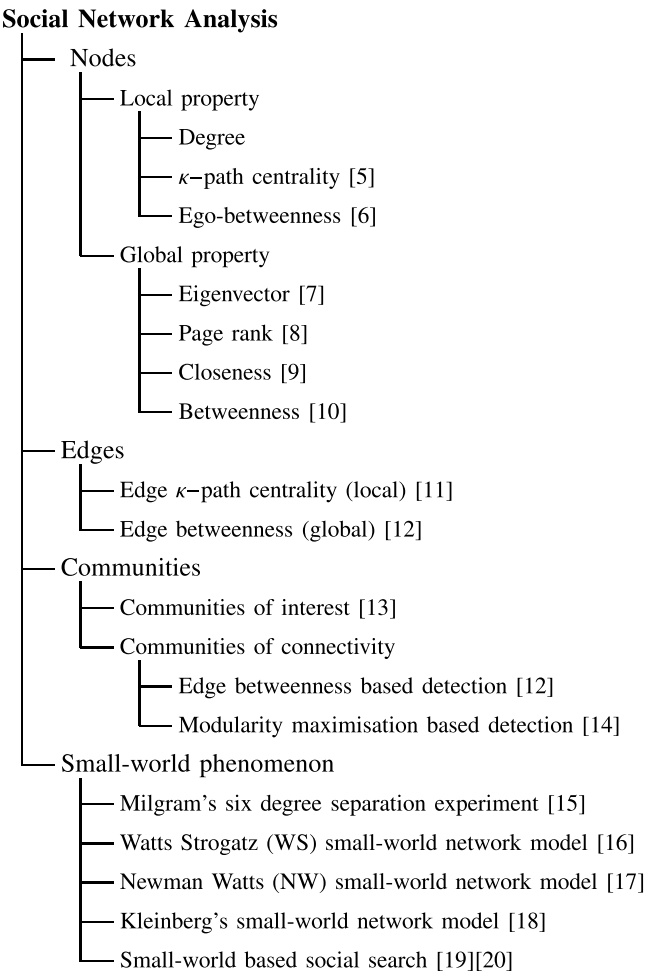

FIGURE 2. **The research in social network analysis.**

club (karate classes and club meetings). The social network of Fig.3(a) is an unweighted and undirected graph, which indicates that all the social links have the same strength and they are symmetrical. The social network of Fig.3(a) can be characterised by the adjacency matrix A_{kara}, as shown in (1), as shown at the top of the next page. Furthermore, a social link can be assigned a weight for the sake of characterising the strength of the friendship between a pair of social network users. Sometimes, a pair of social users share 'unsymmetrical' friendships, which can be characterised by directional social links in social networks.

2) EVALUATING NODES IN SOCIAL NETWORKS

In order to fully exploit the characteristics of a social network, the identification of the principal social users inside the social network is quite important. Such an identification requires an *importance measure* (also referred to as *centrality*) to weight social users and social links.

The most straightforward approach is to directly count the number of neighbours that a social user is directly connected to in the social network studied, which is referred to as the *degree centrality*. Fig.3(b) portrays the degrees for all the nodes in the social network of the karate club [24]. A darker node that is also characterised by a larger size has a higher value of degree centrality. We observe from Fig.3(b) that 'N01' and 'N34' have the highest degrees, sequentially followed by 'N33' and 'N03'. The degree centrality is also applied often for characterising the 'impact factor' of an academic journal by quantifying how often a specific journal is cited by others. Survey journals of the research community usually have a higher impact factor than pure research journals. However, the degree centrality only characterises the local topological properties of a node in a social network, since only the neighbourhood of a node is taken into account. Unfortunately, this measurement is not capable of characterising the global role of a node in the entire social network.

A natural extension of the degree centrality is the *eigenvector centrality*. In the definition of the degree centrality, every neighbour is equally treated without any bias. By contrast, a more important neighbour may provide a higher weight for the calculation of the eigenvector centrality [7]. As a result, a node having fewer higher-weight neighbours may still outrank another node having more lower-weight neighbours, i.e. if the neighbours of the former node are more important than that of the latter. Fig.3(c) portrays the eigenvector centralities for all the nodes in the social network of the karate club [24]. We observe from Fig.3(c) that 'N03' outranks 'N33', although 'N03' has fewer neighbours than 'N33'. This is because the neighbours of 'N03' are more important than those of 'N33'. The eigenvector centrality is also routinely applied in the citation network of journals for characterising the 'eigenfactor' of an academic journal. As an example, research journals in the communication community often outrank survey journals in terms of their eigenfactor. Furthermore, as a variant of the eigenvector centrality, *PageRank centrality* has been proposed for ranking the webpages provided by the Google search engine [8].

Another global measure is referred to as *closeness centrality* [9]. This measure evaluates how 'close' a node is to all the other nodes in a network. Fig.3(d) portrays the closeness centralities for all the nodes in the social network of the karate club. We observe from Fig.3(d) that 'N17' is the closest node to all the other nodes in the social network, although the number of its neighbours is quite low, as shown in Fig.2(b).

Betweenness centrality [10] is also a global measure, which relies on the idea that in social networks information flows along the *shortest path* in terms of the number of hops between a pair of end-users. As a result, a node would have a high betweenness centrality, if a large number of end-to-end shortest paths cross it. As shown in Fig.3(e), 'N01' has the highest betweenness centrality in the social network of the karate club. The authors of [25] further relaxed the assumption that information only flows along the shortest paths and proposed a new betweenness centrality based on random walks. However, the original computation of betweenness centrality requires the global knowledge of the social network studied. If the social network is quite large, having millions of nodes in it, even the most efficient algorithm for computing

$$A_{kara} = \begin{pmatrix}
0&1&1&1&1&1&1&1&1&0&1&1&1&1&0&0&0&1&0&1&0&1&0&0&0&0&0&0&0&0&0&1&0&0\\
1&0&1&1&0&0&0&1&0&0&0&0&0&1&0&0&0&1&0&1&0&1&0&0&0&0&0&0&0&0&0&1&0&0&0\\
1&1&0&1&0&0&0&1&1&1&0&0&0&1&0&0&0&0&0&0&0&0&0&0&0&0&0&1&1&0&0&0&1&0\\
1&1&1&0&0&0&0&1&0&0&0&0&1&1&0&0&0&0&0&0&0&0&0&0&0&0&0&0&0&0&0&0&0&0\\
1&0&0&0&0&0&1&0&0&0&1&0&0&0&0&0&0&0&0&0&0&0&0&0&0&0&0&0&0&0&0&0&0&0\\
1&0&0&0&0&0&1&0&0&0&1&0&0&0&0&0&1&0&0&0&0&0&0&0&0&0&0&0&0&0&0&0&0&0\\
1&0&0&0&1&1&0&0&0&0&0&0&0&0&0&0&1&0&0&0&0&0&0&0&0&0&0&0&0&0&0&0&0&0\\
1&1&1&1&0&0&0&0&0&0&0&0&0&0&0&0&0&0&0&0&0&0&0&0&0&0&0&0&0&0&0&0&0&0\\
1&0&1&0&0&0&0&0&0&0&0&0&0&0&0&0&0&0&0&0&0&0&0&0&0&0&0&0&0&0&0&1&0&1&1\\
0&0&1&0&0&0&0&0&0&0&0&0&0&0&0&0&0&0&0&0&0&0&0&0&0&0&0&0&0&0&0&0&0&0&1\\
1&0&0&0&1&1&0&0&0&0&0&0&0&0&0&0&0&0&0&0&0&0&0&0&0&0&0&0&0&0&0&0&0&0&0\\
1&0&0&0&0&0&0&0&0&0&0&0&0&0&0&0&0&0&0&0&0&0&0&0&0&0&0&0&0&0&0&0&0&0&0\\
1&0&0&1&0&0&0&0&0&0&0&0&0&0&0&0&0&0&0&0&0&0&0&0&0&0&0&0&0&0&0&0&0&0&0\\
1&1&1&1&0&0&0&0&0&0&0&0&0&0&0&0&0&0&0&0&0&0&0&0&0&0&0&0&0&0&0&0&0&0&1\\
0&0&0&0&0&0&0&0&0&0&0&0&0&0&0&0&0&0&0&0&0&0&0&0&0&0&0&0&0&0&0&0&1&1\\
0&0&0&0&0&0&0&0&0&0&0&0&0&0&0&0&0&0&0&0&0&0&0&0&0&0&0&0&0&0&0&0&1&1\\
0&0&0&0&0&1&1&0&0&0&0&0&0&0&0&0&0&0&0&0&0&0&0&0&0&0&0&0&0&0&0&0&0&0\\
1&1&0&0&0&0&0&0&0&0&0&0&0&0&0&0&0&0&0&0&0&0&0&0&0&0&0&0&0&0&0&0&0&0\\
0&0&0&0&0&0&0&0&0&0&0&0&0&0&0&0&0&0&0&0&0&0&0&0&0&0&0&0&0&0&0&0&1&1\\
1&1&0&0&0&0&0&0&0&0&0&0&0&0&0&0&0&0&0&0&0&0&0&0&0&0&0&0&0&0&0&0&0&1\\
0&0&0&0&0&0&0&0&0&0&0&0&0&0&0&0&0&0&0&0&0&0&0&0&0&0&0&0&0&0&0&0&1&1\\
1&1&0&0&0&0&0&0&0&0&0&0&0&0&0&0&0&0&0&0&0&0&0&0&0&0&0&0&0&0&0&0&0&0\\
0&0&0&0&0&0&0&0&0&0&0&0&0&0&0&0&0&0&0&0&0&0&0&0&0&0&0&0&0&0&0&0&1&0\\
0&0&0&0&0&0&0&0&0&0&0&0&0&0&0&0&0&0&0&0&0&0&0&0&0&1&0&1&0&1&0&0&1&1\\
0&0&0&0&0&0&0&0&0&0&0&0&0&0&0&0&0&0&0&0&0&0&0&0&0&1&0&1&0&0&0&1&0&0\\
0&0&0&0&0&0&0&0&0&0&0&0&0&0&0&0&0&0&0&0&0&0&0&0&0&1&1&0&0&0&0&0&1&0&0\\
0&0&0&0&0&0&0&0&0&0&0&0&0&0&0&0&0&0&0&0&0&0&0&0&0&0&0&0&0&0&1&0&0&0&1\\
0&0&1&0&0&0&0&0&0&0&0&0&0&0&0&0&0&0&0&0&0&0&0&0&0&1&1&0&0&0&0&0&0&0&1\\
0&0&1&0&0&0&0&0&0&0&0&0&0&0&0&0&0&0&0&0&0&0&0&0&0&0&0&0&0&0&0&1&0&1\\
0&0&0&0&0&0&0&0&0&0&0&0&0&0&0&0&0&0&0&0&0&0&0&0&0&1&0&0&1&0&0&0&0&1&1\\
0&1&0&0&0&0&0&0&1&0&0&0&0&0&0&0&0&0&0&0&0&0&0&0&0&0&0&0&0&0&0&0&1&1\\
1&0&0&0&0&0&0&0&0&0&0&0&0&0&0&0&0&0&0&0&0&0&0&0&0&1&1&0&0&1&0&0&0&1&1\\
0&0&1&0&0&0&0&0&1&0&0&0&0&0&1&1&0&0&1&0&1&0&1&1&0&0&0&0&0&1&1&1&0&1\\
0&0&0&0&0&0&0&0&0&1&1&0&0&0&1&1&1&0&0&1&1&1&0&0&1&0&0&1&1&1&1&1&1&1&0
\end{pmatrix} \tag{1}$$

the betweenness centrality has the complexity of $O(MN)$ [26], where M and N represent the number of edges and of nodes, respectively. As a further advance, the authors of [5] proposed *κ-path centrality*, where the computation only relies on the information flows along the paths that are shorter than κ hops. They found that the κ-path centrality metric matches the original betweenness centrality well, while significantly reducing the complexity of its computation to $O(\kappa^3 N^{2-2\alpha} \log N)$. The *egocentric network* concept of [27] represents the network surrounding the individual studied within a radius of 1 hops. Moreover, the *ego-betweenness* [6] is a special case of *κ-path centrality* for $\kappa = 2$.

The aforementioned betweenness centralities of nodes can be readily extended in order to characterise the *betweenness centralities for edges*, which plays a vital role in community detection [12]. Similar to [5], a *κ-path edge betweenness* was proposed in [11] and the corresponding computational complexity was reduced to $O(\kappa M)$, where M is the number of edges in the social network studied.

TABLE 1 exemplifies the calculation process of the degree, of the eigenvector, the closeness and the betweenness centralities for the node 'N06' in the social network of the karate club, as shown in Fig.3.

3) COMMUNITY DETECTION

According to different node classification principles, we have the following two types of community:

- A *community of interest*, which is "a set of people assembled around a topic of common interest. Its members take part in the community to exchange information, to obtain answers to personal questions or problems, to improve their understanding of a subject, to share common passions or to play" [13].
- A *community of connectivity*, which is a group of nodes in social networks densely connected to each other and weakly coupled with nodes residing outside the community itself.

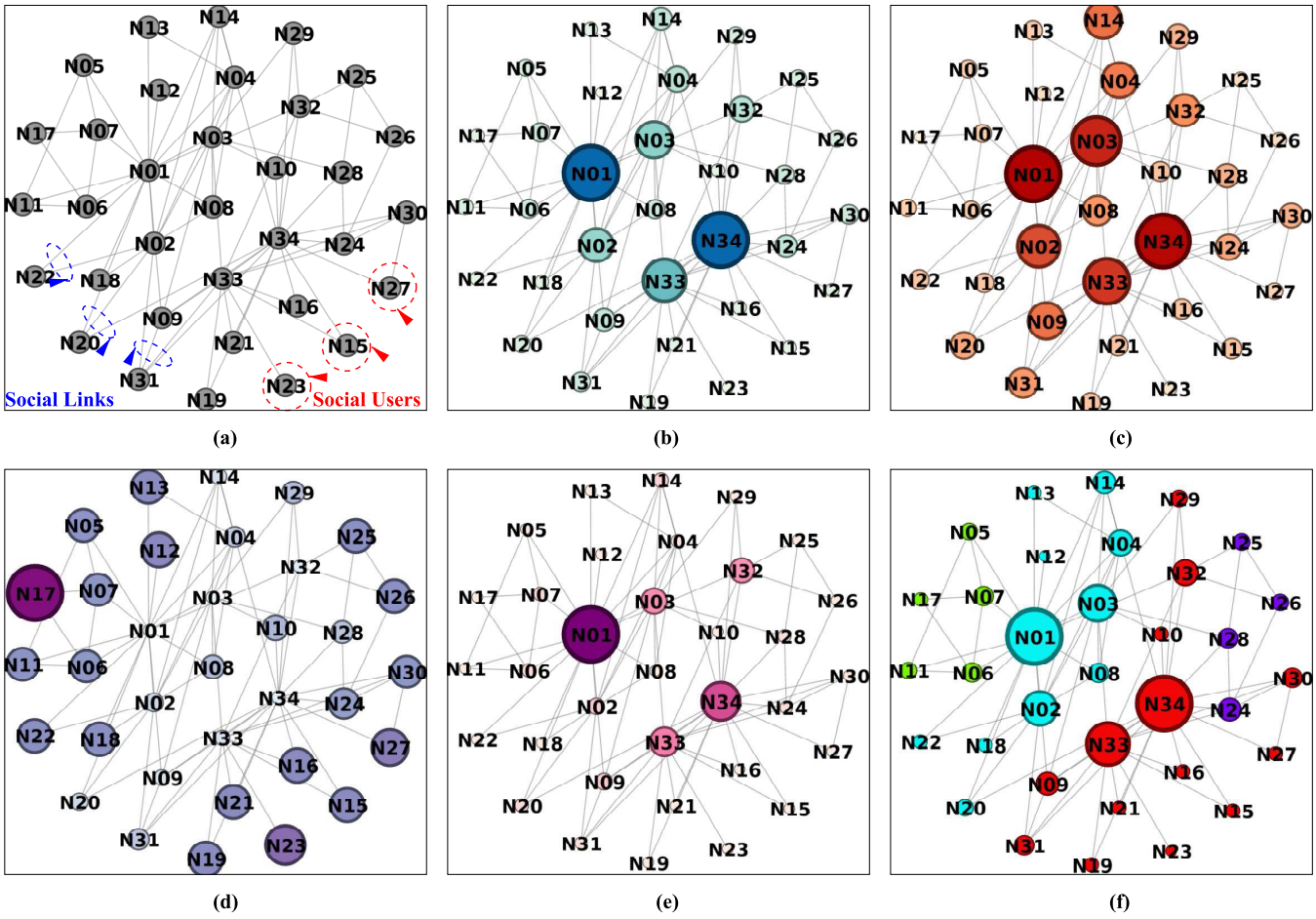

FIGURE 3. **Unweighted and undirected friendship network between members of a karate club. This social network shows the pattern of friendships between the members of a karate club at an American university. The data were collected and published in [24]. The calculation process of degree, eigenvector, closeness, and betweenness centralities for the node 'N06' is exemplified in TABLE 1. (a) Original social networks. (b) Degree centrality. (c) Eigenvector centrality. (d) Closeness centrality. (e) Betweenness centrality. (f) Community detection.**

These two types of community may convert into each other. People sharing common interest are often tightly connected to each other in social networks. Vice versa, people that are strongly connected to each other may tend to cultivate common interests due to frequent communication with each other. It is the community of interest, which is the focus of our research in the following sections. However, in this section, we would like to briefly introduce the detection of communities of connectivity.

As mentioned above, edge betweenness was invoked in the community detection algorithm developed in [12]. After calculating the betweenness centralities for all edges, the specific edge having the highest betweenness is removed. Then, the betweenness centralities of the edges affected by the former removal edge is recalculated. This procedure is repeated until the underlying community structure of the network is completely discovered.

Modularity was designed to quantify the grade of division across a network into modules [29]. The authors of [14] develop a community detection algorithm based on modularity maximisation, which iteratively optimises the formulation of local communities until the achievable global modularity can no longer be improved by tentatively imposing perturbations on the current community state. This algorithm is exploited for discovering the community structure of the social network, such as the karate club, as shown in Fig.3(f). We observe from Fig.3(f) that the social network is divided into four communities and different communities are filled by different colours and patterns. The largest community has 14 members, while the smallest community has only 4 members.

4) SMALL-WORLD PHENOMENON

The small-world phenomenon of social networks was firstly revealed by Milgram's famous experiment [15]:

In order to deliver a letter from a source person to a target person, the source would initially be given basic information about the target, including his address and occupation. Then the source would be instructed to send the letter to someone on a first-name basis in an effort to transmit the letter to the target as efficaciously as possible. Anyone subsequently receiving the letter would be given the same instructions,

TABLE 1. Various centralities of node 'N06' in the social network of Fig.3.

Centrality	Calculation Process	Value	Complexity[a]
Degree	Node N06 has 4 neighbours in total, which are N01, N07, N11 and N17. The number of neighbours is derived by summing the entries in the 6-th row of the adjacent matrix A_{kara} of (1).	Deg(N06) = 4	$O(\min(M, N))$
Eigenvector	Given the adjacency matrix A_{kara} of (1), according to the formula $A_{kara}x = \lambda x$, find the eigenvalue $\lambda_{\max} = 6.67$ having the largest absolute value and derive its corresponding eigenvector x. The eigenvector centrality of N06 is the 6^{th} entry of the eigenvector x.	Eig(N06) = 0.226	$O(C \cdot N^2)$ [28], C is the No. of the iterations in the invoked algorithm.
Closeness	Given the adjacency matrix A_{kara} of (1), we find the shortest path between N06 and an arbitrary node j. Calculate the number of hops of this shortest path, defined as $d_{6,j}$. For example, the shortest path between N06 and N12 is $N06 \rightarrow N01 \rightarrow N12$ having $d_{6,12} = 2$ hops. Repeat this computing process for all the nodes. Then the closeness of N06 is derived as $\sum_{j=1, j\neq 6}^{34} 1/d_{6,j}$.	Clo(N06) = 2.6	$O(M + N \log N)$ [9]
Betweenness	Given the adjacency matrix A_{kara} of (1), we find all the shortest paths between an arbitrary pair of nodes, i and j. The total number of these paths is g_{ij}. Amongst these paths, $g_{ij}(k)$ paths cross node k. For example, there are $g_{7,11} = 3$ shortest paths between N07 and N11. Amongst these, only $g_{7,11}(6) = 1$ shortest path cross N06. Repeat this computing process for all possible pairs. Then the betweenness of N06 is derived as $\sum_{i=1}^{34} \sum_{j=1}^{34} g_{ij}(6)/g_{ij}/2$, for $i \neq 6$ and $j \neq 6$.	Bet(N06) = 15.8	$O(MN)$ [26]

[a] M and N represent the number of edges and of nodes, respectively.

and the chain of communication would continue until the target was reached.

Over many trials, Milgram found that the average number of hops in successful chains lie between five and six, which is referred to as the 'six degrees of separation' principle. Generally speaking, a small-world network is a type of mathematical graph in which most nodes are not neighbours of one another, but most nodes can be reached from every other by a small number of hops or steps.

There are two models that may be used for constructing a small-world network from a regular network, namely the Watts-Strogatz (WS) [16] model and the Newmann-Watts (NW) model [17]. In the WS model, a small-world network is constructed via rewiring a few links in an existing regular network [16]. By contrast, in the NW model [17], a small-world network is constructed via adding a few new links without changing any existing links of the original regular networks. Moreover, the link rewiring probability (or the link adding probability) in the WS (or the NW) model can be expressed by $p \propto 1/(d_{i,j})^{\beta}$ [18], where $d_{i,j}$ represents the minimum number of hops spanning from node i to node j and β is a basic structural parameter that quantifies how clustered the network is. This model is known as Kleinberg's small-world network model. In a nutshell, small-world networks typically have a high clustering coefficient, but a low average path length quantified in terms of the number of hops. Furthermore, the authors of [19] and [20] theoretically confirmed the result of Milgram's experiment in the context of the NW model, which is exploited for evaluating the performance of the social search.

The major contributions in SNA research are summarised in TABLE 2.

B. WHEN SOCIAL NETWORKS MEET TELECOMMUNICATION NETWORKS

At the time of writing, there are remarkable advances in the cross-disciplinary research area of SNA aided telecommunication networking and signal processing, which seamlessly bridge telecommunication networks and social networks [30]. These advances are portrayed in Fig.4. The central box of Fig.4 summarises the commonly-adopted SNA tools, which have been detailed in Section I-A. The outer shell of boxes in Fig.4 provides a glimpse of some of the applications of the SNA in the research of the telecommunication. We will briefly introduce these applications in the rest of Section I-B.

1) COMMUNICATION NETWORK MODELLING

Firstly, SNA can be exploited for modelling generic communication networks. The authors of [31] modelled the telephone call network (TCN) by a scale-free social network [32], where nodes represent telephone numbers and two nodes are connected if calls are made between the corresponding telephone numbers. Based on this social network model, a preferential call blocking scheme was proposed in order to mitigate the adverse effect of a sudden surge

TABLE 2. Major contributions in the SNA research.

Year	Author	Contribution
1934	Moreno *et al.* [21]	pioneered the SNA research.
1969	Milgram *et al.* [15]	identified the small-world phenomenon in social networks by a letter delivery experiment.
1977	Zachary [24]	constructed a social network by observing people's behaviours in a karate club.
	Freeman [10]	proposed betweenness centrality for evaluating the importance of nodes.
1982	Freeman [27]	defined the centred graphs and studied the structure of ego networks.
1988	Freeman [23]	investigated the capabilities of humans in processing social information based on data collected by observation.
1998	Watts *et al.* [16]	constructed a small-world network by rewiring a few links in a regular network.
1999	Newman *et al.* [17]	constructed a small-world network by adding some new links without changing any existing links of the original regular network.
2000	Kleinberg [18]	modelled the link rewiring probability as an inversely-proportional value of the social separation in terms of the number of hops in the social network.
2001	Newman [26]	proposed an algorithm for computing betweenness, whose complexity is $O(MN)$.
2002	Marsden [6]	proposed ego-betweenness centrality for egocentric networks.
	Girvan *et al.* [12]	proposed a community detection algorithm based on the edge betweenness centrality.
2003	Henri *et al.* [13]	provided the definition of the community of interest.
2005	Newman [25]	proposed a new betweenness centrality by assuming that the information flows in the social network according to the random walk law.
2006	Newman [29]	designed modularity to quantify the grade of division across a network into modules.
2007	Bonacich [7]	proposed the eigenvector centrality concept for evaluating the importance of the nodes.
2008	Chen *et al.* [9]	summarised the closeness centrality in the social network.
	Blondel *et al.* [14]	proposed an algorithm in order to detect the community structure of the social network with the aid of the modularity concept.
2011	Tripathi *et al.* [5]	proposed the κ–path centrality relying on the information flows along the paths that are shorter than κ hops.
2012	Meo *et al.* [11]	proposed the κ–path centrality for characterising the importance of an edge in a social network.
2014	Inaltekin *et al.* [20]	mathematically demonstrated Milgram's 'six degrees of separation' theory in the context of the social search.

in the number of telephone calls potentially resulting in an overloaded telephone network. The authors of [33] studied the performance of generic communication networks and link the degree as well as betweenness centrality to the node activation probability. Following indepth experiments relying on various mathematical network models as well as on the Internet constructed at the autonomous system level [34], their proposed resource allocation scheme based on the node activation probability was shown to outperform both the uniform and the degree-based schemes.

2) MOBILITY MODEL DESIGN

Secondly, SNA can be exploited for designing mobility models, which are capable of reflecting the social relationships amongst the Mobile Users (MUs). Based on the mobile phone data collected by the Reality Mining project [35], the self-reported social relationship between a pair of individuals exhibits a distinctive behavioural signature as quantified in terms of their physical proximity and calling patterns. The landmark research disseminated in [35] confirms that the social relationships amongst the MUs affect their mobility patterns. Relying on this fact, the authors of [36] proposed a Community-based Mobility Model (CMM). In CMM, a MU is more likely to move towards a specific place, where most of his/her friends are staying. The CMM captures the behaviours of MUs moving in groups and between groups. As an evolution of CMM, the Home-cell Community-based Mobility Model (HCMM) is proposed in [37]. Apart from the friendship cohesion inherited from CMM, HCMM also accounts for the associated spatial attraction, where a MU may be inclined to move towards a specific place defined as 'home'.

3) CONTACT TRACE BASED RELATIONSHIP MODELLING

Thirdly, SNA can be exploited for modelling the social relationship between a pair of MUs according to their contact trace. In a Mobile Ad Hoc NETwork (MANET), when a pair of MUs enters each other's transmission range, their contact can be readily established. During an observation period, if a MU encounters another MU, we establish a social relationship between them. However, the qualities of the social

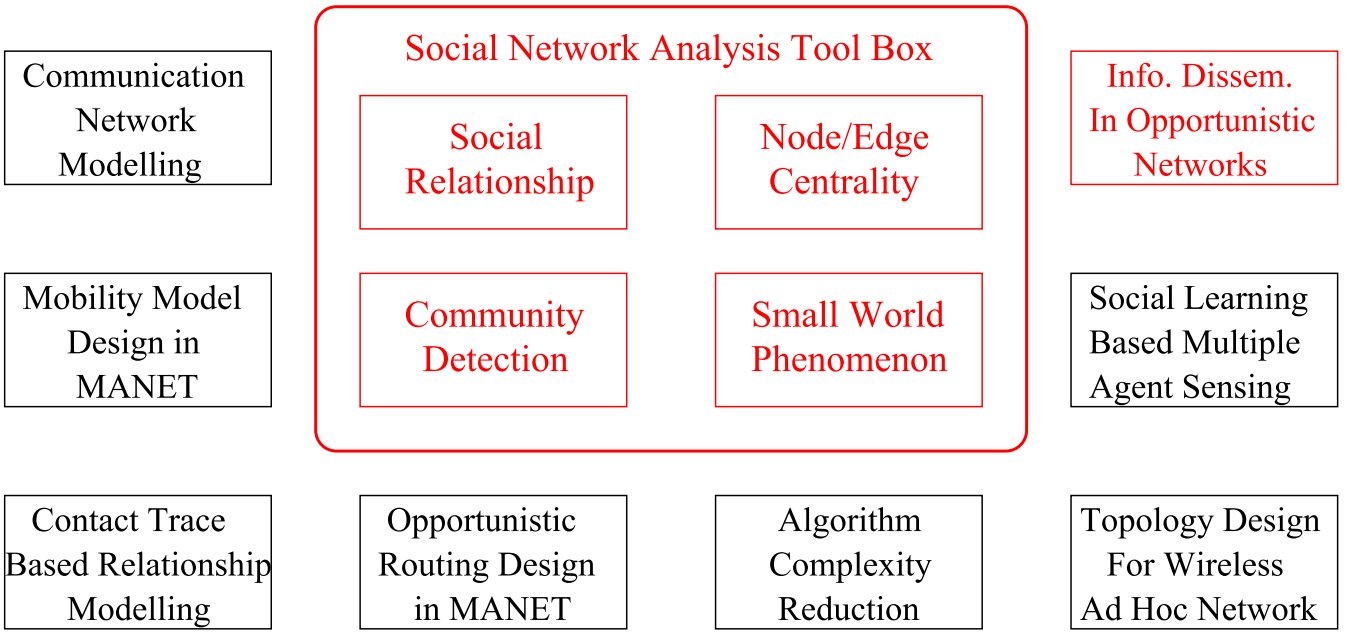

FIGURE 4. The cross-disiplinary research in social network analysis aided telecommunications.

relationships vary amongst the different MU pairs. In [38], the qualities of the social relationships are characterised by the associated encounter frequency, the total or average contact period and the average separation period. Furthermore, the Social Pressure Metric (SPM) is proposed in [39] for overcoming the deficiencies of the above-mentioned metrics and for accurately characterising the qualities of the social relationships.

4) OPPORTUNISTIC ROUTING DESIGN

Fourthly, SNA can be exploited for efficient routing design in MANETs. Due to the intermittent nature of MANETs, data forwarding is realised by opportunistic contacts amongst MUs. When modelling the social relationship between any pair of MUs with the aid of the contact trace, their contact opportunities can be characterised by the associated social graph. Hence various centralities can be invoked for evaluating the personal importance of the MUs in a MANET. In [40], the degree of connectivity is exploited for formulating a data forwarding strategy. The so-called BUBBLE forwarding algorithm [41] is capable of accounting for the global betweenness centralities of the MUs. Furthermore, SimBet [42] routing policy is proposed by exploiting the local ego-betweenness [6].

5) ALGORITHMIC COMPLEXITY REDUCTION

Fifthly, SNA can be exploited for reducing the algorithmic complexity. A coalitional game approach is proposed in [43] in order to cooperatively deliver packets in hybrid wireless mobile networks. Since a pair of MUs separated by multiple hops have less influence on each other, the MUs are divided into communities according to their contact traces. Following the community detection phase, finding the gaming-aided solution of the game model is carried out independently for all the communities. As a result, compared to finding the global gaming-aided solution, the complexity of finding the solution of the game model is significantly reduced with the aid of the community detection technique.

6) TOPOLOGY DESIGN FOR WIRELESS AD HOC NETWORKS

Furthermore, the small-world phenomenon can be utilised for constructing wireless ad hoc networks. In [44], the probability of creating a direct wireless link between a pair of communication nodes is jointly determined by considering the residual battery energy of nodes as well as by the multi-hop transmission distance and the geographical distance between the nodes, whilst also taking the constraints of the radio transmission range between nodes into account. As a result, an energy efficient wireless network topology may be created by relying on the small-world principle. Directional beamforming (BF) is invoked in [45] for creating a direct link, which is referred to as a 'short cut' in the SNA, between a pair of 'central' nodes in a wireless ad hoc networks in order to preserve the validity of the small-world phenomenon.

7) SOCIAL LEARNING BASED MULTI-AGENTS SENSING

Additionally, an agent, which could be either a 'physical sensor'[1] or a 'social sensor',[2] may make a sensing decision by

[1]Examples of physical sensors include sound sensors, chemical sensors and temperature sensors. A physical sensor aims to detect a state change of a natural phenomenon.

[2]Examples of social sensors include Twitter posts, Facebook status updates, and ratings on line reputation systems such as Yelp and Tripadvisor. A social sensor aims to infer social relationships and human activities.

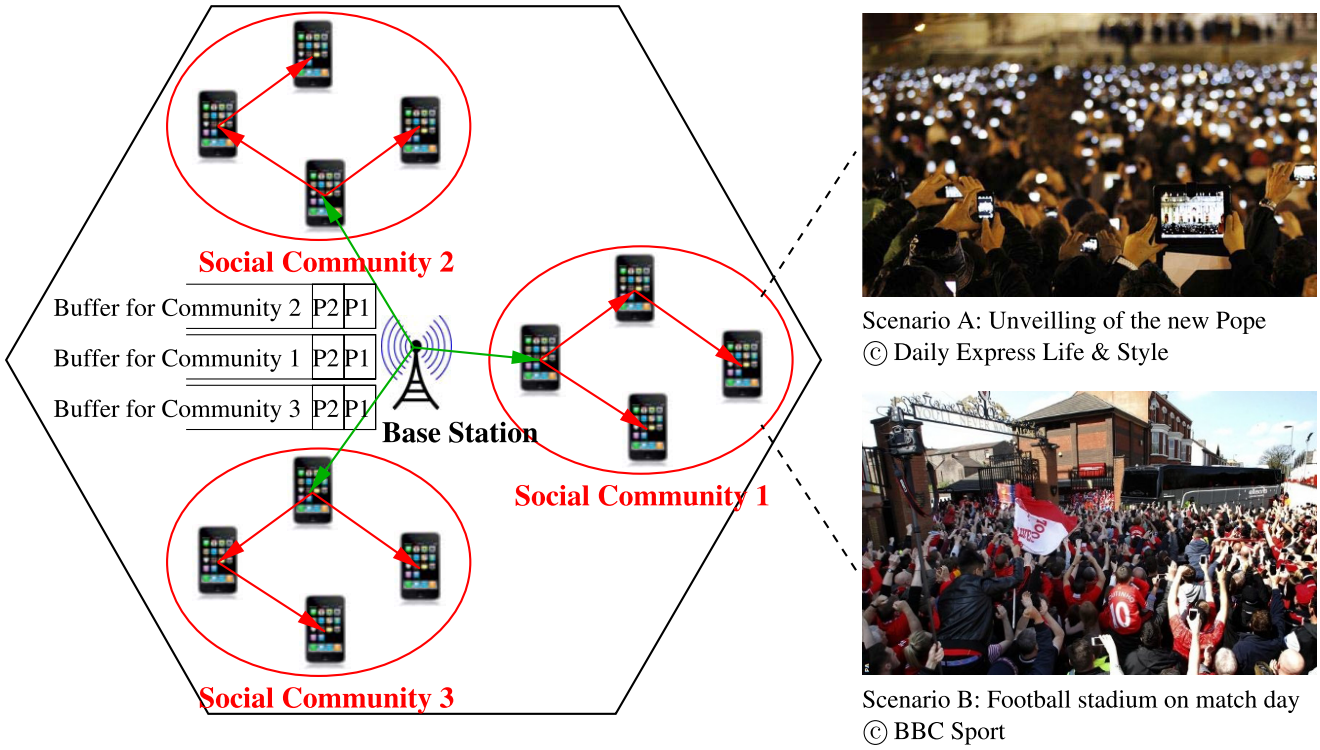

FIGURE 5. People form communities of interest for disseminating the IoCI.

jointly exploiting both its own local observation as well as the decisions made by the surrounding agents. This is regarded as social learning based multi-agent aided sensing [46]. In this application, by exchanging information with their peers, agents form a community in order to collaboratively achieve a common goal with a better 'utility' than that achieved by them individually. In [46], a social learning protocol was discussed in detail and a strategy of making a global sensing decision was proposed for the sake of minimising both the detection delay and the false alarm penalties. Furthermore, based on this original social learning protocol, the authors of [47] resolved the associated privacy concern as well as the biased sensing-induced misinformation propagation.

8) INFORMATION DISSEMINATION IN OPPORTUNISTIC NETWORKS

Finally, SNA can be exploited for realising information dissemination in opportunistic networks. In this application, MUs form a community of interest, as introduced in Section I-A. Based on the multifunctional mobile devices owned by numerous subscribers, the Information of Common Interest (IoCI) can be spontaneously disseminated across the community without the aid of any Centralised Infrastructure (CI). For instance, the crowds participating in the inauguration of the new Pope's identity may form a community of interest in order to share close-up video-clips of the Pope on the podium. Similarly, supporters in a football stadium may also form a community of interest so as to share video-clips of a spectacular goal from different angles or the score updates from another stadium, as exemplified by Fig.5. The tools of SNA are capable of assisting us in designing an efficient strategy for information dissemination. In the following parts of this treatise, we mainly focus our attention on revealing the details of information dissemination in integrated cellular and opportunistic networks.

The major contributions in SNA aided telecommunication research are summarised in TABLE 3.

II. MOTIVATIONS AND CONTRIBUTIONS

A. DESIGN DILEMMAS OF INFORMATION DISSEMINATION IN CI BASED SYSTEM

As discussed, an increasing number of MUs share common interests in the same information. For instances, drivers have to receive the traffic information in rural areas; urban residents are interested in the weather forecast before they go to work; Attendees are keen on reading the program before their conference gets started; Football fans in the stadium are curious about the score update from their championship contender's match... However, CI based techniques exhibit the following limitations in disseminating the IoCI:

1) INTERMITTENT CONNECTIVITY IN RURAL AREAS

Suffering from coverage limitations of the CI in rural areas, the wireless links between the MUs and Base Stations (BSs) are prone to intermittent connections due to the high mobilities of the MUs. The same limitations are encountered,

TABLE 3. Major contributions in the SNA aided telecommunication research.

Year	Authors	SNA Tool	Contribution
2005	Eagle *et al.* [35]	Social Relationship	found a close match between the self-reported social relationships of the MUs and the mobility behaviours of the MUs.
2007	Musolesi *et al.* [36]	Social Relationship	designed a mobility model based on social network theory.
2008	Costa *et al.* [40]	Degree Centrality	designed a routing protocol based on degree centrality.
2009	Tam *et al.* [31]	Social Network	modelled a telephone network by a social network prototype.
	Li *et al.* [38]	Social Relationship	modelled the qualities of the social relationships by the encounter frequency, average/total contact duration/separation period.
	Daly *et al.* [42]	Ego-Betweenness	designed a routing protocol based on ego-betweenness centrality.
2010	Boldrini *et al.* [37]	Social Relationship	designed a mobility model based on both social network theory and spatial attraction.
2011	Hui *et al.* [41]	Betweenness and Community Detec.	designed a routing protocol based on betweenness centrality as well as community detection.
2012	Bulut *et al.* [39]	Social Relationship	proposed SPM so as to accurately model the quality of the contact trace based social relationships.
	Banerjee *et al.* [45]	Small-World Phenomenon	invoked a directional BF technique so as to preserve the small-world phenomenon in wireless ad hoc networks.
2013	Wu *et al.* [33]	Degree Centrality Betweenness	proposed a resource allocation scheme based on node activation probability, which is defined by their degree and betweenness.
	Niyato *et al.* [43]	Community Detection	reduced the complexity of finding a game-solution by exploiting the community detection technique.
	Zhang *et al.* [44]	Small-World Phenomenon	created an energy efficient wireless ad hoc network topology by exploiting the small-world phenomenon.
	Krishnamurthy *et al.* [46]	Social Network	proposed a social learning protocol for multi-agent aided sensing by exploiting information exchange in social networks.
2014	Krishnamurthy *et al.* [47]	Social Network	resolved privacy and misinformation propagation issues in social learning.

when most of the CI is destroyed by a natural disaster [48], such as an earthquake, a tsunami etc. The traditional measures of improving and recovering the wireless connection include building more BSs in the rural area, and increasing the transmit power of the existing BSs so as to cover a larger geographic area as well as deploying more relay stations. However, due to the sparse user distribution in rural areas, the aforementioned measures are believed to be of low-return investment for the network operators.

2) OVERLOADED CENTRALISED INFRASTRUCTURE

As we witness an explosive growth of the tele-traffic demand, most of the existing BSs are overloaded, which results in significant degradation of the quality of service (QoS) for the MUs. The traditional measures of increasing the network capacity include the employment of small-cells [49] in order to offload the potentially excessive data traffic from the macro-cells. The increasing tele-traffic imposes serious inter-cell interference (ICI) [50]. In order to further increase the attainable network capacity and to mitigate the adverse effects of ICI, WiFi hotspots are deployed by the network operators for offloading tele-traffic from cellular networks [51], because the 802.11 WiFi systems [52] operate in a spectrum band different from that of classic cellular communication. However, these traditional measures are based on the centralised management of the entire CI, which imposes a high cost on the network operators in terms of both deployment and maintenance expenses.

3) INEFFICIENT DATA SERVICE IN DENSELY POPULATED AREA

In the densely populated scenarios, such as a football stadium, an open air festival and a conference venue, there are likely to be hundreds of MUs crowding in a very small area having a radius of 50 meters. Since people temporarily get together for a specific event and rarely visit this place again after the event, it is unwise to invest into costly CI for these scenarios. The traditional measure of efficiently delivering the IoCI is to allow the BS to multicast the IoCI by exploiting the broadcast nature of wireless channels rather than to consume excessive resources for establishing dedicated channels [53]. However, when the number of requesters is huge, the CI will impose both a long delay and a low throughput during the multicasting of the IoCI to all the requesters [54].

Fortunately the smart multifunctional mobile devices that are equipped both with large storage capacity and with multiple communication modes are popular amongst the MUs. These devices are capable of receiving, carrying and forwarding the IoCI to their peers, hence they can be 'employed'

by BSs in order to more efficiently deliver the information to the targets. As a result, it is possible for us to solve the aforementioned design dilemma of CI based information dissemination by exploiting the opportunistic communication amongst the MUs based on either opportunistic contacts[3] [55] within the large-scale opportunistic networks or with the aid of opportunistic multicast scheduling[4] [56] in the small-scale opportunistic networks. Here, the adjective 'large-scale' indicates a large area covered by the opportunistic networks, which has a size of several kilometres and it is far larger than the transmission range of the MUs. Moreover, having a 'large-scale' opportunistic network also indicates imposing a longer latency on delivering the IoCI, which may even be on the order of hours. By contrast, the terminology of 'small-scale' indicates a small area quantified in terms of metres, which is comparable to the transmission range of MUs. Moreover, having a 'small-scale' opportunistic network also indicates a lower latency in delivering the IoCI, which is on the order of a transmission frame duration, say milliseconds.

B. CONTRIBUTIONS

In the rest of this treatise, we will demonstrate how integrated cellular and opportunistic networks solve the aforementioned three design dilemmas of the information dissemination. The contributions of this paper are listed below:

- We first deliver a detailed tutorial on the information dissemination process of integrated cellular and large-scale opportunistic networks, and discuss its typical applications both in the scenario of improving connectivity of classic cellular networks and in the scenario of off-loading tele-traffic from cellular networks to opportunistic networks.
- In the above tutorial, we characterised the impact of both the mobility-related factors and that of a range of other factors on the information dissemination process. Specifically, we demonstrated that the contact duration between a pair of MUs obeying a random direction mobility model is approximately exponentially distributed. However, the contact duration between a BS (static node) and a MU can be closely approximated by the Gamma distribution.
- By jointly considering both the contact duration as well as the well-known exponentially distributed inter-contact duration, we model the information dissemination process as a Continuous-Time-Pure-Birth Markov Chain (CT-PBMC) when a homogeneous mobility model is assumed for all the MUs. Furthermore, we additionally demonstrate that heterogeneous mobility can also be handled by an equivalent mathematical transformation.
- Furthermore, the tools of SNA are invoked for carefully selecting the initial receiver set in the scenario of off-loading tele-traffic from cellular networks to opportunistic networks.
- Following this tutorial, we propose a hybrid information dissemination scheme for integrated cellular and small-scale opportunistic networks. This scheme consists of two main stages, namely the BS-aided single-hop multicast and the cooperative multicast aided spontaneous dissemination. In order to avoid any interference amongst Information Multicasters (IMs), a Time-Division-Multiple-Access (TDMA) scheme is implemented.
- The varying distances between the transmitters and receivers, which are incurred by the MUs' mobility, result in varying Path Loss (PL). By jointly considering the PL and the multipath fading in the PHYsical (PHY) layer as well as the classic round-robin resource scheduling in the Medium-Access-Control (MAC) layer, we firstly analyse the average throughput of both the cellular links and of the opportunistic links. Then, we model the hybrid information dissemination scheme by a Discrete-Time-Pure-Birth Markov Chain (DT-PBMC).
- With the aid of this DT-PBMC, we obtain the closed-form results for the group delay characterising a specific group of MUs successfully receiving the IoCI. The group delay is a generic form subsuming various delay metrics. When the group size is one, it is equivalent to the end-to-end delay. When the group size is equal to the total number of MUs in the area studied, it is equivalent to the total dissemination delay, which is the time required to serve all of the MUs. Furthermore, the average energy dissipation of disseminating the IoCI is also derived.
- We observe from the simulation results that a more vigorous social interaction of the MUs is capable of significantly reducing both the dissemination delay and the energy dissipation. The tools of SNA can also be exploited for further improving the information dissemination performance of integrated cellular and small-scale opportunistic networks, as we detailed in [57].

The rest of this treatise is organised as follows. In Section III, we provide a tutorial on the information dissemination process of integrated cellular and large-scale opportunistic networks, where two specific application scenarios are introduced, namely that of improving the connectivity of cellular networks and offloading tele-traffic from cellular networks. In Section IV, we propose a hybrid information dissemination scheme for our integrated cellular and small-scale opportunistic networks in order to reduce both the delay and energy dissipation required for disseminating the IoCI. Finally, we conclude and compare the main features of the family of integrated large-scale/small-scale opportunistic networks in Section IV.

[3]The information delivery is completed by the opportunistic contacts of the source and the target, when they enter each other's transmission range. No pre-decided deterministic routing is required.

[4]All the MUs holding the IoCI are potential relays for the next stage of multicast. No pre-decided deterministic relay selection is required.

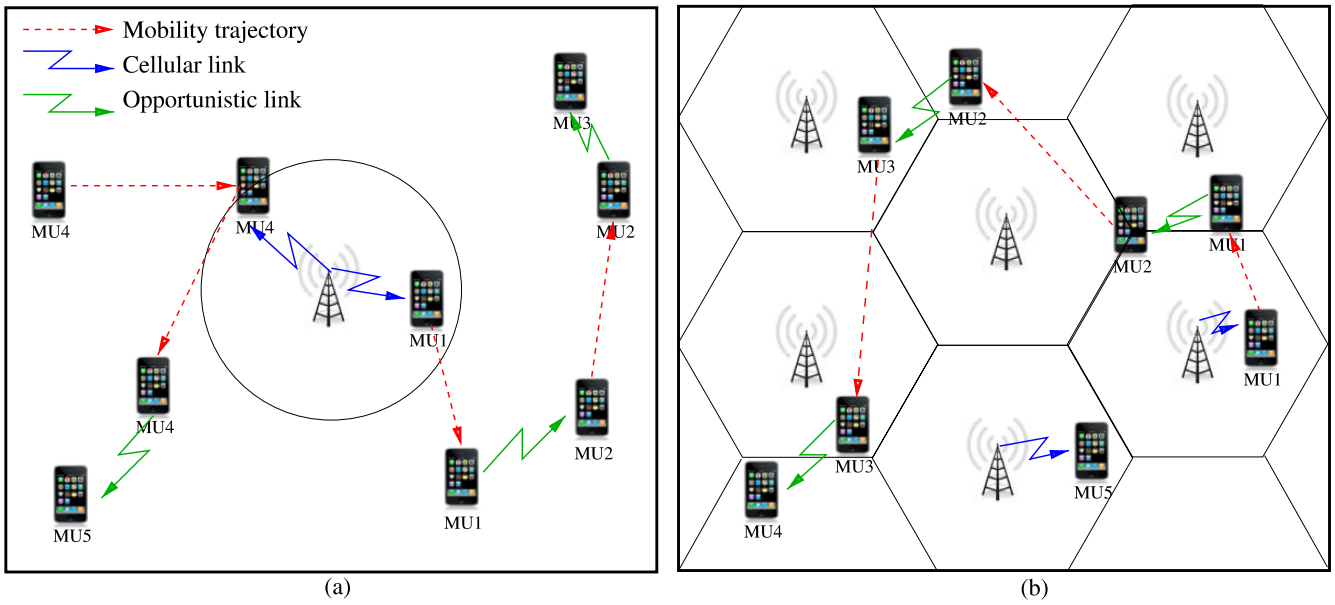

FIGURE 6. Two application scenarios for the integrated cellular and large-scale opportunistic networks. (a) Extending the coverage of the cellular networks. (b) Off-loading tele-traffic from cellular networks.

III. INFORMATION DISSEMINATION IN INTEGRATED CELLULAR AND LARGE-SCALE OPPORTUNISTIC NETWORKS

In order to disseminate the IoCI to all the MUs, the store-carry-forward mode of [58] is exploited. Once a MU receives the IoCI, it first saves the IoCI in its own storage, then carries the IoCI as it moves and forwards it to other hitherto unserved MUs (uMUs). However, in large-scale opportunistic networks, MUs are sparsely distributed across a large area, and their transmission range is much smaller than the size of the area studied. Any information exchange can only be completed, when the MUs are within each other's transmission range. Moreover, since it rarely occurs that an uMU simultaneously enters the transmission range of multiple Information Owners (IOs) or vice versa, sophisticated MAC protocols, such as interference/contention avoidance and resource scheduling [59], become dispensable. As a consequence, the information dissemination is dominated by the mobility pattern of MUs, and the corresponding delay metrics exhibit similar to the *inter-contact duration*[5] between a pair of MUs, which is the main feature of Delay-Tolerant Networks (DTNs) [60].

A. TWO APPLICATION SCENARIOS

As portrayed in Fig.6, integrated cellular and large-scale opportunistic networks can be applied in the following two scenarios, for example.

1) IMPROVING CONNECTIVITY OF CELLULAR NETWORKS

If the BSs are sparsely distributed in a large area [61], the MUs may lose their connections to the BSs since they are likely to be out of the BSs' coverage. In this case, opportunistic communication between a pair of MUs can be invoked for the sake of disseminating important messages. As shown in Fig.6(a), when MU1 and MU4 move into the coverage of the BS, they successfully receive the IoCI from the BS. Thereafter, they carry the IoCI and roam within the area studied. Once they meet other uMUs, the IoCI is delivered via the opportunistic links between them. As a result, opportunistic communication increases the chance of the IoCI's successful reception for those MUs that are not within the coverage of the BS. This integrated network can be exploited for supporting emergency communication as well when most of the BSs are destroyed by a natural disaster [48]. Furthermore, if we consider the BS to be a roadside unit (RU), the scenario of Fig.6(a) can be naturally extended to a hybrid vehicular network [62], where RU-to-vehicle and vehicle-to-vehicle communications cooperate in order to disseminate the important traffic information, for example. In Section III-E, we will introduce a mathematical tool for analysing the delay metrics of this scenario.

2) OFF-LOADING TELE-TRAFFIC FROM CELLULAR NETWORKS

Due to the intrinsic unicast nature of cellular communications, multiple dedicated cellular links have to be established for the sake of disseminating the IoCI to all the requesters, which absorbs a large fraction of the BSs's resources. Apart from improving connectivity of cellular networks, large-scale opportunistic networks are also capable of off-loading some tele-traffic from cellular networks so as to save BSs' precious resources [63]. As shown in Fig.6(b), the BSs firstly inject some copies of the IoCI into the

[5]The statistical properties of the inter-contact duration will be introduced in Section III-C.

opportunistic network. Thereafter, the IoCI is disseminated via opportunistic contacts of MUs as well as via direct injections from the BSs. Since all the MUs are covered by the cellular network, the information delivery of a cellular link is prompt and the delay is substantially shorter than the inter-contact duration of MUs. In Section III-G, we will highlight the specific characteristics of this scenario.

B. FACTORS INDEPENDENT OF THE MOBILITY OF MUs

Let us first introduce the factors affecting the performance of the integrated cellular and large-scale opportunistic networks, which are unrelated to the mobility of MUs.

1) TRANSMISSION RANGE

In practice, the transmission range r is determined by a specific short-range communication technique employed for information transmission. For instance, the transmission range is up to 60 meters for Bluetooth [64], whilst it could be upto 250 meters for WiFi according to the family of 802.11 protocols [52]. Theoretically, the transmission range is jointly determined by transmit power, wireless channel's attenuation, as well as by the interference. For instance, *effective transmission range* [65] is defined as the maximum value of the transmission range satisfying the condition that the received power remains higher than a pre-defined threshold with a high probability.

2) FILE SIZE AND TRANSMISSION RATE

Since the wireless link can only be established when the source and the target are within each other's transmission range, as to whether the file can be successfully delivered or not depends on the file size L, on the transmission rate B and on their contact duration.[6] The file size varies from Kilobytes (for text messages) to Megabytes (for multimedia contents), while the transmission rate depends on bandwidth and transmit power, on the channel attenuation, on the interference, as well as on the specific choice of the modulation and coding schemes. Since adaptive power control [66] is widely adopted in practical communication, a minimum transmission rate B can usually be achieved at the receiver end. If this is the case, the transmission duration becomes L/B time units.

3) LIFE TIME OF THE IoCI

IoCI considered in this treatise may belong to the category of time-sensitive information, such as weather forecast, traffic information etc. This type of information would only attract the interest of MUs for a short period, which is defined by the life time T_L [67]. Once the IoCI is firstly generated, it would be disseminated in the integrated cellular and large-scale opportunistic networks for a period of T_L. After this period, the uMUs might lose their interest in it and the IoCI might be discarded since it is no longer up-to-date. The value of T_L depends on the mobile application's specific requirements.

[6]This will be introduced in Section III-C.

C. MOBILITY-RELATED-FACTORS

Apart from the factors which are unrelated to the mobility of the MUs, the mobility-related factors also crucially affect the performance of the integrated networks.

1) INTER-CONTACT DURATION

Let MU_i and MU_j move according to a specific mobility model. These two MUs are within each other's transmission range at time 0, and then they move out of range at time instant t_1. If these two MUs next come within the transmission range of each other again at time t_2, then the time duration $T_{IC} = (t_2 - t_1)$ is defined as the inter-contact duration of MU_i and MU_j.

Let us consider the following random direction mobility model [68] as an example.

Definition 1 [Random Direction (RD) Mobility Model]: In this model, a MU uniformly assumes a specific speed from the region $[V_{\min}, V_{\max}]$ and uniformly chooses a particular direction from the region $[0, 2\pi)$. Then this MU moves along the chosen direction with the chosen speed for an exponentially distributed travelling time. After this movement, the MU again randomly chooses a speed, a direction and a travelling time for its next movement.

According to [69], the expected inter-contact duration between two MUs obeying the RD mobility model is given by

$$\overline{T}_{IC} = \frac{S}{2rV^*}, \tag{2}$$

where S is the area of the square-shaped mobility region, r is the transmission range and V^* is the average relative speed[7] between a pair of MUs, whose value is given by [70]

$$V^* = 1.27\overline{V} = \frac{1.27(V_{\min} + V_{\max})}{2}. \tag{3}$$

Furthermore, the *contact rate* is defined as $\lambda_s = 1/\overline{T}_{IC}$, and the number of contacts can be modelled as a Poisson process with an arrival rate of λ_s [69]. In our following discourse, we denote the rate of contact occurrences between the BS and a MU as λ_b.

As demonstrated in [69], the inter-contact duration of the RD model and that of the Random Way-Point (RWP) model [68] strictly obey the exponential distribution, while the inter-contact duration of the Random Walk (RW) model [68] also has an exponentially distributed tail. The inter-contact duration may be approximated by a certain inverse power-law [71], but this approximation is believed to be over-pessimistic. Furthermore, the authors of [72] found that most of the realistic mobility traces, such as those of the InfoCom [71] and UCSD [73] datasets, can be well approximated by a mixed power-law and exponential distribution. After a characteristic time, which may be on the order of half a day, the complementary cumulative distribution function (CCDF) of the inter-contact duration

[7]The average relative speed between a moving node and a static node is $V^* = \overline{V}$, which can be substituted in (2) for the sake of calculating the average inter-contact duration between the BS and a MU.

decays exponentially. Since the delay metrics of the information dissemination are usually on the same order, it is reasonable for researchers to assume the exponentially distributed inter-contact duration in the delay analysis of large-scale opportunistic networks [74], [75].

2) CONTACT DURATION

Let MU_i and MU_j move according to a specific mobility model. We assume that these two MUs come within the transmission range of each other at time instant 0. The contact duration T_C is defined as the time duration during which they initially remain in contact with each other before they move out of each other's transmission range.

Let us again consider the RD mobility model as an example. According to [76], the average contact duration between a pair of MUs is given by

$$\overline{T}_C = \frac{\pi r}{2V^*}, \tag{4}$$

where r is the transmission range and V^* is the average relative speed given by (3).

However, the CCDF of the contact duration has not been characterised in the open literature for the popular synthetic mobility models, such as the RD, RWP and RW mobility models. The authors of [77] found that the contact duration obeys the Pareto distribution for the encounter trace based on Bluetooth devices. By contrast, the authors of [78] found that for vehicular mobility traces, the contact duration is well approximated by a mixed power-law and exponential distribution. In contrast to the inter-contact duration reported in [72], the CCDF of the contact duration exponentially decays before reaching a specific characteristic time, which is on the order of 100 seconds.

The authors of [79] proposed a contact-duration-aware data replication scheme by assuming Pareto-distributed contact duration. However, the impact of contact duration on the information dissemination of large-scale opportunistic networks has been to a degree neglected in the existing literature. Researchers often assume that the bandwidth provided for the transmission between a pair of MUs is extremely high and the file size is relatively small [40]–[42]. Even if the file size is large, the file is assumed to be divided into small data chunks. Consequently, the existing studies do not focus on transmitting the entire file but on transmitting a single data chunk [80], [81]. According to these assumptions, if a pair of MUs is in contact, the file (or the data chunk) may be delivered promptly. Hence, it has been deemed unnecessary to account for the contact duration when characterising the information dissemination performance. However, these assumptions are somewhat impractical.

In this treatise, we assume that the success of file delivery depends on the following two events:

- The target MU enters the transmission range of the source MU with a rate of λ_s;
- The contact duration between the source and the target MUs must be longer than the required transmission time that is defined as L/B, where L is the file size and B is the transmission rate.

As a result, the probability of successfully delivering a file during a single contact is given by $F_{T_C}(L/B) = P(T_C > L/B)$, which is the CCDF of the contact duration T_C. For this reason, we propose a thinned Poisson process for the *effective contact* model between a pair of MUs with a rate of $\widetilde{\lambda}_s = F_{T_C}(L/B)\lambda_s$. Since both the original contact processes and the contact durations between any pairs of MUs are independent of each other [69], the *effective contact* processes are independent as well.

3) SOME RESULTS

Let us now consider some simulation results obtained from the following RD mobility model:

- The simulation area is a 2000×2000 (m^2) square area;
- The BS is located at the centre of the square area.
- The duration of a single movement obeys an exponential distribution with a mean of 10 minutes;
- The speed of a single movement is uniformly chosen from the region of $[2, 4]$ (m/s);
- The direction of a single movement is also uniformly chosen from the region of $[0, 2\pi)$;
- A MU would bounce back if he/she hits the boundary of the square area during a single movement.

The most important parameters of the RD mobility model are also summarised in TABLE 4 for the readers' convenience.

TABLE 4. Simulation parameters for the RD mobility model.

Description	Simulation Parameters
Simulation Area	A 2000×2000 m^2 square area
BS Location	The centre of the square area
Average Duration	10 minutes
Speed region	2 m/s ~ 4 m/s
Direction region	0 radian ~ 2π radian

The CCDFs of both the inter-contact duration and the contact duration are plotted in Fig.7, where r denotes the transmission range of MUs, and R denotes the transmission range of the BS. As shown in Fig.7(a)(b), the CCDFs of the inter-contact duration between a pair of MUs and that between the BS and a MU are both closely approximated by the exponential distributions, while the contact rates are calculated as the reciprocal of (2).

As shown in Fig.7(c), the CCDFs of the contact duration between a pair of MUs are closely approximated by the exponential distributions, which have means calculated by (4). In Fig.7(d), we observe that the CCDFs of the contact duration between the BS and a MU are accurately approximated by the *Gamma distribution* [82]. In order to obtain the accurate value of the shape parameter m and that of the scale parameter θ, we have to derive the closed-form results for the mean and the variance of the contact duration. Although the mean is given by (4), we have not derived the

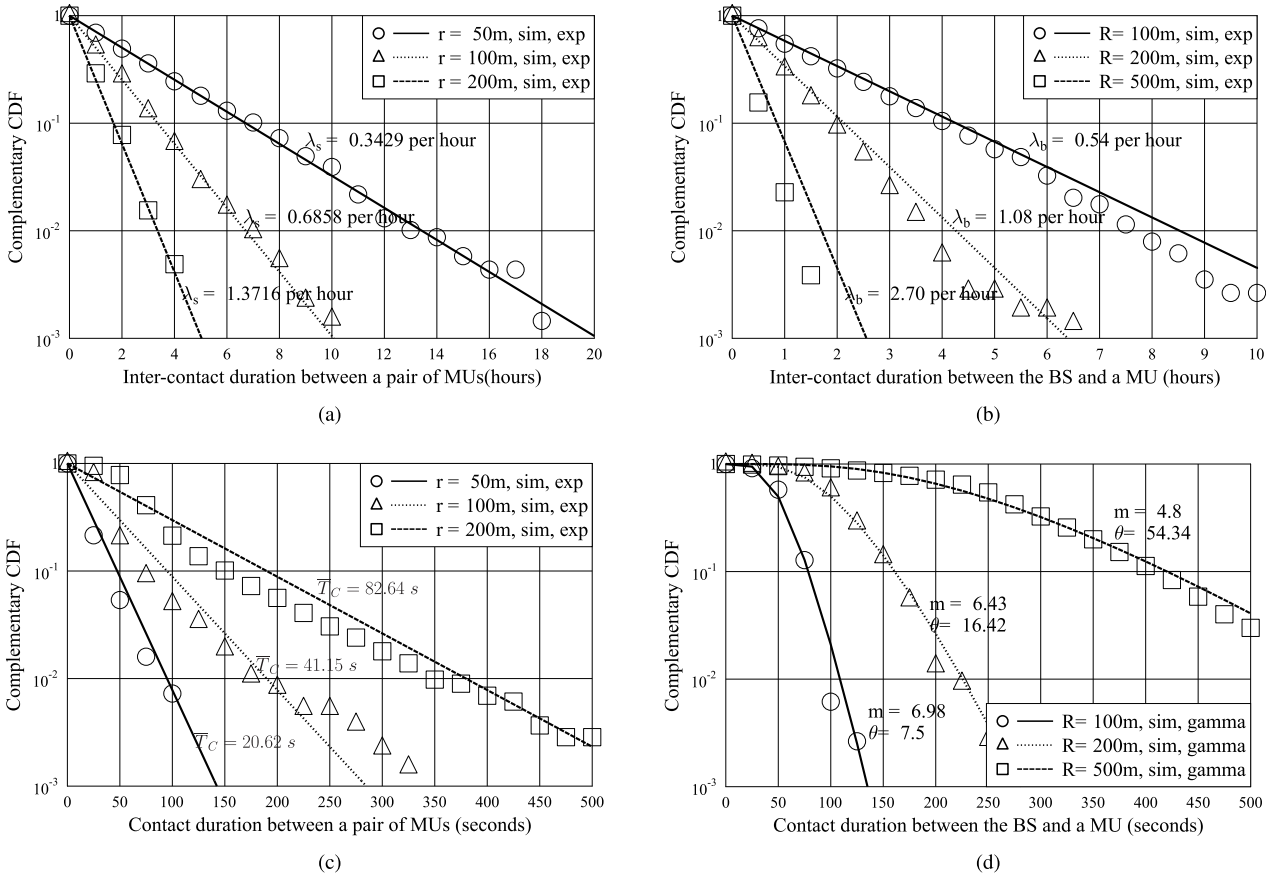

FIGURE 7. Opportunistic contact properties of the RD mobility model. (a) CCDF inter-contact duration between a pair of MUs. (b) CCDF inter-contact duration between the BS and a MU. (c) CCDF contact duration between a pair of MUs. (d) CCDF contact duration between the BS and a MU.

accurate variance, which we expect to derive in our future work. At this stage, we embark on numerically deriving the variance of the contact duration.

D. PROTOCOLS FOR INFORMATION DISSEMINATION

In the open literature, there are three commonly-adopted protocols for information dissemination.

1) DIRECT TRANSMISSION

In this protocol, information is disseminated only by the BSs without any assistance from the opportunistic communication between the MUs [83]. All the MUs receive the IoCI only when they move into the transmission range of the BSs.

2) TWO-HOP RELAYING

In this protocol, only the specific MUs that receive the IoCI from the BSs are relied upon for disseminating the IoCI to the other hitherto uMUs [80].

3) EPIDEMIC RELAYING

In this protocol, the MUs carrying the IoCI may deliver it to any hitherto uMUs that are within their transmission range [84]. The epidemic relaying protocol is often criticised for its low efficiency in supporting end-to-end communication because multiple copies of information are generated, which consumes a large fraction of the resources. However, this low-efficiency problem does not exist in the scenario of information dissemination, because all the MUs in the community are innately interested in the information distributed.

E. CONTINUOUS-TIME-PURE-BIRTH MARKOV CHAIN AIDED DELAY ANALYSIS

Let us now introduce the mathematical tool of analysing the delay metrics of integrated cellular and large-scale opportunistic networks. We first consider its application in the scenario of improving connectivity of cellular networks, as shown in Fig.6(a). A slight adjustment of this methodology makes it fit also for the scenario of off-loading tele-traffic from the cellular networks, as shown in Fig.6(b).

We assume that all the N MUs roam in a bounded area, and the IoCI is disseminated according to the *epidemic relaying* protocol. The number of contacts between any pair of MUs obeys an independent homogeneous Poisson process with a rate of λ_s. Correspondingly, the contact duration between any pair of MUs also obeys an independent homogeneous distribution, whose CCDF is $F_{T_C,s}(t_C)$. If the size of the IoCI is L, and the transmission rate provided for opportunistic

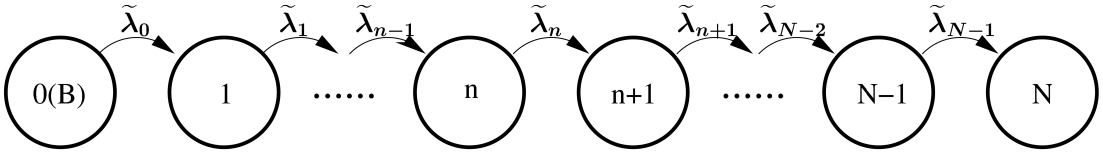

FIGURE 8. Continuous-Time-Pure-Birth Markov Chain.

links is B_s, the successful IoCI delivery during a single contact is achieved with a probability of $F_{T_C,s}(L/B_s)$. As a result, the number of *effective contacts* between any pair of MUs can be modelled by a thinned Poisson process [82] with a rate of $\widetilde{\lambda}_s = \lambda_s F_{T_C,s}(L/B_s)$.

We assume having only a single BS in the area studied, as shown in Fig.6(a), and the number of contacts between any MU and the BS also obeys an independent homogeneous Poisson process with a rate of λ_b. Correspondingly, the contact duration between any MU and the BS also obeys an independent homogeneous distribution, whose CCDF is $F_{T_C,b}(t_C)$. Similarly, the number of *effective contacts* between any MU and the BS can be modelled by another homogeneous thinned Poisson process having a rate of $\widetilde{\lambda}_b = \lambda_b F_{T_C,b}(L/B_b)$.

As a result, we may model the information dissemination process by a CT-PBMC, as shown in Fig.8. State n of the CT-PBMC represents that currently there are n MUs having the information, which are referred to as IOs. Observe from Fig.8 that there are two special states. The first one is the *initial state* 0, which represents that only the BS owns the IoCI at the beginning of the information dissemination process. The other one is the final state N, namely the *absorbing state*, which represents that all the MUs successfully receive the IoCI. The rest of the states are defined as the *transient states*.

Furthermore, $\{\widetilde{\lambda}_n, n = 0, 1, \cdots, (N-1)\}$ represent the rates of the state transitions from state n to state $(n+1)$. Specifically, for state n, we have n IOs and $(N-n)$ uMUs. Consequently, the transition rate is given by

$$\widetilde{\lambda}_n = (N-n)\widetilde{\lambda}_b + n(N-n)\widetilde{\lambda}_s, \tag{5}$$

where $\widetilde{\lambda}_s$ and $\widetilde{\lambda}_b$ have already been defined in the second and third paragraphs of Section II-E, respectively. The $(N \times N)$-element transition rate matrix [85] is given by

$$\Theta = \begin{pmatrix} -\widetilde{\lambda}_0 & \widetilde{\lambda}_0 & 0 & \cdots & 0 \\ 0 & -\widetilde{\lambda}_1 & \widetilde{\lambda}_1 & \cdots & 0 \\ \vdots & \ddots & \ddots & \ddots & \vdots \\ 0 & 0 & \ddots & -\widetilde{\lambda}_{N-2} & \widetilde{\lambda}_{N-2} \\ 0 & 0 & 0 & \cdots & -\widetilde{\lambda}_{N-1} \end{pmatrix}. \tag{6}$$

Given this transition rate matrix, we are able to derive some delay metrics with the aid of the CT-PBMC.

1) THE DISSEMINATION DELAY

The dissemination delay T_D is defined as the time that is spent for disseminating the IoCI to all the N MUs in the area studied. According to the properties of the CT-PBMC, a specific transition delay T_n from state n to state $(n+1)$ obeys an exponential distribution with a rate of $\widetilde{\lambda}_n$. Therefore, the dissemination delay is obtained as $T_D = \sum_{n=0}^{N-1} T_n$, which obeys a hypo-exponential distribution [82]. Since the state transition delays $\{T_n, n = 0, 1, \cdots, (N-1)\}$ are independent of each other, the expectation of the dissemination delay is derived as

$$\mathcal{E}[T_D] = \sum_{n=0}^{N-1} \frac{1}{\widetilde{\lambda}_n} = \sum_{n=0}^{N-1} \frac{1}{(N-n)\widetilde{\lambda}_b + n(N-n)\widetilde{\lambda}_s}. \tag{7}$$

The dissemination delay T_D may be expressed as a phase-type distribution [85], whose CCDF is give by

$$P(T_D > t_D) = \boldsymbol{\alpha}^T \times \exp(t_D\Theta) \times \mathbf{1}, \tag{8}$$

where $\boldsymbol{\alpha}$ is a $(N \times 1)$-elements column vector, whose first element is one and all the other elements are zero, $\mathbf{1}$ is a $(N \times 1)$-elements column vector, whose elements are all ones. Thanks to the existence of the term $(N-n)\widetilde{\lambda}_b$ in (5), the transition rate obeys $\widetilde{\lambda}_n \neq \widetilde{\lambda}_m$ for all $n \neq m$. Hence, we may directly formulate the CCDF of the hypo-exponential distributed dissemination delay T_D [82] as

$$P(T_D > t_D) = \sum_{n=0}^{N-1} \left(\prod_{m=0, m\neq n}^{N-1} \frac{\widetilde{\lambda}_m}{\widetilde{\lambda}_m - \widetilde{\lambda}_n} \right) \exp(-\widetilde{\lambda}_n t_D), \tag{9}$$

which is based on an equivalent transformation of (8).

2) THE INDIVIDUAL DELAY

The individual delay T_I of a specific MU is defined as the time of this MU successfully receiving the IoCI. This is also the end-to-end delay between the BS and a specific MU when the epidemic relaying protocol is invoked for the information dissemination. The target MU may receive the IoCI during any of the states spanning from 1 to N in the sequence of the state transitions of the CT-PBMC. When considering the transition from state n to $(n+1)$ $(0 \le n \le N-1)$, the target MU may successfully receive the IoCI with a probability of $1/(N-n)$, and it may fail to receive it with a probability of $(N-n-1)/(N-n)$. Specifically, the probability $P_{n+1}^{(I)}$ of the target MU receiving the IoCI at state $(n+1)$, which naturally implies that it has not received the IoCI at any of the previous states, may be expressed as

$$P_{n+1}^{(I)} = \frac{1}{N-n} \prod_{m=0}^{n-1} \frac{N-m-1}{N-m} = \frac{1}{N}, \quad 0 \le n \le (N-1). \tag{10}$$

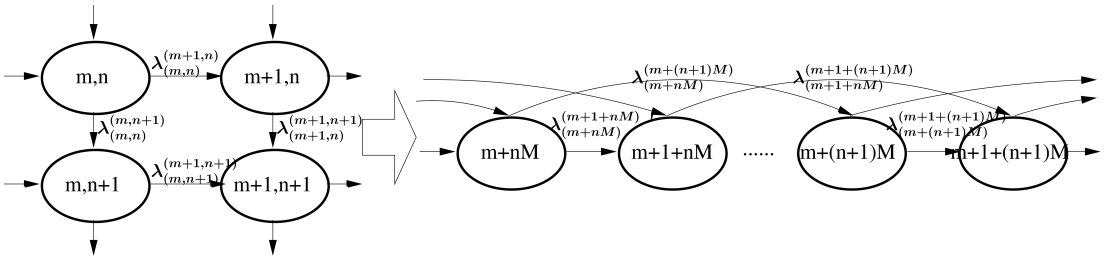

FIGURE 9. Two-dimensional CT-PBMC for capturing the heterogeneous MUs' mobility.

Given that the target MU receives the IoCI at state $(n+1)$, the CT-PBMC can be considered as being absorbed at this state. Similarly to (8), the conditional expectation and the CCDF of T_I is expressed as

$$\mathcal{E}[T_I|n+1] = \sum_{m=0}^{n} \frac{1}{\widetilde{\lambda}_m}, \quad 0 \le n \le (N-1), \tag{11}$$

$$P(T_I > t_I|n+1) = \boldsymbol{\alpha}^T \times \exp(t_I\Theta) \times \mathbf{1}_{n+1}, \tag{12}$$

where $\mathbf{1}_{n+1}$ is a $(N \times 1)$-element column vector, whose first $(n+1)$ elements are one and all the other elements are zero. After further manipulations relying on the Bayesian principle [82], the CCDF of T_I may be expressed as

$$\begin{aligned} P(T_I > t_I) &= \sum_{n=0}^{N-1} P(T_I > t_I|n+1)P_{n+1}^{(I)} \\ &= \sum_{n=0}^{N-1} \frac{\boldsymbol{\alpha}^T \times \exp(t_I\Theta) \times \mathbf{1}_{n+1}}{N} \\ &= \frac{\boldsymbol{\alpha}^T \times \exp(t_I\Theta)}{N} \times \sum_{n=0}^{N-1} \mathbf{1}_{n+1} \\ &= \frac{\boldsymbol{\alpha}^T \times \exp(t_I\Theta) \times \boldsymbol{\eta}}{N}, \end{aligned} \tag{13}$$

where $\boldsymbol{\eta} = (N, N-1, \cdots, 1)^T$. Similarly, the expectation of T_I may be expressed as

$$\begin{aligned} \mathcal{E}[T_I] &= \sum_{n=0}^{N-1} \mathcal{E}[T_I|n+1]P_{n+1}^{(I)} \\ &= \sum_{n=0}^{N-1} \frac{1}{N} \sum_{m=0}^{n} \frac{1}{\widetilde{\lambda}_m} = \sum_{n=0}^{N-1} \frac{N-n}{N} \frac{1}{\widetilde{\lambda}_n}, \end{aligned} \tag{14}$$

where $\widetilde{\lambda}_n$ in (14) is given by (5).

3) THE NUMBER OF THE IOs AT AN ARBITRARY TIME INSTANT

As introduced in Section II-B, if the IoCI has a useful life time T_L, it is important for us to determine how many MUs can successfully receive the IoCI before it expires. The following theorem provides the closed-form expression for calculating the probability of the CT-PBMC remaining in an arbitrary state at an arbitrary time instant.

Theorem 1: Let us denote the probability of the CT-PBMC remaining in state n at time instant t as $p_n(t)$ for $0 \le n \le N$. The closed-form expression of $p_n(t)$ is formulated as:

$$p_n(t) = \begin{cases} \exp(-\widetilde{\lambda}_0 t), & n = 0, \\ \left(\prod_{m=0}^{n-1} \widetilde{\lambda}_m\right) \sum_{i=0}^{n} \frac{\exp(-\widetilde{\lambda}_i t)}{\prod_{j=0, j\neq i}^{n} (\widetilde{\lambda}_j - \widetilde{\lambda}_i)}, & 0 < n < N, \\ 1 - \sum_{n=0}^{N-1} p_n(t), & n = N. \end{cases} \tag{15}$$

Proof: Please refer to Appendix A for the proof. ■

Let $t = T_L$ in Theorem 1, we may derive the average number of MUs successfully receiving the IoCI before the IoCI expires, which is expressed as $\overline{n} = \sum_{n=0}^{N} n p_n(T_L)$.

F. HETEROGENEOUS MOBILE USERS

Assuming a homogeneous mobility pattern in the above analysis is somewhat idealised for adequately reflecting the real characteristics of the MUs. In the existing literature [86], [87], often the multi-dimensional Markov chain is invoked for capturing the heterogeneous MU's mobility pattern. In this section, we will show that after some equivalent mathematical transformations, the analytical framework introduced in Section III-E can be further exploited for deriving various performance metrics, when the MUs' heterogeneous mobility patterns are taken into account.

The authors of [86] modelled the epidemic relaying protocol based end-to-end communication by a two-dimensional CT-PBMC, as shown in Fig.9. Let us first consider how to map their model onto the analytical framework of Section II-E. In their model, two types of MUs are assumed, namely M number of super MUs and N number of ordinary MUs. Jointly considering the impact of both the inter-contact duration and contact duration, the *effective contact* rate between a pair of super MUs is $\widetilde{\lambda}_{\mathcal{SS}}$, and that between a pair of ordinary MUs is $\widetilde{\lambda}_{\mathcal{NN}}$, while that between a super MU and a ordinary one is $\widetilde{\lambda}_{\mathcal{SN}}$. Additionally, the *effective contact* rate between a super MU and the BS is $\widetilde{\lambda}_{\mathcal{BS}}$, while that between an ordinary MU and the BS is $\widetilde{\lambda}_{\mathcal{BN}}$.

As portrayed in Fig.9, state (m, n) represents that we currently have m super MUs and n ordinary MUs that have successfully received the IoCI. When the epidemic relaying protocol is implemented, the transition rates from this state to

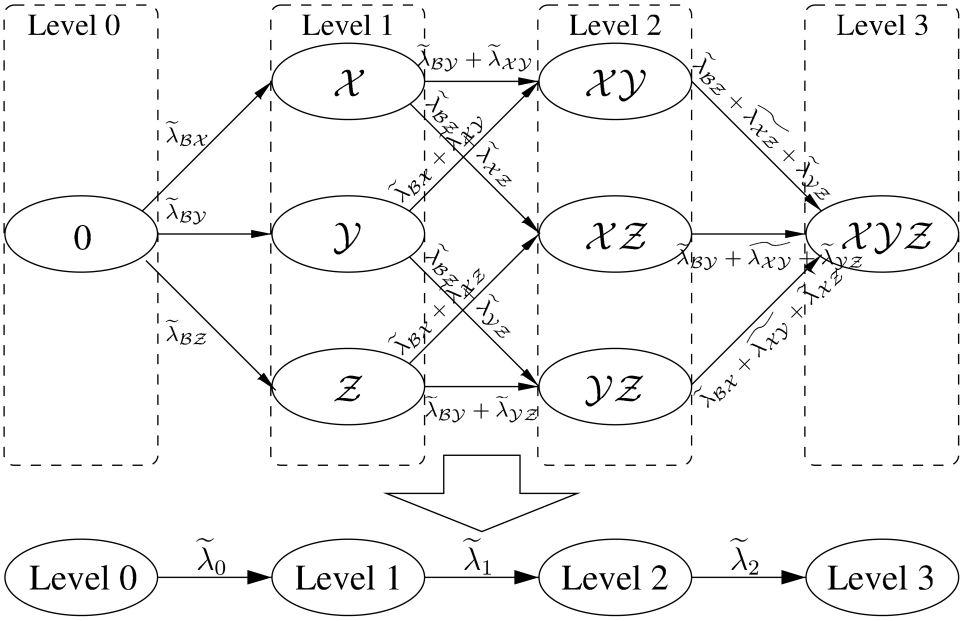

FIGURE 10. The CT-PBMC for completely heterogeneous mobility of MUs.

its neighbouring states may be expressed as

$$\begin{cases} \lambda_{(m,n)}^{(m+1,n)} = (M-m)(\widetilde{\lambda}_{\mathcal{BS}} + m\widetilde{\lambda}_{\mathcal{SS}} + n\widetilde{\lambda}_{\mathcal{NS}}), \\ \lambda_{(m,n)}^{(m,n+1)} = (N-n)(\widetilde{\lambda}_{\mathcal{BN}} + m\widetilde{\lambda}_{\mathcal{NS}} + n\widetilde{\lambda}_{\mathcal{NN}}). \end{cases} \tag{16}$$

However, before analysing any of the performance metrics of this two-dimensional CT-PBMC, we have to equivalently transform it into a one-dimensional CT-PBMC, as shown in Fig.9. State (m, n) for $0 \leq m \leq M$ and $0 \leq n \leq N$ in the two-dimensional CT-PBMC can be transformed into state $(m + nM)$ in its transformed one-dimensional version. Furthermore, the corresponding transition rates $\lambda_{(m,n)}^{(m+1,n)}$ and $\lambda_{(m,n)}^{(m,n+1)}$ are also equivalently transformed into $\lambda_{(m+nM)}^{(m+1+nM)}$ and $\lambda_{(m+nM)}^{(m+(n+1)M)}$, respectively. After this transformation, our analytical framework introduced in Section II-E can be invoked for analysing the various performance metrics. However, we have to employ a phase-type-distribution similar to that of (8), for the sake of characterising the performance of this two-dimensional CT-PBMC. This methodology can then be naturally extended to the multi-dimensional CT-PBMC.

Similarly, the authors of [87] relied on a pair of communities for their model. The MUs in the same community share the same mobility pattern, while the MUs belonging to the different communities have different mobility patterns. Hence, we classify the solutions provided in both [86] and [87] into the same category.

The authors of [81] assumed a completely heterogeneous mobility model for the MUs. We extend this model to our integrated cellular and large-scale opportunistic network. We denote the set of the MUs in the networks as $\boldsymbol{\mathcal{N}}$. When jointly considering the impact of both the inter-contact duration and the contact duration, any pairs of MUs have different *effective contact* rates, which are denoted as $\{\widetilde{\lambda}_{\mathcal{XY}} | \mathcal{X}, \mathcal{Y} \in \boldsymbol{\mathcal{N}}\}$. Furthermore, the *effective contact* rates between the BS and any MUs are different as well, which are denoted as $\{\widetilde{\lambda}_{\mathcal{BX}} | \mathcal{X} \in \boldsymbol{\mathcal{N}}\}$.

Fig.10 portrays an example of CT-PBMC for the completely heterogeneous mobility pattern of MUs in an integrated network, which consists of three MUs, say $\boldsymbol{\mathcal{N}} = \{\mathcal{X}, \mathcal{Y}, \mathcal{Z}\}$. According to the number of MUs successfully receiving the IoCI, the CT-PBMC is divided into three levels. In Level 0, only the BS owns the IoCI. Level 1 is comprised of three states, say states $\mathcal{X}$, $\mathcal{Y}$ and $\mathcal{Z}$, representing the corresponding MUs that own the IoCI. Level 2 is comprised of three states as well, say states $\mathcal{XY}$, $\mathcal{XZ}$ and $\mathcal{YZ}$. Finally, level 3 only has a single state, which is state $\mathcal{XYZ}$, representing that all the MUs have received the IoCI. Let us consider a single state transition example, say from state $\mathcal{X}$ to state $\mathcal{XY}$, in order to explain how to derive the corresponding transition rate. MU $\mathcal{Y}$ can only successfully receive the IoCI if $\mathcal{Y}$ 'meets' either $\mathcal{X}$ or the BS. Hence, the corresponding state transition delay is equal to the minimum of two exponential variables associated with the rates of $\widetilde{\lambda}_{\mathcal{XY}}$ and $\widetilde{\lambda}_{\mathcal{BY}}$. Therefore, this minimum is also an exponential random variable with a rate of $\widetilde{\lambda}_{\mathcal{BY}} + \widetilde{\lambda}_{\mathcal{XY}}$.

If we extend the CT-PBMC of Fig.10 to a more generic model having $|\boldsymbol{\mathcal{N}}| = N$ MUs, level n, which represents that n MUs have successfully received the IoCI, consists of $\binom{N}{n}$ different states. We further establish a simplified one-dimensional CT-PBMC, whose states represent the different levels of the original CT-PBMC, as shown at the bottom of Fig.10. As demonstrated in [81], if the specific values of the transition rates $\{\widetilde{\lambda}_{\mathcal{XY}} | \mathcal{X}, \mathcal{Y} \in \boldsymbol{\mathcal{N}}\}$ obey a distribution with a mean of $\widehat{\lambda}_s$ and those of the transition rates $\{\widetilde{\lambda}_{\mathcal{BX}} | \mathcal{X} \in \boldsymbol{\mathcal{N}}\}$ obey another distribution with a mean of $\widehat{\lambda}_b$, then the transition rate between state n and state $(n + 1)$ in the

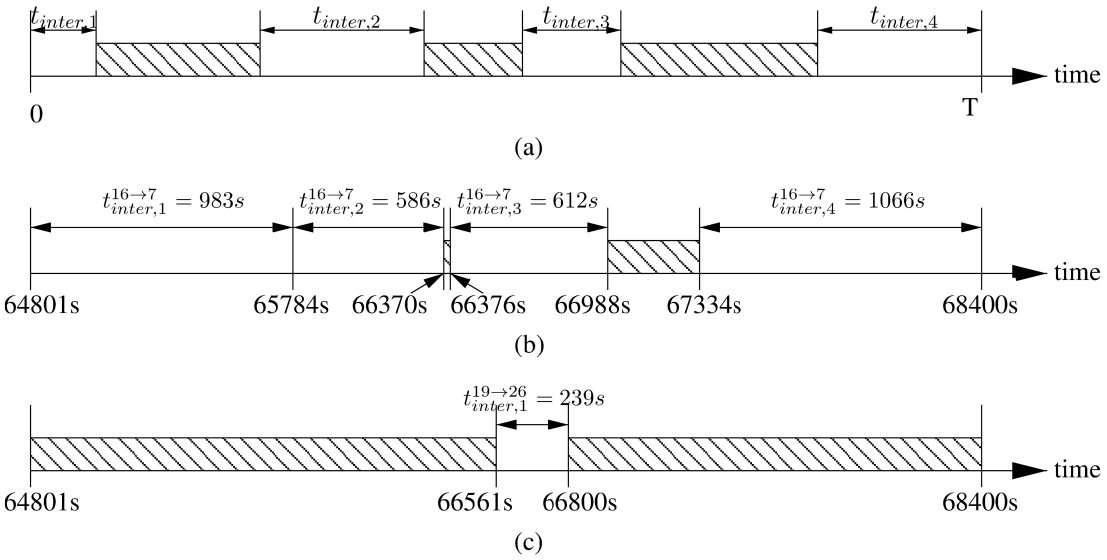

FIGURE 11. Examples of the contact trace between a pair of MUs in the time interval [0, *T*]. For the Infocom2006 contact trace, the observation period is $T = 3600$ second(s). Shaded boxes represent the contact duration between MUs. Both the SPMs and the 'friendship' weights of the contact traces as presented in (b) and (c) are provided in TABLE 5. (a) A generic form of the contact trace between a pair of MUs in the time interval [0, *T*]. (b) Contact trace between MU16 and MU07 in Infocom2006 from 8:01am to 9:00am. (c) Contact trace between MU19 and MU26 in Infocom2006 from 8:01am to 9:00am.

simplified one-dimensional CT-PBMC should be $\widetilde{\lambda}_n = (N-n)(\widehat{\lambda}_b + n\widehat{\lambda}_s)$. As a result, the model characterising completely heterogeneous mobility patterns of the MUs can also be found using the analytical framework of Section III-E.

G. TELE-TRAFFIC OFF-LOADING

As shown in Fig.6(b), in the application of off-loading tele-traffic from the cellular system, all the MUs roam within the coverage of a cellular network. As a result, the contact rates between the BSs and the MUs are infinite, which indicates that the inter-contact duration is zero and that the MUs are always capable of connecting to the BSs. Moreover, the transmission delay from the BSs to the MUs only depends on the transmission rate of the wireless channels connecting them, which is far shorter than the inter-contact duration between the MUs. Hence, it is reasonable to assume that the information transmission between the BSs and the MUs can be promptly completed [81].

However, transmitting the IoCI to multiple requesters via multiple dedicated cellular links imposes a heavy traffic load on the BSs. Consequently, opportunistic communication amongst MUs is adopted for off-loading tele-traffic from the overloaded BSs. To this end, the BSs initially disseminate some copies of the IoCI to a group $\mathcal{D}$ of MUs via dedicated cellular links, whose size is $|\mathcal{D}| = D$. Then, the IoCI is disseminated to the rest of the MUs by their peers via opportunistic communication. During this information dissemination process, the BSs might further inject the IoCI into the large-scale opportunistic network at any time instant. However, in order to reduce the IoCI copies to be injected by the BS, the optimal strategy to be adopted by the BSs is demonstrated in [81] to be that of initially sending the IoCI to some MUs before embarking on information dissemination across the opportunistic network and finally transmitting the IoCI to the uMUs, when the IoCI expires.

According to aforementioned optimal strategy in [81], after the initial IoCI injection, we have $|\mathcal{D}| = D$ MUs that have successfully received the IoCI and the BSs are no longer invoked for disseminating the IoCI before it expires. Hence, the initial state of the CT-PBMC as shown in Fig.8 is state D, rather than state 0. Furthermore, the state transition rate is re-derived after deleting all the BS-related terms. After this slight adjustment, our analytical framework of Section III-E can also be exploited for analysing the performance metrics in the specific application of off-loading tele-traffic from cellular networks.

Another issue in this application scenario is how to select the initial receiver set $\mathcal{D}$ for receiving the IoCI from the BSs before information dissemination via the opportunistic network so that more MUs can receive the IoCI before it expires. In order to achieve this goal, the concept of 'centrality' borrowed from the tools of SNA [88] is exploited for evaluating the specific significance of an individual MU on the opportunistic network.

Before evaluating the centrality[8] of an individual MU, we have to extract a social contact graph from the contact traces and quantify the grade of 'friendship' between a pair of MUs according to their contact-history, as shown in Fig.11. We account for the encounter-related properties with the aid of the so-called *social pressure metric* (SPM) [39]. Explicitly, the SPM between MU_i and MU_j is defined

[8]Centrality describes how 'central' a node is in a network [88]. There are various types of centrality, such as degree, betweenness, closeness, as introduced in Section I-A.

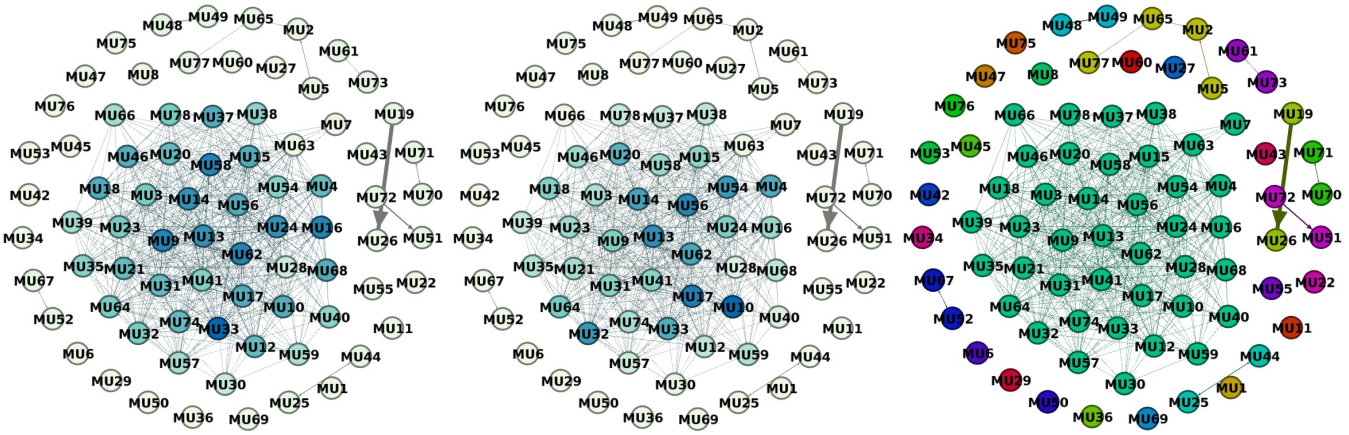

FIGURE 12. The social contact graph extracted from the InfoCom 2006 mobility trace [71]. (a) Out-degree. (b) Betweenness. (c) Component.

TABLE 5. Calculating the SPMs and the 'friendship' weights between two pairs of MUs in Infocom2006 from 8:01am to 9:00am. The contact traces in this observation period are provided in Fig.11.

Pair	Calculation	SPM	Weight	Verdict
MU16→MU07	Observe from Fig.11(b) that for this pair, there are 3 contact events in the observing period. Hence, we have 4 inter-contact durations, namely $t_{inter,1}^{16\to7}$ = 983s, $t_{inter,2}^{16\to7}$ = 586s, $t_{inter,3}^{16\to7}$ = 612s and $t_{inter,4}^{16\to7}$ = 1066s. Then the SPM is derived as $SPM = \left((t_{inter,1}^{16\to7})^2 + (t_{inter,2}^{16\to7})^2 + (t_{inter,3}^{16\to7})^2 + (t_{inter,4}^{16\to7})^2\right)/2/3600$. The weight is the reciprocal of this SPM.	391.7	0.0026	< 0.0033 Discard
MU19→MU26	Observe from Fig.11(c) that for this pair, there are 2 contact events in the observing period. Hence, we have 1 inter-contact duration, namely $t_{inter,1}^{19\to26}$ = 239s. Then the SPM is derived as $SPM = (t_{inter,1}^{19\to26})^2/2/3600$. The weight is the reciprocal of this SPM.	7.934	0.1260	>0.0033 Retain

as $SPM_{i,j} = (\sum_{x=1}^{n} t_{inter,x}^2)/(2T)$, whose reciprocal $\omega_{i,j} = (2T)/(\sum_{x=1}^{n} t_{inter,x}^2)$ represents the weight of the 'friendship' between MUs. The larger the value of $\omega_{i,j}$, the closer the friendship and hence the higher the forwarding probability between MU_i and MU_j.

Let us consider the realistic mobility trace of Infocom 2006 [71] as an example. We study the contact traces of the $N = 78$ MUs (exclude all the static nodes and external nodes) for 1 hours, between 8:01am and 9:00am on April 24th, 2006, namely on the opening day of the conference. The SPMs between any pair of MUs are calculated for this time period, whose reciprocals are invoked for defining the weight of their friendships. The length of the observing period is $T = 3600$ s. The weight threshold is set to be 1/5 min^{-1} (0.0033 s^{-1}). All the friendships, whose weights are lower than this threshold, are discarded. In TABLE 5, we exemplify the calculation of the SPMs and the 'friendship' weights for the pair of MU16 and MU07 as well as for the pair of MU19 and MU26. As a result, we obtain a directed social contact graph for the 78 MUs, as shown in Fig.12. With the aid of the tools of SNA, the following strategies may be designed for the selection of the initial receiver set.

- *Random Selection:* Without considering any social network features, the initial receiver set $\mathcal{D}$ is randomly selected. Although we cannot guarantee a better delivery ratio before the IoCI expires, improved fairness amongst MUs can be achieved, as claimed in [81].
- *Out-Degree-Based Selection: Out-degree* of a MU is defined as the number of the social links that emerge from this MU and terminate at its neighbours in the directed social contact graph [88]. As shown in Fig.12(a), the nodes filled by darker colours exhibit higher out-degree values. Before the information dissemination commences, the MUs having the $|\mathcal{D}| = D$ highest out-degrees are selected as the initial receivers.
- *Betweenness-Based Selection:* The betweenness [88] for MU k is calculated as

$$C_B(k) = \sum_{j=1,\, j\neq k}^{N} \sum_{i=1, i\neq k}^{N} \frac{g_{i,j}(k)}{g_{i,j}},$$

where $g_{i,j}$ is the total number of shortest paths, in terms of the number of hops, linking MU i and MU j in the social contact graph, and $g_{i,j}(k)$ is the number of those shortest paths that include MU k. The betweenness

identifies 'bridge MUs' that act as links between different node clusters. As shown in Fig.12(b), the nodes filled by darker colours have higher values of betweenness. Before the information dissemination process, the MUs having the $|\mathcal{D}| = D$ highest betweenness values are selected as the initial receivers.

- *Component-Based Selection:* As shown in Fig.12(c), the social contact graph is naturally divided into different components. The MUs in the same component are connected to its peers via direct links or multi-hop links, while the MUs in different components are disconnected. In Fig.12(c), the nodes belonging to the same component are filled by the same colour. The social contact graph of Fig.12(c) is comprised of 28 components, amongst which the largest one has 40 MUs. In order to allow more MUs receive the IoCI via the opportunistic network, the initial receivers should cover as many different components as possible. We sort the components according to their sizes and select a MU belonging to a component having the highest betweenness as the component 'head'. All these component 'heads' have higher priorities to be included into the initial receiver set than other MUs, and by the same rationale, the 'head' of a larger component has a higher priority to be selected than the head of a smaller component. According to this principle, we may obtain the initial receiver set $\mathcal{D}$.

Apart from the aforementioned ones, there are other types of centralities conceived for different purposes. Google's well-known ranking algorithm, namely *page rank*, measures the likelihood of nodes having important friends in a social graph [89]. Ego-betweenness [6] is exploited for designing the opportunistic routing protocol in [42] without any global knowledge of the network. In contrast to traditional centralities that are based on unweighted networks, the *cumulative contact probability* concept of [90] is used for reflecting the properties of weighted networks. Interested readers may refer to the related references for further information.

H. NUMERICAL RESULTS

Let us now consider some performance results for the aforementioned two application scenarios.

1) IMPROVING CONNECTIVITY OF CELLULAR NETWORKS

In this scenario, we adopt a homogeneous RD mobility model for all the MUs. The parameters of this RD model are the same as those used for obtaining Fig.7 in Section III-C-3, which have been summarised in TABLE 4. Furthermore, as shown in TABLE 6, we assume that the transmission range of the BS is 100 m, while that of the MUs is 50 m. The transmission rate of the cellular link is $B_b = 1$ Mbps and that of the opportunistic link is $B_s = 2$ Mbps. The file size of the IoCI is set to 40 Mb (5 MB). Once the uMUs enter the transmission range of the IOs (including the BS and the served MUs), their cellular/opportunistic links are established for delivering the IoCI. However, if the IoCI cannot be perfectly delivered during this contact, the data received by the uMUs are discarded.

TABLE 6. Simulation parameters for improving the cellular networks' connectivity.

	BS to MUs	MUs to MUs
Tx Range	$R = 100$ m	$r = 50$ m
Tx Rate	$B_b = 1$ Mbps	$B_s = 2$ Mbps
File Size	$L = 40$ Mb (5 MB)	
File Life Time	From 1 hour to 2 hour	
Number of MUs	From 10 to 100	

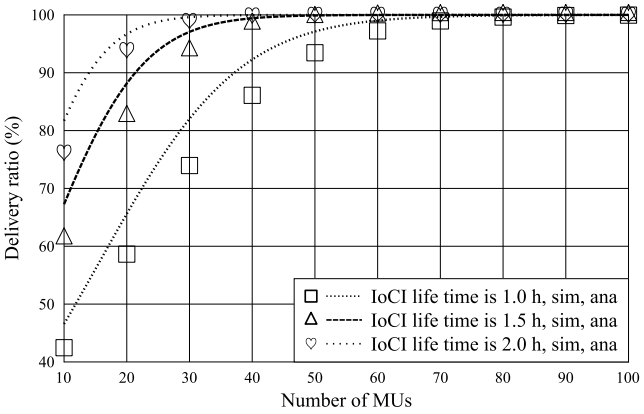

FIGURE 13. The average successful delivery ratio before the expiry of the IoCI. RD mobility model defined in Section III-C-3 is invoked for modelling the movement of the MUs. The mobility-related parameters are provided by TABLE 4, while the other parameters are given by TABLE 6.

The average successful delivery ratio before the IoCI expires is plotted in Fig.13. The analytical results (ana) in Fig.13 are obtained by the following steps:

- Both the contact process between the BS and the MUs and that between a pair of MUs are modelled by a Poisson process. The contact rate λ_b between the BS and the MUs is approximated to be $\lambda_b = 0.54$ per hour according to (2), while the contact rate λ_s between a pair of MUs is approximately $\lambda_s = 0.3429$ per hour according to (2).
- The contact duration between the BS and the MUs is modelled by a Gamma distribution having a shape parameter of $m = 6.98$ and a scale parameter of $\theta = 7.5$, as shown in Fig.7(d). The contact duration between a pair of MUs is modelled by an exponential distribution having a mean of $\overline{T}_C = 20.62$ seconds, which is derived from (4).
- With the aid of CT-PBMC, as introduced in Section II-E, the state probabilities $\{p_n(T_L)\}$ are calculated by (15) when the life time $T_L = \{1.0, 1.5, 2.0\}$ hours are achieved. Furthermore, the average successful delivery ratio is obtained as $\overline{n}/N = \sum_{n=0}^{N} np_n(T_L)/N$, where N is the total number of MUs in the area studied.

TABLE 7. Centralities of the initial receiver set according to different selection schemes. (a) Out-degree based selection. (b) Betweenness based selection. (c) Component based selection.

(a)

	MU33	MU09	MU16	MU58	MU62	MU13	MU14	MU24	MU10	MU15
Out-degree	**23**	**21**	**21**	**21**	**21**	**20**	**20**	**20**	**18**	**18**
Betweenness	33.6	20.0	21.9	21.2	34.6	37.6	35.1	28.1	42.9	24.6
Com.ID(size)	2(40)	2(40)	2(40)	2(40)	2(40)	2(40)	2(40)	2(40)	2(40)	2(40)

(b)

	MU10	MU17	MU56	MU13	MU32	MU54	MU14	MU62	MU04	MU33
Out-degree	18	18	18	20	16	14	20	21	17	23
Betweenness	**42.9**	**39.8**	**39.0**	**37.7**	**36.4**	**36.4**	**35.1**	**34.6**	**33.9**	**33.6**
Com.ID(size)	2(40)	2(40)	2(40)	2(40)	2(40)	2(40)	2(40)	2(40)	2(40)	2(40)

(c)

	MU10	MU65	MU19	MU25	MU48	MU51	MU52	MU61	MU70	MU76
Out-degree	18	1	1	1	1	1	1	1	1	0
Betweenness	42.9	1	0	0	0	0	0	0	0	0
Com.ID(size)	**2(40)**	**1(4)**	**6(2)**	**8(2)**	**17(2)**	**19(2)**	**20(2)**	**24(2)**	**26(2)**	**28(1)**

As shown in Fig.13, we observe that having more MUs may significantly increase the delivery ratio, since the probability of successfully delivering the IoCI is greatly enhanced, when more MUs participate in the information dissemination process. The delivery ratio increases from 45% to 100%, when the life time of the IoCI is one hour, as the number of MUs increases from 10 to 80. Naturally, if the MUs can tolerate a longer latency of receiving the IoCI, which indicates a longer life time, the delivery ratio is also improved.

2) TELE-TRAFFIC OFF-LOADING

On the opening day of an academic conference, the organisers are keen on finding an efficient way of disseminating the conference program to the attendees. Again, as an example, the contact traces of InfoCom 2006 [71] is employed. We study the period spanning from 8:00 am to 9:00 am on the opening day of the conference, April 24th, 2006, in order to study how much the opportunistic network would assist us in disseminating the IoCI. Since the traces were collected via Bluetooth devices, we assume that the opportunistic link between a pair of MUs is realised by Bluetooth and the transmission rate is 1 Mbps. Bluetooth is a half-duplex peer-to-peer communication technique. Hence, while a source is transmitting data to a target, extra links cannot be established even if another uMU enters the transmission range of the source. Furthermore, corresponding to [63], we assume that an uMU will acquire the IoCI from his/her geographic neighbours with a probability of $p_{pull} = 0.001$ during every contact. The file size of the IoCI is 40 Mb (5 MB).

Moreover, random selection, out-degree based selection and betweenness based selection as well as component based selection are invoked for appointing the initial receiver set directly acquiring the IoCI from the CI. Based on the social contact graph of the MUs, as shown in Fig.12, the initial receiver set is determined as follows, if the number of initial receivers is 10:

- For the random selection, by definition, the initial receiver set is randomly selected for every round of the simulation.
- For the out-degree based selection, the initial receiver set is determined from Fig.12(a) as {MU33, MU9, MU16, MU58, MU62, MU13, MU14, MU24, MU10, MU15}. The out-degrees and other centralities of this receiver set are listed in TABLE 7(a).
- For the betweenness based selection, the initial receiver set is determined from Fig.12(b) as {MU10, MU17, MU56, MU13, MU32, MU54, MU14, MU62, MU4, MU33}. The betweenness and other centralities of this receiver set are listed in TABLE 7(b).
- For the component based selection, the initial receiver set is determined from Fig.12(c) as {MU10, MU65, MU19, MU25, MU48, MU51, MU52, MU61, MU70, MU76}. The component IDs and the component sizes as well as other centralities of this receiver set are listed in TABLE 7(c).

The computation process of the above-mentioned metrics, including the out-degree, the betweenness and the component ID as well as the component size, is omitted for reasons of space-economy, since it obeys the same methodology as shown in TABLE 1.

As shown in Fig.14, we study the impact of the number of the initial receivers on the number of MUs served by the opportunistic network. The number of MUs served by the opportunistic network also indicates the amount of tele-traffic off-loaded from the CI. Observe from Fig.14 that the number of MUs served by the opportunistic network firstly increases as we increase the number of initial receivers. But after reaching the peak, it then slowly reduces as we further increase the

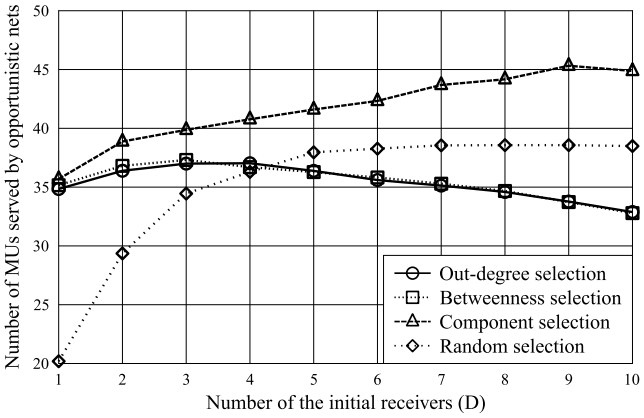

FIGURE 14. The average number of MUs receiving the IoCI via the opportunistic network. The period spanning from 8:01am to 9:00am on April 24th during InfoCom 2006 is studied.

number of the initial receivers. For different initial receiver selection approaches, the peaks appear at different positions. Specifically, for both the out-degree and betweenness based selection approaches, the peaks appear when the number of the initial receivers is 3; for component-based selection, the peak appears when the number of the initial receivers is 9; for random selection, the peak appears when the number of the initial receivers is 8.

Furthermore, as shown in Fig.14, the pair of centrality based selection methods have nearly the same performance because all the initial receivers selected by these two methods belong to the largest component, as shown in Fig.12(c). Therefore, the MUs belonging to the other 27 components cannot receive the IoCI via the opportunistic network. Observe from Fig.14 that the component selection performs the best, because more isolated components are covered by the initial receivers. Moreover, when the number of initial receivers is low, the random selection perform worst, because the MUs belonging to an isolated component are likely to be selected, which seriously degrades the performance. However, when the number of initial receivers is high, the random selection outperforms the two centrality-based methods, because they are more likely to cover more MUs in the opportunistic network.

IV. INFORMATION DISSEMINATION IN INTEGRATED CELLULAR AND SMALL-SCALE OPPORTUNISTIC NETWORKS

In densely populated areas, such as a football stadium and open air festivals, MUs always experience limitations, when they rely on the data services supported by the CI, such as WiFi access points and cellular BSs. For instance, in a circular area having a radius of 50 meters in one of the above-mentioned scenarios, there may be hundreds of MUs, which may impose a heavy tele-traffic load on the CI. Moreover, the range of WiFi [52] in outdoor scenarios can be up to 250 m. If the diameter of the circular area studied is lower than this transmission range, it is reasonable for us to assume that the MUs are always in the transmission range of each other. As a result, in contrast to integrated cellular and large-scale opportunistic networks, as introduced in Section III, the information dissemination in this densely populated area is no longer dominated by the encounter-properties of the MUs' mobility. However, the varying distance between a pair of MUs incurred by their movement would impose a fluctuating signal strength at the receiver end. Such fluctuations can be treated as another type of fading further aggravating the multi-path effects [91]. Apart from the fading incurred by the varying distance and the multi-path effects, sophisticated MAC layer protocols are needed for efficiently scheduling the resources so as to minimise the adverse effects of interference and to optimise the information dissemination performance. All these features differentiate integrated cellular and small-scale opportunistic networks from their large-scale counterparts.

As a remedy, cooperative multicast (co-multicast) techniques may be introduced for improving the attainable performance by relying on multiple information multicasters (IMs) during the information dissemination process. In [92], the concept of multi-hop wireless multicast was proposed for the sake of enhancing the achievable multicast coverage, where a node having received the IoCI in a previous hop is randomly selected for further multicast. In order to exploit the diversity gain provided by multiple IMs, a multi-stage co-multicast scheme was proposed in [93]. Moreover, it was argued in [94] that the employment of two-stage co-multicast is more practical than that of its multi-stage counterpart. Therefore, the attainable performance of two-stage co-multicast was analysed in [95], while the associated optimum power allocation was characterised in [96]. Furthermore, in [97] and [98], the authors studied the benefits of relay selection techniques in the context of two-stage co-multicast. Specifically, in [97], the best relay was selected for maximizing the end-to-end co-multicast capacity. By contrast, in order to avoid unnecessary power wastage, in [98], the relays were activated only if there were unserved nodes within their transmission range.

In this section, we will introduce a mathematical framework for analysing the performance of the information dissemination in integrated cellular and small-scale opportunistic networks.

A. HYBRID INFORMATION DISSEMINATION SCHEME

As shown in Fig.15, our hybrid information dissemination scheme is comprised of two main stages, which are the BS-aided multicast and the co-multicast aided spontaneous dissemination, respectively. For integrated cellular and small-scale networks, communications work in a discrete-time manner, where the basic time unit is the duration of a transmission frame. We assume that all the MUs and the BS are synchronously operated at the frame level, which can be readily realised since the MUs normally exchange control signalling with the BS.

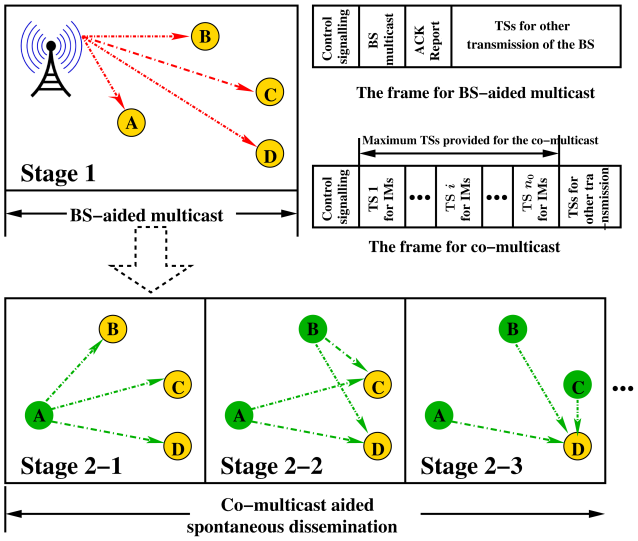

FIGURE 15. Hybrid information dissemination scheme.

1) BS-AIDED MULTICAST

At the first main stage, the cellular BS initially tries to multicast the IoCI to all the MUs in the studied area. The frame structure employed at this stage is portrayed in Fig.15. At the beginning of the frame, several Time Slots (TSs) are reserved for control signalling exchange between the MUs and BS. Next, a single TS is invoked by the BS for multicasting the IoCI. Afterwards, several TSs are allocated to the MUs for reporting their feedback. If a MU successfully receives the IoCI, an acknowledgement (ACK) message is reported to the BS. The BS repeats multicasting the IoCI in the next frame, until it receives a single ACK at least. In this case, the BS-aided multicast completes.

2) CO-MULTICAST AIDED SPONTANEOUS DISSEMINATION

During the second main stage, the IoCI is spontaneously disseminated by the IMs to the hitherto uMUs via co-multicast techniques, until all the MUs in the studied area successfully receive the information. As shown in Fig.15, we have an increasing number of IMs during this stage, and this may substantially speed up the information dissemination process. Furthermore, in order to avoid any collisions incurred by multiple IMs, a TDMA scheme is introduced.[9]

During this stage, the BS may play the role of a controller. The frame structure of this stage is also portrayed in Fig.15, which consists of several TSs for relevant control signalling exchange between the MUs and the controller as well as n_0 TSs for IMs' multicast. During the TSs for control signalling exchange, the following tasks are completed.

- The IMs report their willingness of sharing the IoCI to the controller;
- The uMUs send requests to the controller for the IoCI;
- The controller schedules the available resources of n_0 TSs to the IMs, and then broadcasts the resource scheduling scheme to all the IMs and uMUs. The detail of the resource scheduling scheme invoked in our model is introduced in Section IV-B.

Following the control signalling exchange, the IMs multicast the IoCI to the uMUs during the allocated TSs. Finally, if the controller does not receive any requests from the uMUs at the beginning of a frame, it will inform all the IMs that the information dissemination process is completed.

B. ROUND-ROBIN (RR) RESOURCE SCHEDULING FOR THE SPONTANEOUS DISSEMINATION

In order to fully exploit the n_0 TSs provided by the TDMA system for the co-multicast aided spontaneous dissemination, the classic round-robin (RR) scheme is invoked for scheduling the n_0 TSs of the current transmission frame to the IMs. After collecting the IMs' willingness of sharing the IoCI at the beginning of the frame, the controller randomly sorts the IMs into a set of $\mathcal{IM}$, whose size is $|\mathcal{IM}| = n$. Each TS in the available TS set $\mathcal{TS} = \{TS_i | 1 \leq i \leq n_0\}$ is allocated to a IM belonging to the $\mathcal{IM}$ set. If the size of $\mathcal{IM}$ is larger than n_0, only the first n_0 IMs of $\mathcal{IM}$ are assigned with a single TS for their own multicast. If the size of $\mathcal{IM}$ is smaller than n_0, the controller continues to allocate the remaining TSs to the IMs belonging to $\mathcal{IM}$ in the same order for another round after every IM in $\mathcal{IM}$ set has already been assigned with a single TS in the first round of scheduling. This process continues until all the TSs in the $\mathcal{TS}$ set are allocated. The details of the RR scheduling algorithm are shown in ALGORITHM 1.

ALGORITHM 1 RR Resource Scheduling Algorithm

Initialise the set $\mathcal{IM} \leftarrow$ randomly sort the IMs during the current frame;
Set $n \leftarrow |\mathcal{IM}|$, the size of $\mathcal{IM}$;
Set $n_0 \leftarrow$ the size of the available TSs for multicast;
Initialise the available TSs set $\mathcal{TS} \leftarrow \{TS_i | 1 \leq i \leq n_0\}$;
Set $indexTS = 1$; $indexIM = 1$;
for $indexTS = 1$ to n_0 **do**
  $\mathcal{TS}[indexTS]$ is allocated to $\mathcal{IM}[indexIM]$;
  $indexIM \leftarrow indexIM + 1$;
  if $indexIM > n$ **then**
    $indexIM \leftarrow 1$;
  end if
end for

According to this algorithm, there are $mod(n_0, n)$ IMs receiving $\lceil n_0/n \rceil$ TSs for each of them, while there are $[n - mod(n_0, n)]$ IMs receiving $\lfloor n_0/n \rfloor$ TSs for each of them. Here, $mod(n_0, n)$ represents the remainder after the division of n_0 by n, $\lceil n_0/n \rceil$ represents the first integer that is higher than the real value n_0/n, while $\lfloor n_0/n \rfloor$ represents the first integer that is lower than the real value n_0/n. These results will be exploited in the derivation of the state transition probabilities in Section IV-F.

[9]TDMA is one of the possible solutions that are capable of providing orthogonal channel access. The TDMA scheme in distributed WiFi system has already been thoroughly studied in [99] in terms of synchonisation, contro overhead, which makes it an available solution for our model. Other solutions, e.g. OFDMA, CDMA, and CSMA can be invoked as well.

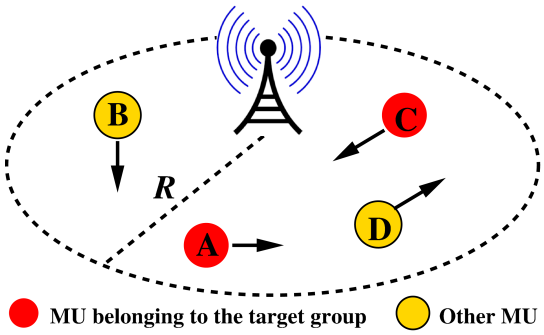

FIGURE 16. Random mobile networks.

C. RANDOM MOBILE NETWORKS

We assume that N MUs roam in a cell, which is a circular area having a radius of R, as shown in Fig.16. Naturally, the BS is assumed to be located at the center of the circular area. In line with the mobility model introduced in [100] and [101], the position of the ith MU during frame t is denoted by $\mathbf{P}_i(t)$, which represents a stationary and ergodic process having a stationary uniform distribution in the circular area. In other words, $\mathbf{P}_i(t)$ *is unchanged during a transmission frame but varies from one frame to another.* Moreover, the positions of the different MUs are independent and identically distributed (i.i.d.). As a result, the CDF and the PDF of the distance Y_b between the BS and a MU can be formulated as

$$F_{Y_b}(y_b)=\frac{y_b^2}{R^2},\quad f_{Y_b}(y_b)=\frac{dF_{Y_b}(y_b)}{dy_b}=\frac{2y_b}{R^2},\quad 0\le y_b\le R. \tag{17}$$

By contrast, the CDF of the distance Y_s between a pair of MUs [102] can be expressed as

$$F_{Y_s}(y_s)=\frac{2}{\pi}\left\{4\left(\frac{y_s}{2R}\right)^2\arccos\left(\frac{y_s}{2R}\right)+\arcsin\left(\frac{y_s}{2R}\right)-\left[\frac{y_s}{2R}+2\left(\frac{y_s}{2R}\right)^3\right]\sqrt{1-\left(\frac{y_s}{2R}\right)^2}\right\}, \tag{18}$$

while the corresponding PDF can be derived as

$$f_{Y_s}(y_s)=\frac{8}{\pi R}\frac{y_s}{2R}\left[\arccos\left(\frac{y_s}{2R}\right)-\frac{y_s}{2R}\sqrt{1-\left(\frac{y_s}{2R}\right)^2}\right], \tag{19}$$

for $0\le y_s\le 2R$. However, in order to make our following analysis tractable, we use the approximated PDF derived in [103] for (19), which is expressed as

$$\widetilde{f_{Y_s}}(y_s)=C_{Y_s}\cdot\frac{8}{\pi R}\left(\frac{\pi}{2}\frac{y_s}{2R}+\sum_{n=0}^{n_{\max}}C_n\left(\frac{y_s}{2R}\right)^{2n+2}\right), \tag{20}$$

where we have

$$C_{Y_s}=\frac{\pi}{4}\left(\pi+\sum_{n=0}^{n_{\max}}\frac{4C_n}{2n+3}\right)^{-1},$$

$$C_n=\frac{2\cdot(2n)!}{4^n(n!)^2(2n+1)(2n-1)}.$$

D. PHYsical (PHY) LAYER MODEL

1) PATH LOSS (PL)

Given the distance y between a transmitter-receiver pair, which is assumed to be longer than the reference distance d_0 determining the edge of the near-field, the PL model is defined by the following equation

$$\Omega(y)=\frac{P_0}{P_r}=\left(\frac{y}{d_0}\right)^{\kappa},\quad y\ge d_0, \tag{21}$$

where P_r is the power received at the receiver, P_0 is the power received at the reference point that is d_0 m away from the transmitter and κ is the PL exponent. The free-space PL model [104] is exploited for calculating the PL from the transmitter to the reference point, which is expressed as

$$\Omega_0=\frac{P_t}{P_0}=\frac{(4\pi)^2d_0^2}{\lambda^2}=\left(\frac{4\pi d_0}{c/f_c}\right)^2, \tag{22}$$

where $\lambda=c/f_c$ is the wave-length, c is the speed of light, f_c is the carrier frequency, and P_t is the transmit power. We note that the subscript 't' represents either 'b' for the BS, or 's' for MUs. Thus, the received reference power P_0 is obtained as $P_0=P_t/\Omega_0$. Unfortunately, (22) is invalid for calculating the PL in the near-field of the transmit antenna. As a result, we assume that, when the distance y between the transmitter and receiver is shorter than d_0, the received power P_r is equal to the transmit power P_t. In a nutshell, given an arbitrary distance y, the PL model in our system is defined as

$$\Omega(y)=\frac{P_0}{P_r}=\begin{cases}1/\Omega_0, & 0\le y<d_0,\\ (y/d_0)^{\kappa}, & y\ge d_0.\end{cases} \tag{23}$$

2) SMALL-SCALE FADING

The small-scale fading is modelled by uncorrelated stationary Rayleigh flat-fading. *The channel's amplitude $|h(t)|$ during the t-th TS, which varies from one TS to another, is a Rayleigh distributed random variable.* Consequently, the square of the channel amplitude $|h(t)|^2$ obeys an exponential distribution associated with $\mathcal{E}[|h(t)|^2]=1$. The PDF and CDF of $X=|h(t)|^2$ are $f_X(x)=\exp(-x)$, $F_X(x)=1-\exp(-x)$, $x>0$, respectively.

E. THROUGHPUT ANALYSIS OF WIRELESS LINKS

We assume that a packet can only be successfully received during a TS, if the instantaneously received Signal-to-Noise-Ratio (SNR) exceeds a pre-defined SNR threshold γ. Given the distance y_i between a transmitter-receiver pair, the successful packet delivery probability μ_i during a single TS is derived as

$$\mu_i(y_i)=\mathrm{P}\left[\frac{P_{0,i}|h(t)|^2}{N_0W_i\cdot\Omega(y_i)}\ge\gamma\right]=\begin{cases}\exp(-B_i), & 0\le y_i<d_0,\\ \exp(-A_i{y_i}^{\kappa}), & y_i\ge d_0,\end{cases} \tag{24}$$

where $A_i=(\gamma N_0W_i)/(P_{0,i}d_0^{\kappa})$, $B_i=(\gamma N_0W_i)/P_i$, N_0 is the noise power spectrum density (PSD), W_i is the available bandwidth, P_i is the transmit power and $P_{0,i}$ is the

associated received reference power. According to [105], $\mu_i(y_i)$ is also equivalent to the normalized throughput of the link connecting the transmitter and receiver, whose unit is 'packets/frame'. We should note that the subscript 'i' of (24) represents 'b' for the transmission between the BS and MUs, and represents 's' for the transmission between a pair of MUs.

1) l-TH MOMENT OF THROUGHPUT BETWEEN THE BS AND MUs DURING A TS

Integrating the l-th power of $\mu_b(y_b)$, provided by (24), over the PDF of (17), we can derive the l-th moment of the link throughput between the BS and a MU as

$$\begin{aligned}
&\mathcal{E}[\mu_b^l] \\
&= \int_0^R \mu_b^l(y_b) f_{Y_b}(y_b) dy_b \\
&= \int_0^{d_0} \exp(-lB_b)\frac{2y_b}{R^2}dy_b + \int_{d_0}^R \exp(-lA_b y_b^\kappa)\frac{2y_b}{R^2}dy_b \\
&= \exp(-lB_b)\frac{d_0^2}{R^2} + \frac{2}{R^2}\left[\frac{\Gamma(lA_b d_0^\kappa, 2/\kappa)}{\kappa(lA_b)^{2/\kappa}} - \frac{\Gamma(lA_b R^\kappa, 2/\kappa)}{\kappa(lA_b)^{2/\kappa}}\right],
\end{aligned} \tag{25}$$

where $\Gamma(\cdot,\cdot)$ is the upper incomplete Gamma function. By setting $l = 1$, we obtain the average link throughput $\overline{\mu}_b$ between the BS and a MU, which is also the upper bound of the social unicast throughput derived in [106].

2) l-TH MOMENT OF THROUGHPUT BETWEEN MUs DURING A TS

Integrating the l-th power of $\mu_s(y_s)$, provided by (24), over the PDF of (19) as well as its approximate version of (20), we can derive the l-th moment of the link throughput between a pair of MUs as

$$\begin{aligned}
\mathcal{E}[\mu_s^l] = \int_0^{2R} \mu_s^l(y_s) f_{Y_s}(y_s) dy_s &= \underbrace{\int_0^{d_0} \exp(-lB_s) f_{Y_s}(y_s) dy_b}_{I_1} \\
&+ \underbrace{\int_{d_0}^{2R} \exp(-lA_s y_s^\kappa)\widetilde{f}_{Y_s}(y_s) dy_s}_{I_2}
\end{aligned} \tag{26}$$

The first integral I_1 of (26) may be expressed as

$$I_1 = \exp(-lB_s)\int_0^{d_0} f_{Y_s}(y_s)dy_s = \exp(-lB_s)\cdot F_{Y_s}(d_0),$$

while the second integral I_2 of (26) may be derived as

$$\begin{aligned}
I_2 &= \int_{d_0}^{2R} \exp(-lA_s y_s^\kappa) C_{Y_s}\cdot\frac{8}{\pi R}\left(\frac{\pi}{2}\frac{y_s}{2R} + \sum_{n=0}^{n_{\max}} C_n\left(\frac{y_s}{2R}\right)^{2n+2}\right)dy_s \\
&= \frac{8C_{Y_s}}{\pi R}\left[\frac{\pi}{4R}\frac{\Gamma(lA_s d_0^\kappa, 2/\kappa) - \Gamma(lA_s(2R)^\kappa, 2/\kappa)}{\kappa(lA_s)^{2/\kappa}} + \sum_{n=0}^{n_{\max}}\right. \\
&\left.\times\frac{C_n(\Gamma(lA_s d_0^\kappa, (2n+3)/\kappa) - \Gamma(lA_s(2R)^\kappa, (2n+3)/\kappa)}{\kappa(2R)^{2n+2}(lA)^{(2n+3)/\kappa}}\right].
\end{aligned}$$

By setting $l = 1$, we obtain the average link throughput $\overline{\mu}_s$ between a pair of MUs during a TS, which is also the upper bound of the average social unicast throughput derived in [103].

3) AVERAGE THROUGHPUT DURING A TRANSMISSION FRAME

In the first stage of BS-aided multicast, as detailed in Section IV-A, only a single TS is invoked by the BS for the sake of multicasting the IoCI. As a result, the link throughput during a transmission frame between the BS and a MU is the same as that during a single TS, which is given by substituting $l = 1$ into (25).

By contrast, in the second stage of co-multicast aided spontaneous dissemination, a single IM may be assigned with multiple TSs, say L, for its own multicast. Let us consider an IM and uMU pair as an example. Recalling the mobility model introduced in Section IV-C, the distance y_s is unchanged during the transmission frame. Given the L TSs for the IM's multicast, the packet fails to be conveyed to the uMU only when all the transmission attempts in these L TSs fail. Since the small-scale fading varies independently from one TS to another, the successful packet delivery probability during a transmission frame may be expressed as

$$\begin{aligned}
\lambda_s(y_s, L) &= 1 - [1 - \mu_s(y_s)]^L \\
&= 1 - \sum_{l=0}^{L}\binom{L}{l}(-1)^l[\mu_s(y_s)]^l.
\end{aligned} \tag{27}$$

Integrating $\lambda_s(y_s, L)$ over the PDF $f_{Y_s}(y_s)$ given by (19), the average link throughput during a transmission frame is formulated as

$$\begin{aligned}
\overline{\lambda_s}(L) &= \int\left[1 - \sum_{l=0}^{L}\binom{L}{l}(-1)^l[\mu_s(y_s)]^l\right] f_{Y_s}(y_s)dy_s \\
&= 1 - \sum_{l=0}^{L}\binom{L}{l}(-1)^l\mathcal{E}[\mu_s^l],
\end{aligned} \tag{28}$$

where L is the number of TSs that is allocated to the IM for the multicast during the current transmission frame, and $\mathcal{E}[\mu_s^l]$ is the l-th moment of the link throughput during a single TS that has been derived in (26). Specifically, when no TS is allocated to the IM, namely $L = 0$, we have $\overline{\lambda_s}(L) = 0$.

F. DISCRETE-TIME-PURE-BIRTH-MARKOV CHAIN (DT-PBMC) AIDED DELAY ANALYSIS

In contrast to its large-scale counterpart, the integrated cellular and small-scale opportunistic network is a discrete transmission system, where the basic time unit is the duration of a transmission frame. Since the number of IMs always increases during the information dissemination process, we may model this process as a DT-PBMC, whose states are defined by the number of IMs. Moreover, the BS may also be considerd as a special IM. For example, the state $(1 + n)$ represents that both the BS and n MUs own the IoCI. In the DT-PBMC, the transition from a lower numbered state to a higher numbered one can only occur once during

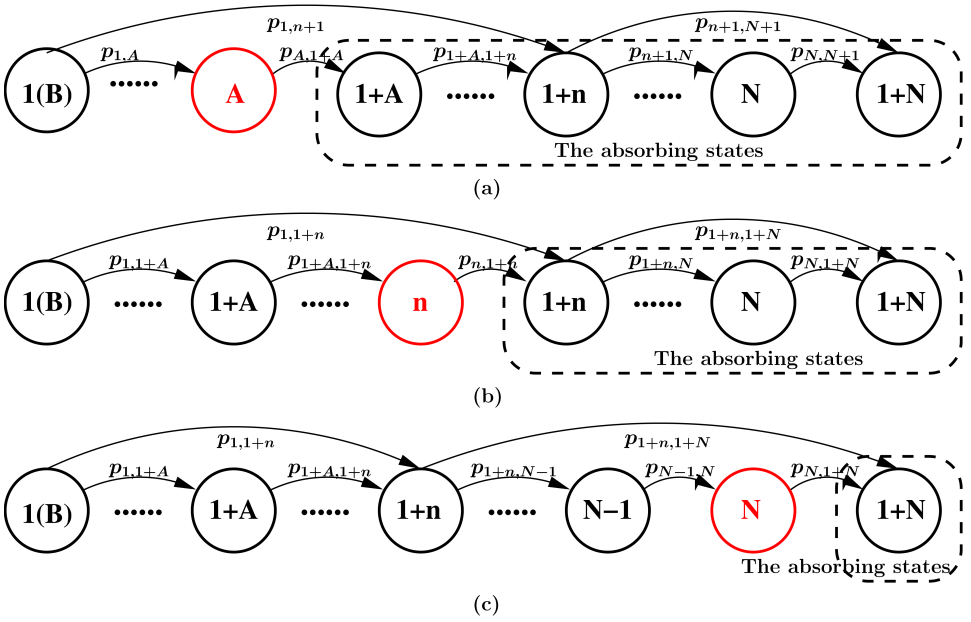

FIGURE 17. The DT-PBMC for the information dissemination in integrated cellular and small-scale opportunistic networks. (a) Group $\mathcal{A}$ receive the information after the transient boundary A. (b) Group $\mathcal{A}$ receive the information after the transient boundary n. (c) Group $\mathcal{A}$ receive the information after the transient boundary N.

a single frame. Consequently, $p_{1+n,1+n+m}(t)$ represents the probability of a transition traversing from state $(1+n)$ to state $(1+n+m)$ during a given frame t. As portrayed in Fig.17, there are two special states in the DT-PBMC, which are the initial state $1(B)$, representing that only the BS owns the IoCI at the beginning of the information dissemination process, and the absorbing state $(1+N)$, representing that all the MUs have obtained the IoCI. Except for state $(1+N)$, the other states are referred to as the transient states.

1) STATE TRANSITION MATRIX

We can collect the state transition probabilities $\{p_{1+n,1+n+m}(t)|0 \le n \le N, 0 \le m \le (N-n)\}$ into a state transition matrix $\mathbf{P}(t)$, which is expressed as (29), shown at the bottom of this page, where the $(N \times N)$-element matrix $\mathbf{Q}(t)$ contains all the state transition probabilities between any pairs of transient states. Hence $\mathbf{Q}(t)$ is referred to as the *transient transition matrix*, while $\mathbf{Q_0}(t)$ is an N-length vector, containing the transition probabilities of traversing from any of the N transient states to the absorbing state $(1+N)$. We note that both the matrix $\mathbf{P}(t)$ and $\mathbf{Q}(t)$ are random matrices, varying from one frame to another. The expectation matrix $\overline{\mathbf{P}}$ is derived by computing the expectation of every entry in $\mathbf{P}(t)$. The elements of the expectation matrix $\overline{\mathbf{P}}$ are denoted as $\{\overline{p}_{1+n,1+n+m},\ 0 \le n \le N, 0 \le m \le (N-n)\}$, which are given by the following lemma:

Lemma 1: Due to the independent mobilities of the MUs, the state transition probability $p_{1+n,1+n+m}(t)$ is an independent time-varying random variable. Its expected value is given by the following formulas:

i) When $n = 0$ and $0 \le m \le N$, the expected value of $p_{1,1+m}(t)$ is expressed as

$$\overline{p}_{1,1+m} = \binom{N}{m} \overline{\mu}_b^m (1-\overline{\mu}_b)^{N-m}, \tag{30}$$

where $\overline{\mu}_b$ can been derived by letting $l = 1$ in (25).

ii) When $0 < n \le N$ and $0 \le m \le (N-n)$, the expected value of $p_{1+n,1+n+m}(t)$ is expressed as

$$\overline{p}_{1+n,1+n+m} = \binom{N-n}{m} \overline{p_i}^m (1-\overline{p_i})^{N-n-m}, \tag{31}$$

$$\mathbf{P}(t) = \begin{pmatrix} p_{1,1}(t) & p_{1,2}(t) & p_{1,3}(t) & p_{1,4}(t) & \cdots & p_{1,N}(t) & p_{1,N+1}(t) \\ 0 & p_{2,2}(t) & p_{2,3}(t) & p_{2,4}(t) & \cdots & p_{2,N}(t) & p_{2,N+1}(t) \\ \vdots & \vdots & \ddots & \vdots & & \vdots & \vdots \\ 0 & 0 & \cdots & p_{n+1,n+1}(t) & \cdots & p_{U,N}(t) & p_{U,N+1} \\ \vdots & \vdots & & & \ddots & \vdots & \vdots \\ 0 & 0 & \cdots & 0 & \cdots & p_{N,N}(t) & p_{N,N+1} \\ 0 & 0 & \cdots & 0 & \cdots & 0 & p_{N+1,N+1} \end{pmatrix} = \begin{pmatrix} \mathbf{Q}(t) & \mathbf{Q_0}(t) \\ \mathbf{0} & 1 \end{pmatrix} \tag{29}$$

where $\overline{p_i}$ is the expected probability of an arbitrary uMU successfully receiving the IoCI, which is formulated as

$$\overline{p_i} = 1 - \left[1 - \overline{\lambda_s}\left(\lceil \frac{n_0}{n} \rceil\right)\right]^{mod(n_0,n)} \cdot \left[1 - \overline{\lambda_s}\left(\lfloor \frac{n_0}{n} \rfloor\right)\right]^{n-mod(n_0,n)}. \quad (32)$$

Proof: Please refer to Appendix B for the proof. ■

Furthermore, the expectation $\overline{\mathbf{Q}}$ of the transient-state transition matrix $\mathbf{Q}(t)$ contains the entries in the first N rows and first N columns of the general state transition matrix $\overline{\mathbf{P}}$.

Various delay metrics can be derived with the aid of the DT-PBMC of Fig.17, including (a) the *group delay* K_G, which is defined as the delay when the entire group $\mathcal{A}$ of MUs has successfully received the IoCI, (b) the *individual delay* K_I, namely the delay of a specific MU receiving the information, (c) the *dissemination delay* K_D, which represents the delay when all the N MUs in the cell have successfully received the information, and, finally (d) the *BS-aided multicast delay* K_b, which is the delay of the BS-aided first stage of information dissemination. Furthermore, in this section, the *BS-aided-Single-hop-Multicast (BSSHM) delay* K^{bm} is also derived and used as a benchmarker.

2) TRANSIENT BOUNDARY

As shown in Fig.17, multiple-step state transitions may occur during a single frame's transmission. For example, the transition can emerge from state $1(B)$ directly to any of the states $(1+n)$ $(0 \le n \le N)$. Consequently, we cannot exactly tell at which state the specific group $\mathcal{A}$ of MUs have first successfully received the IoCI as we dealt with the CT-PBMC of Fig.8 in Section III-E, because within a sample trace of the state transitions traversing from the initial state $1(B)$ to the absorbing state N, certain states might be skipped. However, we may ascertain that this group of MUs must successfully receive the IoCI after a certain state n, which also indicates that not all the MUs belonging to the group $\mathcal{A}$ have successfully received the information during the previous states. As a result, the states emanating from state $(1+n)$ to $(1+N)$ can be equivalently considered together as an absorbing state for the event that all the MUs belonging to the group $\mathcal{A}$ have successfully received the information after state n, as shown in Fig.17(b). Corresponding to the above event, state n may be referred to as the *transient boundary*.

Lemma 2: Let the size of the group $\mathcal{A}$ be defined as $|\mathcal{A}| = A$. The legitimate *transient boundary* may be any of the states spanning from state A to state N, as shown in Fig.17. The probability p_n that the *transient boundary* is at state n $(A \le n \le N)$ is given by the following equation:

$$p_n = \binom{n-1}{A-1} \Big/ \binom{N}{A}, \quad A \le n \le N. \quad (33)$$

Proof: Please refer to Appendix C for the proof. ■

3) GROUP DELAY ANALYSIS

Given that the *transient boundary* is at state n $(A \le n \le N)$, all the MUs belonging to the target group $\mathcal{A}$ receive the IoCI right after state n. Correspondingly, we represent the *group delay* as K_n frames. As shown in Fig.17(b), in this case, the absorbing states for the group $\mathcal{A}$ are comprised of the states $\{n+1, n+2, \cdots, N, N+1\}$. As a result, transition matrix $\mathbf{Q}_n(t)$ of the new DT-PBMC of Fig.17(b) is a sub-matrix of $\mathbf{Q}(t)$ containing its entries in the first n rows and n columns, which is expressed as

$$\mathbf{Q}_n(t) = \begin{pmatrix} p_{1,1}(t) & p_{1,2}(t) & \cdots & p_{1,n}(t) \\ 0 & p_{2,2}(t) & \cdots & p_{2,n}(t) \\ \vdots & \vdots & \ddots & \vdots \\ 0 & 0 & \cdots & p_{n,n}(t) \end{pmatrix}, \quad A \le n \le N. \quad (34)$$

According to (34), for different values of n, $\mathbf{Q}_n$ has different size. In order to unify the size of the matrices $\{\mathbf{Q}_n, n = 1, 2, \cdots, N\}$, we may redefine $\mathbf{Q}_n$ without affecting the result of the matrix product as

$$\widetilde{\mathbf{Q}}_n(t) = \begin{pmatrix} \mathbf{Q}_n(t) & \mathbf{0}_{n,N-n} \\ \mathbf{0}_{N-n,n} & \mathbf{0}_{N-n,N-n} \end{pmatrix}, \quad (35)$$

where $\mathbf{0}_{m,n}$ is a $(m \times n)$-element matrix whose entries are all zeros. Particularly, the expected matrix of $\widetilde{\mathbf{Q}}_n(t)$ is denoted as $\widehat{\mathbf{Q}}_n$, while the entries of $\widehat{\mathbf{Q}}_n$ are defined in (30) and (31).

According to [103, Th. 1], the ij-entry $q_{i,j}$ of the matrix $\widetilde{\mathbb{Q}}_n(k_G) = \prod_{t=1}^{k_G} \widetilde{\mathbf{Q}}_n(t)$ is the probability of state j being reached after k_G frames from the initial state i. Since the information dissemination starts at state 1, as shown in Fig.17, given a series of the i.i.d. transition matrices $\{\widetilde{\mathbf{Q}}_n(t), t = 1, \cdots, k_G\}$, the sum of the entries in the first row of the matrix $\widetilde{\mathbb{Q}}_n^{k_G}$ is the probability of $K_n > k_G$, which is expressed as

$$P(K_n > k_G | \widetilde{\mathbf{Q}}_n(1), \cdots, \widetilde{\mathbf{Q}}_n(k_G)) = \boldsymbol{\tau}^T \widetilde{\mathbb{Q}}_n(k_G)\mathbf{1} = \boldsymbol{\tau}^T \prod_{t=1}^{k_G} \widetilde{\mathbf{Q}}_n(t)\mathbf{1},$$

where $\boldsymbol{\tau}$ is a $(N \times 1)$-element column vector, whose first entry is one and all the other entries are zeros, while $\mathbf{1}$ is a $(N \times 1)$-element column vector, whose entries are all ones. According to the Bayesian principle [82], given n as the transient boundary, the tail distribution of the group delay K_n is derived as presented in (36), as shown at the top of the next page, where $f[\widetilde{\mathbf{Q}}_n(t)]$ denotes the PDF of the random matrix $\widetilde{\mathbf{Q}}_n(t)$.

Since the *transient boundary* may be at any state spanning from state A to state N with the probabilities of $\left\{p_n = \binom{n-1}{A-1} \Big/ \binom{N}{A}, n = A, \cdots, N\right\}$, as shown in Lemma 2, according to the Bayesian principle [82], we may obtain the tail distribution of the *group delay* K_G as

$$P(K_G > k_G) = \sum_{n=A}^{N} P(K_n > k_G) p_n = \sum_{n=A}^{N} \boldsymbol{\tau}^T \widehat{\mathbf{Q}}_n^{k_G} \mathbf{1} \cdot \binom{n-1}{A-1} \Big/ \binom{N}{A} = \boldsymbol{\tau}^T \left(\sum_{n=A}^{N} \frac{\widehat{\mathbf{Q}}_n^{k_G}}{N} \cdot \binom{n-1}{A-1} \Big/ \binom{N}{A} \right) \mathbf{1}. \quad (37)$$

$$P(K_n > k_G) = \int_{\widetilde{\mathbf{Q}}_n(1)} \cdots \int_{\widetilde{\mathbf{Q}}_n(k_G)} P(K_n > k_G | \widetilde{\mathbf{Q}}_n(1), \ldots, \widetilde{\mathbf{Q}}_n(k_G)) f[\widetilde{\mathbf{Q}}_n(1), \ldots, \widetilde{\mathbf{Q}}_n(k_G)] d\widetilde{\mathbf{Q}}_n(1) \cdots d\widetilde{\mathbf{Q}}_n(k_G)$$
$$= \int_{\widetilde{\mathbf{Q}}_n(1)} \cdots \int_{\widetilde{\mathbf{Q}}_n(k_G)} \left(\boldsymbol{\tau}^T \prod_{t=1}^{k_G} \widetilde{\mathbf{Q}}_n(t) \mathbf{1} \right) f[\widetilde{\mathbf{Q}}_n(1), \ldots, \widetilde{\mathbf{Q}}_n(k_G)] d\widetilde{\mathbf{Q}}_n(1) \ldots d\widetilde{\mathbf{Q}}_n(k_G)$$
$$= \boldsymbol{\tau}^T \left(\prod_{t=1}^{k_G} \int_{\widetilde{\mathbf{Q}}_n(t)} \widetilde{\mathbf{Q}}_n(t) f[\widetilde{\mathbf{Q}}_n(t)] d\widetilde{\mathbf{Q}}_n(t) \right) \mathbf{1} = \boldsymbol{\tau}^T \left(\prod_{t=1}^{k_G} \mathcal{E}[\widetilde{\mathbf{Q}}(t)] \right) \mathbf{1} = \boldsymbol{\tau}^T \widehat{\mathbf{Q}}_n^{k_G} \mathbf{1} \quad (36)$$

Furthermore, since K_G is a discrete random variable, its average value may be expressed as $\mathcal{E}[K_G] = \sum_{k_G=0}^{+\infty} P(K_G > k_G)$ [82]. As a result, the average *group delay* can be formulated as

$$\mathcal{E}[K_G] = \sum_{k_G=0}^{+\infty} P(K_G > k_G) = \boldsymbol{\tau}^T \left(\sum_{n=1}^{N} \binom{n-1}{A-1} \Big/ \binom{N}{A} \sum_{k_G=0}^{+\infty} \widehat{\mathbf{Q}}_n^{k_G} \right) \mathbf{1}$$
$$= \boldsymbol{\tau}^T \left(\sum_{n=A}^{N} \frac{1}{(\mathbf{I} - \widehat{\mathbf{Q}}_n)} \binom{n-1}{A-1} \Big/ \binom{N}{A} \right) \mathbf{1}, \quad (38)$$

where the last equal relation is derived with the aid of [103, Th. 2] and [103, Th. 4].

4) INDIVIDUAL DELAY

In order to characterise the statistical properties of the individual delay K_I, we can simply set the size of the target group $\mathcal{A}$ to $|\mathcal{A}| = A = 1$. Consequently, upon substituting $A = 1$ into (37) and (38), the tail distribution of the individual delay K_I can be expressed as

$$P(K_I > k_I) = \boldsymbol{\tau}^T \left(\sum_{n=1}^{N} \frac{\widehat{\mathbf{Q}}_n^{k_I}}{N} \right) \mathbf{1}, \quad (39)$$

while its average value can be derived as

$$\mathcal{E}[K_I] = \boldsymbol{\tau}^T \left(\sum_{n=1}^{N} \frac{(\mathbf{I} - \widehat{\mathbf{Q}}_n)^{-1}}{N} \right) \mathbf{1}. \quad (40)$$

5) DISSEMINATION DELAY

The statistical properties of the dissemination delay K_D can be obtained by setting the size of the target group $\mathcal{A}$ to $|\mathcal{A}| = A = N$. In this case, we have $\widetilde{\mathbf{Q}}_N(t) = \mathbf{Q}(t)$, which is defined in (29). When substituting $A = N$ into (37) and (38), the tail distribution as well as the average of the dissemination delay K_D can be expressed as

$$P(K_D > k_D) = \boldsymbol{\tau}^T \overline{\mathbf{Q}}^k \mathbf{1}, \quad \mathcal{E}[K_D] = \boldsymbol{\tau}^T (\mathbf{I} - \overline{\mathbf{Q}}^k)^{-1} \mathbf{1}, \quad (41)$$

respectively. In (41), $\overline{\mathbf{Q}}$ is the expectation of $\mathbf{Q}(t)$.

6) BS-AIDED MULTICAST DELAY IN THE FIRST STAGE

It can be shown that if the *transient boundary* is at state 1, the transition matrix $\widetilde{\mathbf{Q}}_1(t)$ only has a single non-zero entry $p_{1,1}(t) = \prod_{\text{All MUs}}(1 - \mu_{b,j}(t))$, whose expected value is $\overline{p}_{1,1} = (1 - \overline{\mu}_b)^N$. In this case, the *group delay* K_1 is reduced to the multicast delay K_b that only the BS multicasts during the first stage. Corresponding to (36), the tail distribution of K_b is given by

$$P(K_b > k_b) = (1 - \overline{\mu}_b)^{Nk_b}, \quad (42)$$

while its average value can be expressed as

$$\mathcal{E}[K_b] = \sum_{k_b=0}^{+\infty} P(K_b > k_b) = 1/[1 - (1 - \overline{\mu}_b)^N]. \quad (43)$$

As shown in (43), if N tends to infinity, we have $\lim_{N \to \infty} \mathcal{E}[K_b] = 1$ frame, as expected. This explains that on average only one frame is needed by the first stage of our hybrid information dissemination scheme, when a large number of MUs are supported in the integrated network.

7) BS-AIDED SINGLE-HOP MULTICAST (BSSHM) DELAY

For the sake of comparison, we also consider the delay of the conventional BSSHM. In this case, the BS repeatedly disseminates the IoCI as a sole transmitter until all the MUs have successfully received it. As a result, given the probability $\mu_{b,i}(t)$ of the ith MU successfully receiving the IoCI during the tth frame, the probability $p^{(bm)}_{1+n,1+n+m}(t)$ of traversing from state $(1+n)$ to state $(1+n+m)$ is given by

$$p^{(bm)}_{1+n,1+n+m}(t) = \sum_{\text{All } \mathcal{M}} \prod_{uMU_i \in \mathcal{M}} \mu_{b,i}(t) \prod_{uMU_j \notin \mathcal{M}} (1 - \mu_{b,j}(t)), \quad (44)$$

for $0 \leq n \leq N$ and $0 \leq m \leq N - n$. After taking the expectation, we obtain

$$\overline{p}^{(bm)}_{1+n,1+n+m} = \binom{N-n}{m} \overline{\mu}_b^m (1 - \overline{\mu}_b)^{N-n-m}. \quad (45)$$

Based on (45), the expectation of the state transition matrix $\overline{\mathbf{Q}}^{(bm)}$ can be formed. Upon replacing $\overline{\mathbf{Q}}$ in (41) by $\overline{\mathbf{Q}}^{(bm)}$, we obtain both the tail distribution and the average of the BSSHM delay $K^{(bm)}$.

8) ENERGY ANALYSIS

Apart from the various delay metrics, we may also analyse the average energy required for disseminating the IoCI to all the N MUs. According to the above analysis, at state 1, the energy consumed during a single frame is P_b since the BS

TABLE 8. Parameters of the PHY layer.

	BS to MUs	MUs to MUs
Transmit Power	$P_b = 0 \sim 23$ dBm	$P_s = 0 \sim 20$ dBm
Carrier Freq.	$f_{c,b} = 2$ GHz	$f_{c,s} = 2.4$ GHz
Bandwidth	$W_b = 100$ MHz	$W_s = 10$ MHz
Noise PSD[a]	$N_0 = -174$ dBm/Hz (20^oC)	
SNR Threshold	$\gamma = 10$ dB	
PL Model	$d_0 = 1$ m, $\kappa = 3$	
Studied Area	A circular area having a radius of 200 m	
Mobility Model	Introduced in Section IV-C	

[a]PSD: Power Spectrum Density

only invokes a single TS for multicasting the IoCI. However, at state $(1+n)$, the energy dissipated during a single frame is $n_0 P_s$, as n_0 TSs are allocated to the IMs for their multicast. Hence, the energy dissipation of different states during a transmission frame is denoted by the N-elements column vector $\boldsymbol{\mathcal{P}}$, whose first element is P_b and all the other elements are $n_0 P_s$.

In order to evaluate the average energy dissipation, the number of frames that the system spends in a specific state $(1+n)$ must be known. Thanks to [103, Th. 3], the ij-entry ψ_{ij} of the matrix $\Psi = \sum_{k_D=0}^{\infty} \mathbb{Q}(k_D) = \sum_{k_D=0}^{\infty} \prod_{t=1}^{k_D} \mathbf{Q}(t)$ represents the average number of frames that the system spend at state j when the initial state is i, where $\mathbf{Q}(t)$ is given by (29). Since in our hybrid information dissemination scheme the system emerges from state 1, we only consider the first row of the matrix Ψ. Given a series of matrices $\{\mathbb{Q}(k_D) = \prod_{t=1}^{k_D} \mathbf{Q}(t), k_D = 0, 1, \cdots, \infty\}$, the average energy dissipation until the information dissemination is completed is derived as

$$\mathcal{E}[E_D|\mathbb{Q}(k_D), k_D = 0, 1, \cdots, \infty] = \boldsymbol{\tau}^T \Psi \boldsymbol{\mathcal{P}} = \boldsymbol{\tau}^T \times \sum_{k_D=0}^{\infty} \mathbb{Q}(k_D) \times \boldsymbol{\mathcal{P}}.$$

According to the Bayesian principle [82], we have

$$\begin{aligned}\mathcal{E}[E_D] &= \boldsymbol{\tau}^T \times \left[\sum_{k_D=0}^{\infty} \int_{\mathbb{Q}(k_D)} \mathbb{Q}(k_D) f(\mathbb{Q}(k_D)) d\mathbb{Q}(k_D)\right] \times \boldsymbol{\mathcal{P}} \\ &= \boldsymbol{\tau}^T \times \sum_{k_D=0}^{\infty} \mathcal{E}[\mathbb{Q}(k_D)] \times \boldsymbol{\mathcal{P}} \\ &= \boldsymbol{\tau}^T \times \sum_{k=0}^{\infty} \overline{\mathbf{Q}}^k \times \boldsymbol{\mathcal{P}} = \boldsymbol{\tau}^T \times (\mathbf{I} - \overline{\mathbf{Q}})^{-1} \times \boldsymbol{\mathcal{P}}, \quad (46)\end{aligned}$$

where $f[\mathbb{Q}(k_D)]$ is the PDF of $\mathbb{Q}(k_D)$ and the last equal relation is derived with the aid of [103, Th. 2] and [103, Th. 4].

G. NUMERICAL RESULTS

The parameters of the PHY layer are presented in TABLE 8. For the transmissions from the MUs to MUs, the parameters are in line with the 802.11 protocol [52], while for the transmission from the BSs to MUs, the parameters are in line with the Long-Term-Evolution-Advanced (LTE-A) standard [107]. The radius of the cellular system is set to $R = 200$ m and all the N MUs roam in this circular area. The BS is located at the center of the circular area. The classic RR scheduling is invoked during the information dissemination process.

The performance metrics of our hybrid information dissemination scheme are evaluated by both the analytical (ana) results as well as by the simulation (sim) results, including the average link throughput during a transmission frame, and various delay metrics as well as the average energy required for disseminating the IoCI. All the delay metrics are quantified in terms of the number of frames, while the energy dissipation is quantified in terms of 'mW*TS'. In order to obtain reliable statistical results, we repeatedly run the simulation in MATLAB 10 000 times. The performance of the conventional BSSHM is also presented as a benchmarker.

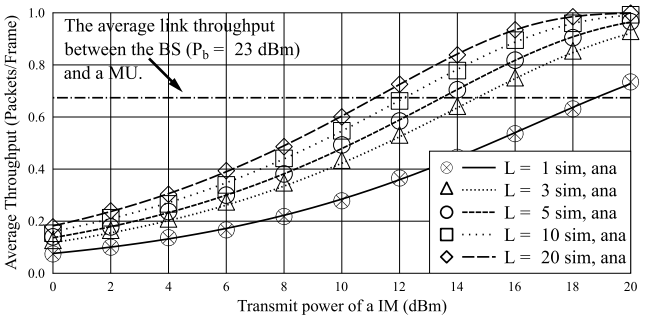

FIGURE 18. The average link throughput during a transmission frame between a IM and uMU pair. The transmit power of the IM varies from 0 dBm to 20 dBm. The number of TSs allocated to the IM for its multicast varies from 1 to 20. As a benchmarker, we also portray the average throughput between the BS and a MU when the transmit power of the BS is 23 dBm. All the other parameters are listed in TABLE 8. The analytical results are derived by evaluating Eq.(28).

1) AVERAGE LINK THROUGHPUT DURING A TRANSMISSION FRAME

We portray the average link throughput during a transmission frame between a IM and uMU pair associated with different number of TSs allocated to the IM in Fig.18. As the transmit power of the IM increases, we observe an increasing trend for the average link throughput. Furthermore, we also observe that the average link throughput during a frame increases, as more TSs are allocated to the IM. The analytical results derived in (28) perfectly match the simulation results.

2) VARIOUS DELAY METRICS

i) Individual Delay: The transmit power of the BS is set to $P_b = 23$ dBm, which is the typical value for picocellular systems, while that of the MUs is $P_s = 4$ dBm, which is the typical value for 802.11 based transmitters. As shown in Fig.19(a), by invoking the BSSHM, the average *individual delay* of a specific MU receiving the IoCI remains near-constant at about 1.5 frames, as the number N of MUs increases from 1 to 100. The reason for this trend is that the *individual delay* in the case of BSSHM is only affected by the

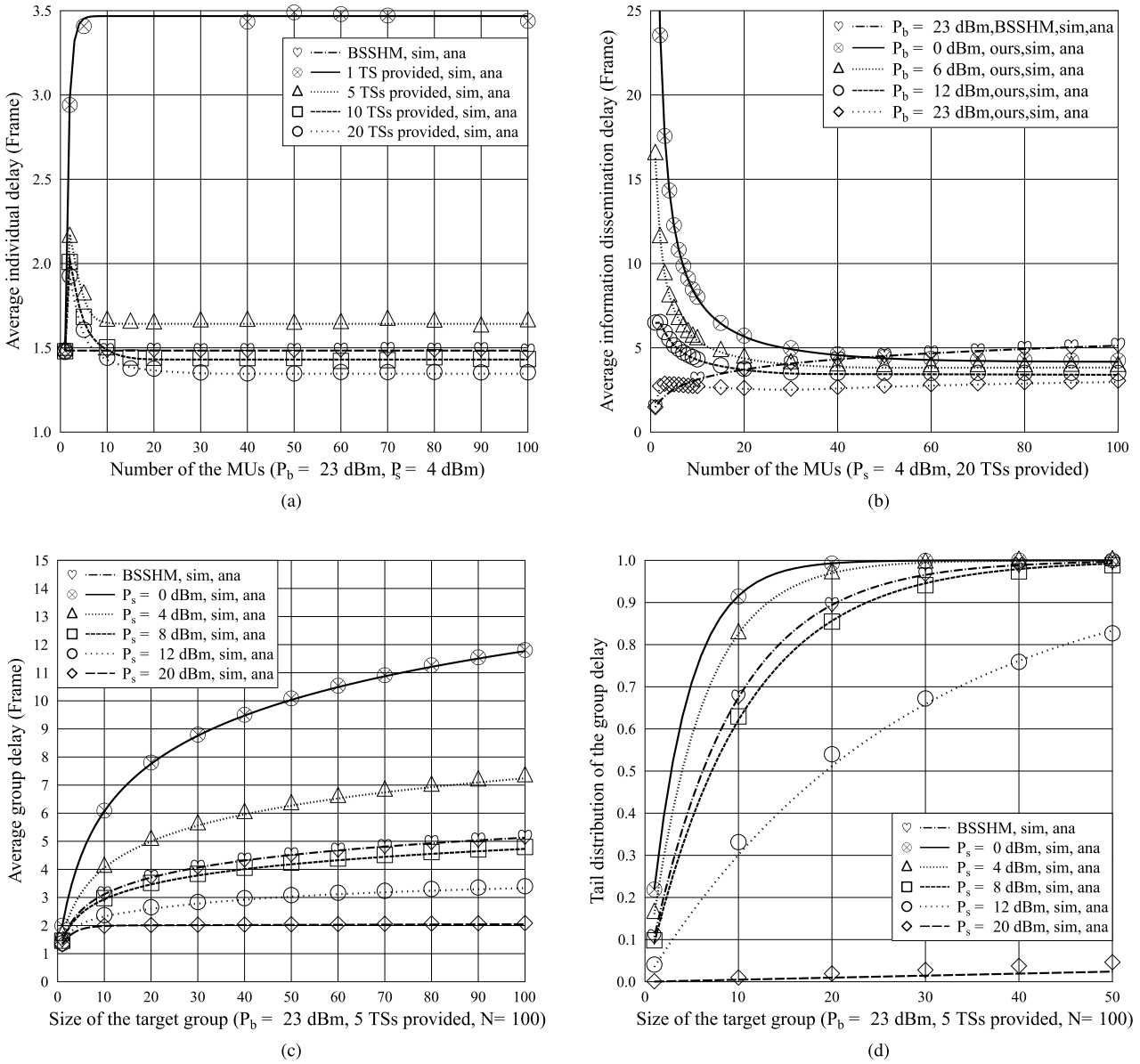

FIGURE 19. **Various delay metrics of our hybrid dissemination scheme. We investigate the impact of the transmit power of both the BS and the MUs, the impact of the number of TSs, and the impact of the number of the MUs in the area studied, as well as the impact of the size of the target group on the average individual delay, the average dissemination delay and the average group delay as well as the tail distribution of the group delay. Apart from the parameters quantified in figures, all the other parameters are provided in TABLE 8. (a) Average individual delay. (b) Average dissemination delay. (c) Average group delay. (d) Tail distribution of group delay.**

wireless link connecting the MU to the BS rather than being related to N. If only a single TS is provided for the second stage of the co-multicast aided spontaneous dissemination, which indicates that only a single IM is selected randomly out of the IOs during each frame, the average *individual delay* firstly increases and then tends to about 3.5 frames as N increases. By contrast, the curves of the average *individual delay* associated with $n_0 = \{5, 10, 20\}$ firstly increases until reaching their peaks, before they start to decay and tend to constant values. Moreover, if more TSs are provided for the spontaneous dissemination, as reflected by higher values of n_0, the average *individual delay* may be reduced. Furthermore, compared to BSSHM, our hybrid information dissemination scheme associated with $n_0 = 20$ TSs may reduce the average *individual delay* by 9% when there are more than 30 MUs.

ii) Dissemination Delay: The transmit power of the MUs is set to $P_s = 4$ dBm, while that of the BS for the first stage of the information dissemination is varied from 0 dBm to 23 dBm. As the benchmarker, the transmit power of the BS used for the BSSHM is set to $P_b = 23$ dBm. We assume that $n_0 = 20$ TSs are provided for multiple IMs' multicast. As shown in Fig.19(b), the BSSHM delay associated with $P_b = 23$ dBm increases steadily as we

increase the number N of the MUs. For our hybrid information dissemination scheme associated with $P_b = \{12, 23\}$ dBm, the average *dissemination delay* first increases until reaching its peak, beyond which it decays. However, for the case of $P_b = \{0, 6\}$ dBm, the average *dissemination delay* continuously decreases. Specifically, our hybrid information dissemination scheme associated with the most economical scenario of $P_b = 0$ dBm, outperforms the BSSHM associated with $P_b = 23$ dBm, when the number of MUs is higher than 50. Furthermore, when $N = 100$, our hybrid information dissemination scheme associated with $P_b = 23$ dBm may reduce the average *dissemination delay* by 40.6%, compared to the BSSHM. Furthermore, the analytical results derived from (41) perfectly match the simulation results.

iii) Group Delay: The transmit power of the BS is still set to $P_b = 23$ dBm, while the transmit power of the MU takes values from the set $\{0, 4, 8, 12, 20\}$ dBm. The maximum number of TSs provided for co-multicast is $n_0 = 5$. The total number of MUs is set to $N = 100$, but the size $|\mathcal{A}| = A$ of the target group $\mathcal{A}$ increases from 1 to 100. Observe in Fig.19(c) that the average *group delay* of all the members in the target group $\mathcal{A}$ receiving the IoCI steadily increases as the group size increases. Moreover, the increased transmit power P_s of the MUs may significantly reduce the average *group delay*. According to Fig.19(c), if P_s is larger than 8 dBm, our hybrid information dissemination scheme may achieve a lower average *group delay* than the BSSHM. Specifically, when $P_s = 12$ dBm and the group size is $A = 50$, compared to the BSSHM, our hybrid information dissemination scheme may reduce the average *group delay* by 33%. Moreover, the analytical results derived from (38) perfectly match the simulation results.

In order to study the tail distribution of the *group delay*, the maximum tolerable delay threshold is set to 2 frames, As shown in Fig.19(d), the probability of the *group delay* exceeding 2 frames increases as the size of the target group increases. A higher P_s leads to a lower 'threshold-violation' probability. Similarly, our hybrid information dissemination scheme associated with $P_s = 8$ dBm outperforms the conventional BSSHM. Furthermore, the analytical results derived from (37) match the simulation results.

3) AVERAGE ENERGY DISSIPATION

Fig.20 portrays the average energy required for disseminating the IoCI to all the MUs, where we have $P_b = 23$ dBm and $P_s = 4$ dBm. The average energy dissipation first decays, as we initially increase N, and then it steadily increases, as we further increase N. As presented in Fig.20, if we provide more TSs for the co-multicast of the IMs, which is represented by a higher n_0 value, more energy is dissipated, but it still remains significantly lower than that of the BSSHM benchmarker. For example, when $N = 100$ and $n_0 = 20$ TSs are provided for co-multicast, our scheme may reduce the average energy dissipation by about 70%, compared to the BSSHM, as evidenced by Fig.20. Furthermore, the analytical results derived from (46) match the simulation results.

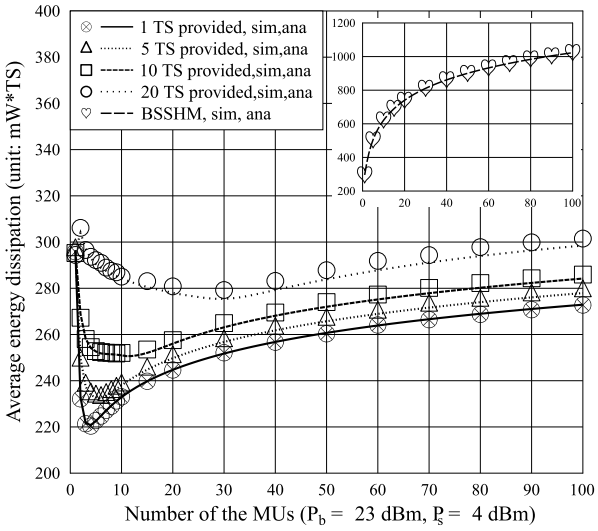

FIGURE 20. The average energy dissipation during exhaustively disseminating the IoCI to all the MUs in the area studied. The transmit power of the BS is 23 dBm, while the transmit power of the MUs is 4 dBm. The number of the MUs in the area studied varies from 1 to 100, while the number of TSs provided by the TDMA system varies from 1 to 20. Other parameters are provided in TABLE 8.

H. CENTRALITY BASED RESOURCE SCHEDULING AND DISCUSSION

The tools of SNA may be exploited in the integrated cellular and small-scale opportunistic network as well for further improving the information dissemination performance. As shown in our previous work [57], various distance-based and transmission rate-based centralities may be conceived, such as the *Shortest-Longest-Distance* centrality, the *Shortest-Shortest-Distance* centrality, and the *Shortest-Sum-Distance* centrality as well as the *Highest-Sum-Rate* centrality. The simulation results of [57] demonstrate the advantage of these centrality based resource scheduling schemes over the traditional RR regime.

V. CONCLUSIONS

In Section I, we provided a rudimentary introduction to the current trends of SNA and to its application in telecommunications, followed by the design dilemmas of information dissemination in current cellular networks in Section II. Then a tutorial was provided in Section III on the information dissemination process of integrated cellular and large-scale opportunistic networks with the goal of improving connectivity of cellular networks as well as for off-loading excess teletraffic to opportunistic networks. Apart from the well-known exponentially distributed inter-contact duration, which is presented in Figs.7(a)(b), we also demonstrated in Fig.7(c) that the contact duration between a pair of MUs obeying RD mobility model can be approximated by an exponential distribution. Surprisingly, the contact duration between the BS (a static node) and a MU closely matches a Gamma distribution, as shown in Fig.7(d). Then in Section III-D, we jointly considered the impact of inter-contact duration

TABLE 9. Comparison between integrated cellular large-scale opportunistic network and its small-scale counterpart.

	Cellular+Large-scale opportunistic networks	Cellular+Small-scale opportunistic networks
Scale	The size of the area studied is far larger than the transmission range of the MUs.	The size of the area studied is comparable to the transmission range of the MUs.
Density	MUs are sparsely distributed in the area studied.	MUs are densely distributed in the area studied.
Mobility factors	MUs move at a high speed. The inter-contact duration and contact duration dominate the information dissemination.	The path loss between a transmitter and receiver pair fluctuates, which affects the information dissemination performance.
Other factors	File size and transmission rate jointly determine the required transmission time. Information life time decides when the information expires.	Path loss, multi-path fading and transmit power jointly determine the received signal strength. Noise power.
Infomattion delivery	The receiver enters the range of the transmitter, while the contact duration is longer than required transmission time.	The signal-to-noise ratio is higher than a pre-defined threshold.
Resource Scheduling	Dispensable. Sparse distribution of MUs makes it unlikely that a receiver is in the transmission range of multiple transmitters.	Indispensable in order to avoid interference, when multiple IOs multicast and in order to efficiently exploit the precious resources.
Protocol	Peer-to-peer communication based epidemic relaying protocol.	Multi-stage cooperative multicast protocol.
Latency order	Similar to the inter-contact duration, normally hours, suitable for delivering delay-tolerant services.	Similar to the duration of a transmission frame, normally milli-seconds, suitable for delivering delay-sensitive services.
Math. tool	Conventional CT-PBMC.	DT-PBMC.
Application Scenarios	Networking in rural areas, emergency communication in large areas, tele-traffic off-loading in macro cellular networks, hybrid vehicular communications.	Networking in densely populated areas, such as shopping malls, football stadiums, open air festivals and small cellular networks.

and contact duration on the performance analysis of the information dissemination by modelling it as a CT-PBMC. With the aid of this CT-PBMC, we analytically derived the dissemination and individual delay as well as the average number of receivers before the IoCI expires. The simulation results of Fig.13 validated the accuracy of our mathematical model and demonstrated that a more active social participation of the MUs is capable of significantly improving the IoCI delivery ratio. Furthermore, the amount of tele-traffic off-loaded by the SNA assisted initial receiver selection is as much as 1.75 times that of the random selection method, as shown in Fig.14.

Then a hybrid information dissemination regime conceived for the integrated cellular and small-scale opportunistic network was proposed in Section IV, which consists of two stages in the densely populated area, namely the BS-aided multicast stage and the co-multicast aided spontaneous dissemination stage. By jointly considering the impact of RR resource scheduling, of the MUs' mobilities, the PL, and the small-scale fading, we modelled this hybrid information dissemination regime as a DT-PBMC and derived the group delay that the system imposes during the dissemination of the IoCI to a specific group of MUs, which is a generic form jointly representing both the dissemination delay and the individual MU delay. Moreover, the average energy dissipation imposed by successfully disseminating the IoCI was also obtained. Furthermore, we demonstrated that our hybrid scheme significantly reduces both the average dissemination delay, as shown in Fig.19(b) and the average energy dissipation, as shown in Fig.20, for example, by 40.6% and 70%, respectively, when compared to the BSSHM.

For the readers' convenience, the major features of the integrated cellular and large-scale/small-scale opportunistic networks are listed in TABLE 9. Based on our studies, we have the vision that owing to the tremendous benefit of future heterogeneous networks relying on the social participation of the MUs, the integrated cellular and opportunistic networks deserve much more joint effort from both the communication community and the social science community.

APPENDIX A
PROOF OF THEOREM 1

For the specific case of $1 \leq n \leq (N-1)$, after a sufficiently short time interval Δt, the probability of the CT-PBMC, shown in Fig.8, remaining in state n is derived as

$$p_n(t+\Delta t) = p_{n-1}(t)\widetilde{\lambda}_{n-1}\Delta t + p_n(t)[1-\widetilde{\lambda}_n\Delta t], \quad (47)$$

where $\widetilde{\lambda}_n\Delta t$ is the probability of the CT-PBMC traversing from state n to state $(n+1)$ during the time interval Δt, whereas $\widetilde{\lambda}_{n-1}\Delta t$ holds a similar meaning. After some

equivalent transformation applied to (47), we arrive at

$$\frac{d}{dt}p_n(t)=\lim_{\Delta t\to 0}\frac{p_n(t+\Delta t)-p_n(t)}{\Delta t}=\widetilde{\lambda}_{n-1}p_{n-1}(t)-\widetilde{\lambda}_n p_n(t). \tag{48}$$

Similarly, we can also derive the corresponding differential equation for the cases of $n=0$ and $n=N$. As a result, the following set of differential equations are obtained

$$\begin{cases}\frac{d}{dt}p_0(t)=-\widetilde{\lambda}_0 p_0(t), & n=0,\\ \frac{d}{dt}p_n(t)=\widetilde{\lambda}_{n-1}p_{n-1}(t)-\widetilde{\lambda}_n p_n(t), & 1\le n\le N-1,\\ \frac{d}{dt}p_N(t)=\widetilde{\lambda}_{N-1}p_{N-1}(t), & n=N.\end{cases} \tag{49}$$

Since only the BS owns the IoCI at the beginning of the information dissemination, the initial condition is given by $\{p_0(0)=1,p_1(0)=0,\cdots,p_N(0)=0\}$. As a result, applying the Laplace transform to the above differential equations, and taking the aforementioned initial condition into account, we arrive at

$$\begin{cases}sP_0(s)=-\widetilde{\lambda}_0P_0(s)+1, & n=0,\\ sP_n(s)=-\widetilde{\lambda}_nP_n(s)+\widetilde{\lambda}_{n-1}P_{n-1}(s), & 1\le n\le N-1,\\ sP_N(s)=\widetilde{\lambda}_{N-1}P_{N-1}(s), & n=N,\end{cases} \tag{50}$$

from which we obtain

$$P_n(s)=\begin{cases}\frac{1}{s+\widetilde{\lambda}_0}, & n=1\\ \frac{1}{s+\widetilde{\lambda}_n}\prod_{m=0}^{n-1}\frac{\widetilde{\lambda}_m}{s+\widetilde{\lambda}_m}, & 0<n<N,\\ \frac{1}{s}\prod_{m=0}^{N-1}\frac{\widetilde{\lambda}_m}{s+\widetilde{\lambda}_m}, & n=N.\end{cases} \tag{51}$$

Finally, applying the inverse-Laplace-transform to the above equations, we may arrive at the closed-form equations for $p_n(t)$, as expressed in (15). The theorem is proved. ■

APPENDIX B
PROOF OF LEMMA 1

A. EXPECTED STATE TRANSITION PROBABILITY $\overline{p}_{1,1+m}$

Since the first main stage of our hybrid information dissemination scheme is the BS-aided multicast, we first derive the state transition probability $p_{1,1+m}(t)$ during the t-th frame for $0\le m\le N$. A series of successful packet delivery probabilities $\{\mu_{b,i}(t),i=1,\cdots,N\}$ are provided during the t-th transmission frame, where $\mu_{b,i}(t)$ is the successful packet delivery probability of the link connecting the i-th MU to the BS. Assuming that the group $\mathcal{M}$ of MUs, whose size is $|\mathcal{M}|=m$, successfully receives the IoCI, while the others fail to do so, $p_{1,1+m}(t)$ can be derived as

$$p_{1,1+m}(t)=\sum_{\text{All }\mathcal{M}}\prod_{MU_i\in\mathcal{M}}\mu_{b,i}(t)\prod_{MU_j\notin\mathcal{M}}(1-\mu_{b,j}(t)), \tag{52}$$

for $0\le|\mathcal{M}|=m\le N$, where 'ALL $\mathcal{M}$' represents all the possible combinations for construction of $\mathcal{M}$. Since the geographic positions of the MUs are i.i.d., which also leads to i.i.d. random variables $\{\mu_{b,i}(t),i=1,\cdots,N\}$, the expected value of $p_{1,1+m}(t)$ is derived as

$$\begin{aligned}\overline{p}_{1,1+m}&=\sum_{\text{All }\mathcal{M}}\prod_{MU_i\in\mathcal{M}}\mathcal{E}[\mu_{b,i}(t)]\prod_{MU_j\notin\mathcal{M}}(1-\mathcal{E}[\mu_{b,j}(t)])\\&=\binom{N}{m}\overline{\mu}_b^{\,m}(1-\overline{\mu}_b)^{N-m},\quad 0\le m\le N,\end{aligned} \tag{53}$$

where $\overline{\mu}_b$ can be obtained by letting $l=1$ in (25). The first part of Lemma 1 is proved. ■

B. EXPECTED STATE TRANSITION PROBABILITY $\overline{p}_{1+n,1+n+m}$

Let us now derive the state transition probability $p_{1+n,1+n+m}(t)$ during the t-th transmission frame for the stage of spontaneous dissemination, where $0<n\le N$ and $0\le m\le(N-n)$. In this case, there are n IMs at state $(1+n)$ and hence we have $(N-n)$ uMUs. The IMs are partitioned into two sets $\mathcal{R}_1=\{IM_{r_1},1\le r_1\le mod(n_0,n)\}$ and $\mathcal{R}_2\{IM_{r_2},1\le r_2\le(n-mod(n_0,n))\}$ according to the number of TDMA TSs that are allocated to them after the RR scheduling. As introduced in Section IV-B, each IM of $\mathcal{R}_1$ is allocated $\lceil n_0/n\rceil$ TDMA TSs, while each IM of $\mathcal{R}_2$ is allocated $\lfloor n_0/n\rfloor$ TDMA TSs. The set of uMUs at state $(1+n)$ is denoted as $\mathcal{M}=\{uMU_i|1\le i\le(N-n)\}$.

We consider a single uMU denoted as uMU_i. The successful packet delivery probabilities from the IMs in $\mathcal{R}_1$ to uMU_i are denoted as $\boldsymbol{\lambda}_{\mathcal{R}_1,i}=\{\lambda_{r_1,i}(t,\lceil\frac{n_0}{n}\rceil),1\le r_1\le mod(n_0,n)\}$, while those from the IMs in $\mathcal{R}_2$ to uMU_i are denoted as $\boldsymbol{\lambda}_{\mathcal{R}_2,i}=\{\lambda_{r_2,i}(t,\lfloor\frac{n_0}{n}\rfloor),1\le r_2\le mod(n_0,n)\}$. Since the positions of different IMs are i.i.d. random variables, all the elements in both $\boldsymbol{\lambda}_{\mathcal{R}_1,i}$ and $\boldsymbol{\lambda}_{\mathcal{R}_2,i}$ are independent of each other. As a result, as long as at least one IM from $\mathcal{R}_1$ or $\mathcal{R}_2$ successfully delivers the packet to uMU_i, the packet can be successfully received. Therefore, the successful packet reception probability $p_i(t)$ of uMU_i is derived as

$$\begin{aligned}p_i(t)=1-&\prod_{IM_{r_1}\in\mathcal{R}_1}\left[1-\lambda_{r_1,i}\left(t,\lceil\frac{n_0}{n}\rceil\right)\right]\\&\times\prod_{IM_{r_2}\in\mathcal{R}_2}\left[1-\lambda_{r_2,i}\left(t,\lfloor\frac{n_0}{n}\rfloor\right)\right].\end{aligned} \tag{54}$$

The expectation of $p_i(t)$ is derived as

$$\begin{aligned}\overline{p_i}&=1-\prod_{IM_{r_1}\in\mathcal{R}_1}\left\{1-\mathcal{E}\left[\lambda_{r_1,i}\left(t,\lceil\frac{n_0}{n}\rceil\right)\right]\right\}\\&\quad\cdot\prod_{IM_{r_2}\in\mathcal{R}_2}\left\{1-\mathcal{E}\left[\lambda_{r_2,i}\left(t,\lfloor\frac{n_0}{n}\rfloor\right)\right]\right\}\\&=1-\left[1-\overline{\lambda_s}\left(\lceil\frac{n_0}{n}\rceil\right)\right]^{mod(n_0,n)}\\&\quad\cdot\left[1-\overline{\lambda_s}\left(\lfloor\frac{n_0}{n}\rfloor\right)\right]^{n-mod(n_0,n)}.\end{aligned} \tag{55}$$

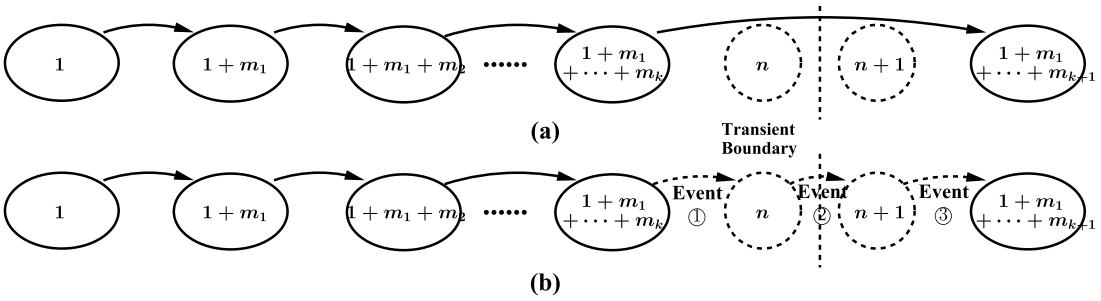

FIGURE 21. A possible trace of the state transitions. (a) Original trace of the state transitions. (b) Equivalent trace of the state transitions.

Furthermore, we assume that a subset $\mathcal{M}' \subseteq \mathcal{M}$ of uMUs, whose size is $|\mathcal{M}'| = m$, successfully receive the IoCI during the t-th frame, while $\mathcal{M}/\mathcal{M}'$ of uMUs fail to do so. As a result, the state transition probability $p_{1+n,1+n+m}(t)$ can be expressed as

$$p_{1+n,1+n+m}(t) = \sum_{\text{All } \mathcal{M}'} \prod_{uMU_i \in \mathcal{M}'} p_i(t) \prod_{uMU_j \in \mathcal{M}/\mathcal{M}'} (1 - p_j(t)). \tag{56}$$

Since the positions of different uMUs are i.i.d. random variables, $\{p_i(t), uMU_i \in \mathcal{M}\}$ are i.i.d. random variables as well. Hence, the expectation of $p_{1+n,1+n+m}(t)$ is derived as

$$\overline{p}_{1+n,1+n+m} = \binom{N-n}{m} \overline{p_i}^m (1 - \overline{p_i})^{N-n-m}, \tag{57}$$

where $\overline{p_i}$ is given by (55). The second part of Lemma 1 is proved. ■

APPENDIX C
PROOF OF LEMMA 2

Assuming that the *transient boundary* is at state n, we portray in Fig.21(a) a sample trace of the state transitions emerging from the initial state 1 to state $(1 + m_1 + \cdots + m_{k+1})$, which is the first state after crossing the *transient boundary* n. Naturally, when state n is the *transient boundary*, according to the above assumption, we have $(1 + \sum_{i=1}^{k} m_i) \leq n$ and $(1 + \sum_{i=1}^{k+1} m_i) \geq (n + 1)$. Let us denote the set of the uMUs whose members have successfully received the IoCI during the i-th frame as $\mathcal{M}_i$, with its cardinality $|\mathcal{M}_i| = m_i$, where $1 \leq i \leq (k+1)$. Let us denote the MUs simultaneously belonging to $\mathcal{M}_i$ and to the target group $\mathcal{A}$ as the set $\mathcal{A}_i$ with a cardinality of $|\mathcal{A}_i|$. As shown in Fig.21(a), since all the members of the target group $\mathcal{A}$ have successfully received the IoCI until the $(k+1)$th frame, we have $\mathcal{A} = \bigcup_{i=1}^{k+1} \mathcal{A}_i$, and $\{\mathcal{A}_i \bigcap \mathcal{A}_j = \phi | i \neq j\}$. Note that the cardinality $|\mathcal{A}_i|$ of the group $\mathcal{A}_i$ is a random integer assuming a value in $[0, m_i]$ subject to the constraint of $\sum_{i=1}^{k+1} |\mathcal{A}_i| = A$. As a specific case during the i-th frame, we have $|\mathcal{A}_i| = a_i$, where a_i is a possible sample for the random integer $|\mathcal{A}_i|$ and $a_i \in [0, m_i]$. As a result, the vector, which reflects the number of newly served MUs belonging to the target group $\mathcal{A}$ from the first frame to the $(k+1)$-th frame, is constructed as $\boldsymbol{a} = (a_1, a_2, \cdots, a_{k+1})^T$, subject to the constraints of $\sum_{i=1}^{k+1} a_i = A$.

Based on the above discussions, we know that before the transition from state $(1 + m_1 + \cdots + m_{i-1})$ to state $(1 + m_1 \cdots + m_i)$, we have $(N - m_1 - \cdots - m_{i-1})$ uMUs, amongst which $(A - a_1 - \cdots - a_{i-1})$ uMUs belong to the group $\mathcal{A}$. After the state transition, $|\mathcal{M}_i| = m_i$ uMUs have successfully received the information, amongst which $|\mathcal{A}_i| = a_i$ uMUs belong to the target group $\mathcal{A}$. Hence, the joint event of $(\mathcal{A}_i \subseteq \mathcal{M}_i, \boldsymbol{a})$ occurs during the i-th frame with the probability of (58), as shown at the bottom of this page.

As a result, the probability that, after the kth frame, $(m_1 + m_2 + \cdots + m_k)$ uMUs have successfully received the IoCI, amongst which $(a_1 + a_2 + \cdots + a_k)$ uMUs belong to the target group $\mathcal{A}$, can be expressed as (59), shown at the bottom of this page.

$$P\left(\mathcal{A}_i \subseteq \mathcal{M}_i, \boldsymbol{a}\right) = \frac{\binom{A - a_1 - \cdots - a_{i-1}}{a_i} \binom{N - m_1 - \cdots - m_{i-1} - A + a_1 + \cdots + a_{i-1}}{m_i - a_i}}{\binom{N - m_1 - \cdots - m_{i-1}}{m_i}} \tag{58}$$

$$P\left(\bigcap_{i=1}^{k} \left(\mathcal{A}_i \subseteq \mathcal{M}_i\right), \boldsymbol{a}\right) = \prod_{i=1}^{k} P\left(\mathcal{A}_i \subseteq \mathcal{M}_i, \boldsymbol{a}\right) = \frac{A!(N-A)!}{N!} \cdot \prod_{i=1}^{k} \frac{m_i!}{a_i!(m_i - a_i)!} \cdot \frac{(N - m_1 - \cdots - m_k)!}{(A - a_1 - \cdots - a_k)!(N - m_1 - \cdots - m_k - A + a_1 + \cdots + a_k)!} \tag{59}$$

$$P\left(\mathcal{A}_{i+1}^{(1)} \subseteq \mathcal{M}_{i+1}^{(1)}, \boldsymbol{a}\right) = \frac{\binom{A-a_1-\cdots-a_k}{a_{k+1}^{(1)}}\binom{N-m_1-\cdots-m_k-A+a_1+\cdots+a_k}{m_{k+1}^{(1)}-a_{k+1}^{(1)}}}{\binom{N-m_1-\cdots-m_k}{m_{k+1}^{(1)}}}$$
$$= \frac{m_{k+1}^{(1)}! \cdot (A-a_1-\cdots-a_k)!}{(m_{k+1}^{(1)}-a_{k+1}^{(1)})! \cdot a_{k+1}^{(1)}!} \frac{(N-m_1-\cdots-m_k-A+a_1+\cdots+a_k)!}{(N-m_1-\cdots-m_k)!/(N-n+1)} \quad (60)$$

P(State n is the transient boundary, $\boldsymbol{a}$)
$$= \underbrace{P\left(\bigcap_{i=1}^{k}\left(\mathcal{A}_i \subseteq \mathcal{M}_i\right), \boldsymbol{a}\right)}_{\text{Eq. (59)}} \cdot \underbrace{P\left(\mathcal{A}_{i+1}^{(1)} \subseteq \mathcal{M}_{i+1}^{(1)}, \boldsymbol{a}\right)}_{\text{Eq. (60)}} \cdot \underbrace{P\left(\mathcal{A}_{i+1}^{(2)} \subseteq \mathcal{M}_{i+1}^{(2)}, \boldsymbol{a}\right)}_{\text{Eq. (61)}} \cdot \underbrace{P\left(\mathcal{A} \bigcap \mathcal{M}_{k+1}^{(3)} = \phi, \boldsymbol{a}\right)}_{\text{Eq. (62)}}$$
$$= \binom{m_1}{a_1} \cdot \binom{m_2}{a_2} \cdot \cdots \cdot \binom{m_k}{a_k} \binom{m_{k+1}^{(1)}}{a_{k+1}^{(1)}} \Big/ \binom{N}{A} \quad (63)$$

As shown in Fig.21(b), given that the *transient boundary* is state n, the last state transition traversing from state $(1+\sum_{i=1}^{k} m_i)$ to state $(1+\sum_{i=1}^{k+1} m_i)$, can be decomposed into three consecutive **virtual events** as follows.

Event ①*:* Firstly, let us consider the virtual transition traversing from state $(1+\sum_{i=1}^{k} m_i)$ to state n. Before this state transition, there are $(N-m_1-\cdots-m_k)$ uMUs, which include $(A-a_1-\cdots-a_k)$ uMUs belonging to the target group $\mathcal{A}$. After the state transition, a set $\mathcal{M}_{k+1}^{(1)}$ of uMUs satisfying $|\mathcal{M}_{k+1}^{(1)}| = m_{k+1}^{(1)} = n-1-\sum_{i=1}^{k} m_i$ have successfully received the IoCI. Here $\mathcal{M}_{k+1}^{(1)}$ includes a set $\mathcal{A}_{i+1}^{(1)}$ of uMUs belonging to $\mathcal{A}$, and we have $|\mathcal{A}_{i+1}^{(1)}| = a_{i+1}^{(1)} = a_{k+1}-1 = A-1-\sum_{i=1}^{k} a_i$. In other words, after this transition, there is only a single uMU in $\mathcal{A}$ who has not received the information. The probability of the above event occurring is derived as (60), shown at the top of this page.

Event ②*:* Secondly, let us consider the virtual transition traversing from state n to state $(1+n)$. After Event ①, there are $(N-n+1)$ uMUs, which include a single uMU belonging to the target group $\mathcal{A}$. After the state transition, a set $\mathcal{M}_{k+1}^{(2)}$ of uMUs with $\left|\mathcal{M}_{k+1}^{(2)}\right| = m_{k+1}^{(2)} = 1$ have successfully received the IoCI. Explicitly, we have $|\mathcal{M}_{k+1}^{(2)}| = m_{k+1}^{(2)} = |\mathcal{A}_{i+1}^{(2)}| = a_{i+1}^{(2)} = 1$. As a result, the probability of this event is

$$P\left(\mathcal{A}_{i+1}^{(2)} \subseteq \mathcal{M}_{i+1}^{(2)}, \boldsymbol{a}\right) = \frac{1}{N-n+1}. \quad (61)$$

Event ③*:* Finally, let us consider the virtual transition traversing from state $(1+n)$ to state $(1+\sum_{i=1}^{k+1} m_i)$. After Event ① and ②, among the remaining $(N-n)$ uMUs, a set $\mathcal{M}_{k+1}^{(3)}$ of uMUs satisfying $\left|\mathcal{M}_{k+1}^{(3)}\right| = m_{k+1}^{(3)} = m_{k+1} - m_{k+1}^{(1)} - m_{k+1}^{(2)}$ have successfully received the IoCI during this virtual state transition. Note that in $\mathcal{M}_{k+1}^{(3)}$, there are no uMUs belonging to the target group $\mathcal{A}$, since all the MUs in the target set $\mathcal{A}$ received the IoCI after Event ① and ②. Consequently, the probability that Event ③ occurs is given by

$$P\left(\mathcal{A} \bigcap \mathcal{M}_{k+1}^{(3)} = \phi, \boldsymbol{a}\right) = 1. \quad (62)$$

In summary of the above three virtual events of ①, ② and ③, when $\boldsymbol{a}$ is assumed, the joint probability that the *transient boundary* is located at state n can be expressed as (63), shown at the top of this page.

Finally, upon summing up (63) over all possible combinations for the elements in $\boldsymbol{a}$, we obtain the probability p_n that the *transient boundary* is located at state n, which is given by

$$p_n = \sum_{\text{All } \boldsymbol{a}} P(\text{State } n \text{ is the transient boundary}, \boldsymbol{a})$$
$$= \sum_{\text{All } \boldsymbol{a}} \binom{m_1}{a_1} \cdot \binom{m_2}{a_2} \cdot \cdots \cdot \binom{m_k}{a_k} \binom{m_{k+1}^{(1)}}{a_{k+1}^{(1)}} \Big/ \binom{N}{A}$$
$$= \binom{n-1}{A-1} \Big/ \binom{N}{A}, \quad (64)$$

for $A \le n \le N$. Note that since $m_{k+1}^{(1)} + \sum_{i=1}^{k} m_i = n-1$ and, for all $1 \le i \le k$, the entries of $\boldsymbol{a}$ are subject to $0 \le a_i \le m_i$ as well as $0 \le a_{k+1}^{(1)} \le m_{k+1}^{(1)}$, while $a_{k+1}^{(1)} + \sum_{i=1}^{k} a_k = A-1$, the combinatorial problem described by the numerator of the second line of (64) is equivalent to that of selecting $(A-1)$ MUs out of the total $(n-1)$ ones. As a result, the third equality of (64) holds, and Lemma 2 is proved. According to (64), we can see that p_n is not related to any specific value of $\{m_i, i = 1, 2, \cdots, k+1\}$ and $\{a_i, i = 1, 2, \cdots, k+1\}$. ■

REFERENCES

[1] (Feb. 2015). *Cisco Visual Networking Index: Global Mobile Data Traffic Forecast Update 2014–2019 White Paper*. [Online]. Available: http://www.cisco.com/c/en/us/solutions/collateral/service-provider/visual-networking-index-vni/white_paper_c11-520862.pdf

[2] M. Peng, Y. Li, T. Q. S. Quek, and C. Wang, "Device-to-device underlaid cellular networks under Rician fading channels," *IEEE Trans. Wireless Commun.*, vol. 13, no. 8, pp. 4247–4259, Aug. 2014.

[3] A. M. Ortiz, D. Hussein, S. Park, S. N. Han, and N. Crespi, "The cluster between Internet of Things and social networks: Review and research challenges," *IEEE Internet Things J.*, vol. 1, no. 3, pp. 206–215, Jun. 2014.

[4] N. Kayastha, D. Niyato, P. Wang, and E. Hossain, "Applications, architectures, and protocol design issues for mobile social networks: A survey," *Proc. IEEE*, vol. 99, no. 12, pp. 2130–2158, Dec. 2011.

[5] T. Alahakoon, R. Tripathi, N. Kourtellis, R. Simha, and A. Iamnitchi, "κ-centrality: a new centrality measure in social networks," in *Proc. 4th Workshop Social Netw. Syst. (SNS)*, 2011, Art. ID 1. [Online]. Available: http://doi.acm.org/10.1145/1989656.1989657

[6] P. V. Marsden, "Egocentric and sociocentric measures of network centrality," *Social Netw.*, vol. 24, no. 4, pp. 407–422, 2002. [Online]. Available: http://www.sciencedirect.com/science/article/pii/S0378873302000163

[7] P. Bonacich, "Some unique properties of eigenvector centrality," *Social Netw.*, vol. 29, no. 4, pp. 555–564, 2007. [Online]. Available: http://www.sciencedirect.com/science/article/pii/S0378873307000342

[8] S. Brin and L. Page, "The anatomy of a large-scale hypertextual Web search engine," *Comput. Netw. ISDN Syst.*, vol. 30, nos. 1–7, pp. 107–117, Apr. 1998. [Online]. Available: http://dl.acm.org/citation.cfm?id=297810.297827

[9] K. Okamoto, W. Chen, and X.-Y. Li, "Ranking of closeness centrality for large-scale social networks," in *Frontiers in Algorithmics*, vol. 5059. Berlin, Germany: Springer-Verlag, Jun. 2008, pp. 186–195. [Online]. Available: http://dx.doi.org/10.1007/978-3-540-69311-6_21

[10] L. C. Freeman, "A set of measures of centrality based on betweenness," *Sociometry*, vol. 40, no. 1, pp. 35–41, Mar. 1977. [Online]. Available: http://moreno.ss.uci.edu/23.pdf

[11] P. De Meo, E. Ferrara, G. Fiumara, and A. Ricciardello, "A novel measure of edge centrality in social networks," *Knowl.-Based Syst.*, vol. 30, pp. 136–150, Jun. 2012. [Online]. Available: http://www.sciencedirect.com/science/article/pii/S0950705112000160

[12] M. Girvan and M. E. J. Newman, "Community structure in social and biological networks," *Proc. Nat. Acad. Sci. USA*, vol. 99, no. 12, pp. 7821–7826, 2002. [Online]. Available: http://www.pnas.org/content/99/12/7821.abstract

[13] F. Henri and B. Pudelko, "Understanding and analysing activity and learning in virtual communities," *J. Comput. Assist. Learn.*, vol. 19, no. 4, pp. 474–487, 2003. [Online]. Available: http://dx.doi.org/10.1046/j.0266-4909.2003.00051.x

[14] V. D. Blondel, J.-L. Guillaume, R. Lambiotte, and E. Lefebvre, "Fast unfolding of communities in large networks," *J. Statist. Mech., Theory Experim.*, vol. 2008, no. 10, Oct. 2008. [Online]. Available: http://stacks.iop.org/1742-5468/2008/i=10/a=P10008

[15] J. Travers and S. Milgram, "An experimental study of the small world problem," *Sociometry*, vol. 32, no. 4, pp. 425–443, 1969.

[16] D. J. Watts and S. H. Strogatz, "Collective dynamics of 'small-world' networks," *Nature*, vol. 393, no. 6684, pp. 440–442, Jun. 1998.

[17] M. E. J. Newman and D. J. Watts, "Renormalization group analysis of the small-world network model," *Phys. Lett. A*, vol. 263, nos. 4–6, pp. 341–346, 1999. [Online]. Available: http://www.sciencedirect.com/science/article/pii/S0375960199007574

[18] J. Kleinberg, "The small-world phenomenon: An algorithmic perspective," in *Proc. 32nd Annu. ACM Symp. Theory Comput. (STOC)*, 2000, pp. 163–170.

[19] H. Inaltekin, M. Chiang, and H. V. Poor, "Average message delivery time for small-world networks in the continuum limit," *IEEE Trans. Inf. Theory*, vol. 56, no. 9, pp. 4447–4470, Sep. 2010.

[20] H. Inaltekin, M. Chiang, and H. V. Poor, "Delay of social search on small-world graphs," *J. Math. Sociol.*, vol. 38, no. 1, pp. 1–46, 2014. [Online]. Available: http://dx.doi.org/10.1080/0022250X.2011.629062

[21] J. L. Moreno and H. H. Jennings, *Who Shall Survive? A New Approach to the Problem of Human Interrelations* (Nervous and Mental Disease Monograph Series No. 58). New York, NY, USA: Nervous and Mental Disease Publishing Company, 1934.

[22] A. Rapoport and W. J. Horvath, "A study of a large sociogram," *Behavioral Sci.*, vol. 6, no. 4, pp. 279–291, 1961. [Online]. Available: http://dx.doi.org/10.1002/bs.3830060402

[23] L. C. Freeman, S. C. Freeman, and A. G. Michaelson, "On human social intelligence," *J. Social Biol. Struct.*, vol. 11, no. 4, pp. 415–425, 1988. [Online]. Available: http://www.sciencedirect.com/science/article/pii/0140175088900802

[24] W. W. Zachary, "An information flow model for conflict and fission in small groups," *J. Anthropol. Res.*, vol. 33, no. 4, pp. 452–473, 1977. [Online]. Available: http://www.jstor.org/stable/3629752

[25] M. E. J. Newman, "A measure of betweenness centrality based on random walks," *Social Netw.*, vol. 27, no. 1, pp. 39–54, 2005. [Online]. Available: http://www.sciencedirect.com/science/article/pii/S0378873304000681

[26] M. E. J. Newman, "Scientific collaboration networks. II. Shortest paths, weighted networks, and centrality," *Phys. Rev. E*, vol. 64, no. 1, p. 016132, Jun. 2001. [Online]. Available: http://link.aps.org/doi/10.1103/PhysRevE.64.016132

[27] L. C. Freeman, "Centered graphs and the structure of ego networks," *Math. Social Sci.*, vol. 3, no. 3, pp. 291–304, 1982. [Online]. Available: http://www.sciencedirect.com/science/article/pii/0165489682900762

[28] M. Panju, "Iterative methods for computing eigenvalues and eigenvectors," *Waterloo Math. Rev.*, vol. 1, no. 1, pp. 9–18, May 2011. [Online]. Available: http://arxiv.org/abs/1105.1185

[29] M. E. J. Newman, "Modularity and community structure in networks," *Proc. Nat. Acad. Sci. USA*, vol. 103, no. 23, pp. 8577–8582, 2006. [Online]. Available: http://www.pnas.org/content/103/23/8577.abstract

[30] K.-C. Chen, M. Chiang, and H. V. Poor, "From technological networks to social networks," *IEEE J. Sel. Areas Commun.*, vol. 31, no. 9, pp. 548–572, Sep. 2013. [Online]. Available: http://ieeexplore.ieee.org/lpdocs/epic03/wrapper.htm?arnumber=6544549

[31] W. M. Tam, F. C. M. Lau, and C. K. Tse, "Complex-network modeling of a call network," *IEEE Trans. Circuits Syst. I, Reg. Papers*, vol. 56, no. 2, pp. 416–429, Feb. 2009.

[32] A.-L. Barabási, R. Albert, and H. Jeong, "Mean-field theory for scale-free random networks," *Phys. A, Statist. Mech. Appl.*, vol. 272, nos. 1–2, pp. 173–187, 1999.

[33] J. Wu, C. K. Tse, F. C. M. Lau, and I. W. H. Ho, "Analysis of communication network performance from a complex network perspective," *IEEE Trans. Circuits Syst. I, Reg. Papers*, vol. 60, no. 12, pp. 3303–3316, Dec. 2013.

[34] M. Faloutsos, P. Faloutsos, and C. Faloutsos, "On power-law relationships of the Internet topology," *ACM SIGCOMM Comput. Commun. Rev.*, vol. 29, no. 4, pp. 251–262, Oct. 1999.

[35] N. Eagle and A. Pentland, "Reality mining: Sensing complex social systems," *Pers. Ubiquitous Comput.*, vol. 10, no. 4, pp. 255–268, Nov. 2005. [Online]. Available: http://dl.acm.org/citation.cfm?id=1122739.1122745

[36] M. Musolesi and C. Mascolo, "Designing mobility models based on social network theory," *ACM SIGMOBILE Mobile Comput. Commun. Rev.*, vol. 11, no. 3, pp. 59–70, 2007. [Online]. Available: http://dl.acm.org/citation.cfm?id=1317433

[37] C. Boldrini and A. Passarella, "HCMM: Modelling spatial and temporal properties of human mobility driven by users' social relationships," *Comput. Commun.*, vol. 33, no. 9, pp. 1056–1074, Jun. 2010. [Online]. Available: http://www.sciencedirect.com/science/article/pii/S0140366410000514

[38] F. Li and J. Wu, "LocalCom: A community-based epidemic forwarding scheme in disruption-tolerant networks," in *Proc. 6th Annu. IEEE Commun. Soc. Conf. Sensor, Mesh Ad Hoc Commun. Netw.*, Jun. 2009, pp. 1–9. [Online]. Available: http://ieeexplore.ieee.org/lpdocs/epic03/wrapper.htm?arnumber=5168942

[39] E. Bulut and B. K. Szymanski, "Exploiting friendship relations for efficient routing in mobile social networks," *IEEE Trans. Parallel Distrib. Syst.*, vol. 23, no. 12, pp. 2254–2265, Dec. 2012.

[40] P. Costa, C. Mascolo, M. Musolesi, and G. P. Picco, "Socially-aware routing for publish-subscribe in delay-tolerant mobile ad hoc networks," *IEEE J. Sel. Areas Commun.*, vol. 26, no. 5, pp. 748–760, Jun. 2008.

[41] P. Hui, J. Crowcroft, and E. Yoneki, "BUBBLE rap: Social-based forwarding in delay-tolerant networks," *IEEE Trans. Mobile Comput.*, vol. 10, no. 11, pp. 1576–1589, Nov. 2011.

[42] E. M. Daly and M. Haahr, "Social network analysis for information flow in disconnected delay-tolerant MANETs," *IEEE Trans. Mobile Comput.*, vol. 8, no. 5, pp. 606–621, May 2009.

[43] K. Akkarajitsakul, E. Hossain, and D. Niyato, "Cooperative packet delivery in hybrid wireless mobile networks: A coalitional game approach," *IEEE Trans. Mobile Comput.*, vol. 12, no. 5, pp. 840–854, May 2013.

[44] T. Zhang, J. Cao, Y. Chen, L. Cuthbert, and M. Elkashlan, "A small world network model for energy efficient wireless networks," *IEEE Commun. Lett.*, vol. 17, no. 10, pp. 1928–1931, Oct. 2013.

[45] A. Banerjee, R. Agarwal, V. Gauthier, C. K. Yeo, H. Afifi, and F. B. Lee, "A self-organization framework for wireless ad hoc networks as small worlds," *IEEE Trans. Veh. Technol.*, vol. 61, no. 6, pp. 2659–2673, Jul. 2012.

[46] V. Krishnamurthy and H. V. Poor, "Social learning and Bayesian games in multiagent signal processing: How do local and global decision makers interact?" *IEEE Signal Process. Mag.*, vol. 30, no. 3, pp. 43–57, May 2013. [Online]. Available: http://ieeexplore.ieee.org/lpdocs/epic03/wrapper.htm?arnumber=6494678

[47] V. Krishnamurthy and H. V. Poor, "A tutorial on interactive sensing in social networks," *IEEE Trans. Comput. Social Syst.*, vol. 1, no. 1, pp. 3–21, Mar. 2014. [Online]. Available: http://ieeexplore.ieee.org/lpdocs/epic03/wrapper.htm?arnumber=6780648

[48] M. Kobayashi, "Experience of infrastructure damage caused by the Great East Japan Earthquake and countermeasures against future disasters," *IEEE Commun. Mag.*, vol. 52, no. 3, pp. 23–29, Mar. 2014.

[49] Y. S. Soh, T. Q. S. Quek, M. Kountouris, and H. Shin, "Energy efficient heterogeneous cellular networks," *IEEE J. Sel. Areas Commun.*, vol. 31, no. 5, pp. 840–850, May 2013.

[50] R. W. Heath, M. Kountouris, and T. Bai, "Modeling heterogeneous network interference using Poisson point processes," *IEEE Trans. Signal Process.*, vol. 61, no. 16, pp. 4114–4126, Aug. 2013.

[51] S. Singh, H. S. Dhillon, and J. G. Andrews, "Offloading in heterogeneous networks: Modeling, analysis, and design insights," *IEEE Trans. Wireless Commun.*, vol. 12, no. 5, pp. 2484–2497, May 2013.

[52] *IEEE Standard for Information Technology—Telecommunications and Information Exchange Between Systems Local and Metropolitan Area Networks—Specific Requirements Part 11: Wireless LAN Medium Access Control (MAC) and Physical Layer (PHY) Specifications*, IEEE Standard 802.11-2012, Nov. 2012.

[53] S. Y. Park and D. J. Love, "Outage performance of multi-antenna multicasting for wireless networks," *IEEE Trans. Wireless Commun.*, vol. 8, no. 4, pp. 1996–2005, Apr. 2009.

[54] J. Wang, S. Park, D. J. Love, and M. D. Zoltowski, "Throughput delay tradeoff for wireless multicast using hybrid-ARQ protocols," *IEEE Trans. Commun.*, vol. 58, no. 9, pp. 2741–2751, Sep. 2010.

[55] A. Clementi, F. Pasquale, and R. Silvestri, "Opportunistic MANETs: Mobility can make up for low transmission power," *IEEE/ACM Trans. Netw.*, vol. 21, no. 2, pp. 610–620, Apr. 2013.

[56] J.-T. Tsai and R. L. Cruz, "Opportunistic multicast scheduling for information streaming in cellular networks," *IEEE Trans. Wireless Commun.*, vol. 10, no. 6, pp. 1776–1785, Jun. 2011.

[57] J. Hu, L.-L. Yang, and L. Hanzo, "Cooperative multicast aided picocellular hybrid information dissemination in mobile social networks: Delay/energy evaluation and relay selection," in *Proc. IEEE WCNC*, Istanbul, Turkey, Apr. 2014, pp. 3207–3212.

[58] Z. Zhang, "Routing in intermittently connected mobile ad hoc networks and delay tolerant networks: Overview and challenges," *IEEE Commun. Surveys Tuts.*, vol. 8, no. 1, pp. 24–37, First Quarter 2006.

[59] A. Jindal and K. Psounis, "Contention-aware performance analysis of mobility-assisted routing," *IEEE Trans. Mobile Comput.*, vol. 8, no. 2, pp. 145–161, Feb. 2009.

[60] P. R. Pereira, A. Casaca, J. J. P. C. Rodrigues, V. N. G. J. Soares, J. Triay, and C. Cervello-Pastor, "From delay-tolerant networks to vehicular delay-tolerant networks," *IEEE Commun. Surveys Tuts.*, vol. 14, no. 4, pp. 1166–1182, Fourth Quarter 2012.

[61] A. Chaintreau, J.-Y. Le Boudec, and N. Ristanovic, "The age of gossip: Spatial mean field regime," *ACM SIGMETRICS Perform. Eval. Rev.*, vol. 37, no. 1, pp. 109–120, Jun. 2009. [Online]. Available: http://doi.acm.org/10.1145/2492101.1555363

[62] T. Wang, L. Song, and Z. Han, "Coalitional graph games for popular content distribution in cognitive radio VANETs," *IEEE Trans. Veh. Technol.*, vol. 62, no. 8, pp. 4010–4019, Oct. 2013.

[63] B. Han, P. Hui, V. S. A. Kumar, M. V. Marathe, J. Shao, and A. Srinivasan, "Mobile data offloading through opportunistic communications and social participation," *IEEE Trans. Mobile Comput.*, vol. 11, no. 5, pp. 821–834, May 2012.

[64] *Specification Bluetooth System v4.1*, Bluetooth Special Interest Group, Kirkland, WA, USA, Dec. 2013.

[65] M. Zhao, Y. Li, and W. Wang, "Modeling and analytical study of link properties in multihop wireless networks," *IEEE Trans. Commun.*, vol. 60, no. 2, pp. 445–455, Feb. 2012.

[66] W. L. Huang and K. B. Letaief, "Cross-layer scheduling and power control combined with adaptive modulation for wireless ad hoc networks," *IEEE Trans. Commun.*, vol. 55, no. 4, pp. 728–739, Apr. 2007.

[67] G. Resta and P. Santi, "A framework for routing performance analysis in delay tolerant networks with application to noncooperative networks," *IEEE Trans. Parallel Distrib. Syst.*, vol. 23, no. 1, pp. 2–10, Jan. 2012.

[68] T. Camp, J. Boleng, and V. Davies, "A survey of mobility models for ad hoc network research," *Wireless Commun. Mobile Comput.*, vol. 2, no. 5, pp. 483–502, 2002.

[69] R. Groenevelt, P. Nain, and G. Koole, "The message delay in mobile ad hoc networks," *Perform. Eval.*, vol. 62, nos. 1–4, pp. 210–228, 2005. [Online]. Available: http://www.sciencedirect.com/science/article/pii/S0166531605000970

[70] T. Spyropoulos, A. Jindal, and K. Psounis, "An analytical study of fundamental mobility properties for encounter-based protocols," *Int. J. Auto. Adapt. Commun. Syst.*, vol. 1, no. 1, pp. 4–40, Jul. 2008. [Online]. Available: http://dx.doi.org/10.1504/IJAACS.2008.019198

[71] A. Chaintreau, P. Hui, J. Crowcroft, C. Diot, R. Gass, and J. Scott, "Impact of human mobility on opportunistic forwarding algorithms," *IEEE Trans. Mobile Comput.*, vol. 6, no. 6, pp. 606–620, Jun. 2007.

[72] T. Karagiannis, J.-Y. Le Boudec, and M. Vojnović, "Power law and exponential decay of intercontact times between mobile devices," *IEEE Trans. Mobile Comput.*, vol. 9, no. 10, pp. 1377–1390, Oct. 2010.

[73] M. McNett and G. M. Voelker, "Access and mobility of wireless PDA users," *ACM SIGMOBILE Mobile Comput. Commun. Rev.*, vol. 9, no. 2, pp. 40–55, Apr. 2005. [Online]. Available: http://doi.acm.org/10.1145/1072989.1072995

[74] D. Niyato, P. Wang, W. Saad, and A. Hjørungnes, "Controlled coalitional games for cooperative mobile social networks," *IEEE Trans. Veh. Technol.*, vol. 60, no. 4, pp. 1812–1824, May 2011.

[75] H. Sun and C. Wu, "Epidemic forwarding in mobile social networks," in *Proc. IEEE Int. Conf. Commun. (ICC)*, Jun. 2012, pp. 1421–1425.

[76] M. Abdulla and R. Simon, "The impact of inter-contact time within opportunistic networks: Protocol implications and mobility models," Dept. Comput. Sci., George Mason Univ., Fairfax, VA, USA, White Paper, 2009. [Online]. Available: http://cs.gmu.edu/~mabdulla/files/papers/dtn-mobility.pdf

[77] W. Wang, V. Srinivasan, and M. Motani, "Adaptive contact probing mechanisms for delay tolerant applications," in *Proc. 13th Annu. ACM Int. Conf. Mobile Comput. Netw. (MobiCom)*, 2007, pp. 230–241. [Online]. Available: http://doi.acm.org/10.1145/1287853.1287882

[78] Y. Li, D. Jin, Z. Wang, L. Zeng, and S. Chen, "Exponential and power law distribution of contact duration in urban vehicular ad hoc networks," *IEEE Signal Process. Lett.*, vol. 20, no. 1, pp. 110–113, Jan. 2013.

[79] X. Zhuo, Q. Li, W. Gao, G. Cao, and Y. Dai, "Contact duration aware data replication in delay tolerant networks," in *Proc. 19th IEEE Int. Conf. Netw. Protocols (ICNP)*, Oct. 2011, pp. 236–245.

[80] Y. Li, M. Qian, D. Jin, P. Hui, Z. Wang, and S. Chen, "Multiple mobile data offloading through disruption tolerant networks," *IEEE Trans. Mobile Comput.*, vol. 13, no. 7, pp. 1579–1596, Jul. 2014.

[81] V. Sciancalepore, D. Giustiniano, A. Banchs, and A. Picu, "Offloading cellular traffic through opportunistic communications: Analysis and optimization," *IEEE J. Sel. Areas Commun.*, Jul. 2015.

[82] P. Van Mieghem, *Performance Analysis of Communications Networks and Systems*. New York, NY, USA: Cambridge Univ. Press, 2005.

[83] R.-S. Chang, W.-Y. Chen, and Y.-F. Wen, "Hybrid wireless network protocols," *IEEE Trans. Veh. Technol.*, vol. 52, no. 4, pp. 1099–1109, Jul. 2003.

[84] A. Vahdat and D. Becker, "Epidemic routing for partially connected ad hoc networks," Dept. Comput. Sci., Duke Univ., Durham, NC, USA, Tech. Rep. CS-200006, Jul. 2000.

[85] M. W. Fackrell, "Characterization of matrix-exponential distributions," Ph.D. dissertation, Dept. Appl. Math., Univ. Adelaide, Adelaide, Australia, 2003.

[86] Y.-K. Ip, W.-C. Lau, and O.-C. Yue, "Performance modeling of epidemic routing with heterogeneous node types," in *Proc. IEEE Int. Conf. Commun.*, May 2008, pp. 219–224.

[87] Y. Li, G. Su, D. O. Wu, D. Jin, L. Su, and L. Zeng, "The impact of node selfishness on multicasting in delay tolerant networks," *IEEE Trans. Veh. Technol.*, vol. 60, no. 5, pp. 2224–2238, Jun. 2011.

[88] J. Hu, L. Yang, and L. Hanzo, "Mobile social networking aided content dissemination in heterogeneous networks," *China Commun.*, vol. 10, no. 6, pp. 1–13, Jun. 2013. [Online]. Available: http://www.chinacommunications.cn/EN/abstract/article_8138.shtml

[89] M. V. Barbera, J. Stefa, A. C. Viana, M. Dias de Amorim, and M. Boc, "VIP delegation: Enabling VIPs to offload data in wireless social mobile networks," in *Proc. Int. Conf. Distrib. Comput. Sensor Syst. Workshops (DCOSS)*, Jun. 2011, pp. 1–8.

[90] W. Gao, Q. Li, B. Zhao, and G. Cao, "Social-aware multicast in disruption-tolerant networks," *IEEE/ACM Trans. Netw.*, vol. 20, no. 5, pp. 1553–1566, Oct. 2012.

[91] Z. Gong and M. Haenggi, "Interference and outage in mobile random networks: Expectation, distribution, and correlation," *IEEE Trans. Mobile Comput.*, vol. 13, no. 2, pp. 337–349, Feb. 2014.

[92] C.-H. Liu and J. G. Andrews, "Multicast outage probability and transmission capacity of multihop wireless networks," *IEEE Trans. Inf. Theory*, vol. 57, no. 7, pp. 4344–4358, Jul. 2011.

[93] B. Niu, H. Jiang, and H. V. Zhao, "A cooperative multicast strategy in wireless networks," *IEEE Trans. Veh. Technol.*, vol. 59, no. 6, pp. 3136–3143, Jul. 2010.

[94] Y. Zhou, H. Liu, Z. Pan, L. Tian, J. Shi, and G. Yang, "Two-stage cooperative multicast transmission with optimized power consumption and guaranteed coverage," *IEEE J. Sel. Areas Commun.*, vol. 32, no. 2, pp. 274–284, Feb. 2013.

[95] H. V. Zhao and W. Su, "Cooperative wireless multicast: Performance analysis and power/location optimization," *IEEE Trans. Wireless Commun.*, vol. 9, no. 6, pp. 2088–2100, Jun. 2010.

[96] J.-H. Wui and D. Kim, "Optimal power allocation between unicast and multicast messages in wireless relay-multicasting networks using superposition coding," *IEEE Commun. Lett.*, vol. 15, no. 11, pp. 1159–1161, Nov. 2011.

[97] I.-H. Lee, H. Lee, and H.-H. Choi, "Exact outage probability of relay selection in decode-and-forward based cooperative multicast systems," *IEEE Commun. Lett.*, vol. 17, no. 3, pp. 483–486, Mar. 2013.

[98] J. Lee, Y. M. Lim, K. Kim, S. G. Choi, and J. K. Choi, "Energy efficient cooperative multicast scheme based on selective relay," *IEEE Commun. Lett.*, vol. 16, no. 3, pp. 386–388, Mar. 2012.

[99] V. Sevani, B. Raman, and P. Joshi, "Implementation-based evaluation of a full-fledged multihop TDMA-MAC for WiFi mesh networks," *IEEE Trans. Mobile Comput.*, vol. 13, no. 2, pp. 392–406, Feb. 2014.

[100] M. Grossglauser and D. N. C. Tse, "Mobility increases the capacity of ad hoc wireless networks," *IEEE/ACM Trans. Netw.*, vol. 10, no. 4, pp. 477–486, Aug. 2002.

[101] H. Zhang, Z. Zhang, and H. Dai, "Gossip-based information spreading in mobile networks," *IEEE Trans. Wireless Commun.*, vol. 12, no. 11, pp. 5918–5928, Nov. 2013.

[102] C. Bettstetter, H. Hartenstein, and X. Pérez-Costa, "Stochastic properties of the random waypoint mobility model," *Wireless Netw.*, vol. 10, no. 5, pp. 555–567, Sep. 2004. [Online]. Available: http://dx.doi.org/10.1023/B:WINE.0000036458.88990.e5

[103] J. Hu, L.-L. Yang, and L. Hanzo, "Distributed multistage cooperative-social-multicast-aided content dissemination in random mobile networks," *IEEE Trans. Veh. Technol.*, vol. 64, no. 7, pp. 3075–3089, Jul. 2015.

[104] T. S. Rappaport, *Wireless Communications: Principles and Practice*, 2nd ed. Upper Saddle River, NJ, USA: Prentice-Hall, 2001.

[105] J. Hu, L.-L. Yang, and L. Hanzo, "Maximum average service rate and optimal queue scheduling of delay-constrained hybrid cognitive radio in Nakagami fading channels," *IEEE Trans. Veh. Technol.*, vol. 62, no. 5, pp. 2220–2229, Jun. 2013.

[106] J. Hu, L.-L. Yang, and L. Hanzo, "Throughput and delay analysis of wireless multicast in distributed mobile social networks based on geographic social relationships," in *Proc. IEEE WCNC*, Istanbul, Turkey, Apr. 2014, pp. 1874–1879.

[107] G. Yuan, X. Zhang, W. Wang, and Y. Yang, "Carrier aggregation for LTE-advanced mobile communication systems," *IEEE Commun. Mag.*, vol. 48, no. 2, pp. 88–93, Feb. 2010.

JIE HU (S'11) received the B.Eng. degree in communication engineering and the M.Eng. degree in communication and information system from the School of Communication and Information Engineering, Beijing University of Posts and Telecommunications, in 2008 and 2011, respectively.

He is currently pursuing the Ph.D. degree with the Communication, Signal Processing and Control Group, University of Southampton, Southampton, U.K. His research interests in wireless communications include cognitive radio and cognitive networks, queuing analysis, resource allocation and scheduling, ad hoc wireless networks, and mobile social networks.

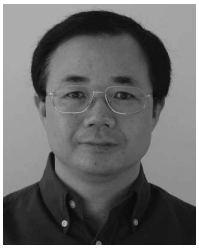

LIE-LIANG YANG (M'98–SM'02) received the B.Eng. degree in communications engineering from Shanghai Tiedao University, Shanghai, China, in 1988, and the M.Eng. and Ph.D. degrees in communications and electronics from Beijing Jiaotong University, Beijing, China, in 1991 and 1997, respectively. In 1997, he was a Visiting Scientist with the Institute of Radio Engineering and Electronics, Academy of Sciences of the Czech Republic. Since 1997, he has been with the University of Southampton, U.K., where he is currently a Professor of Wireless Communications with the School of Electronics and Computer Science. His research has covered a wide range of topics in wireless communications, networking, and signal processing. He has authored over 300 research papers in journals and conference proceedings, authored or co-authored three books, and also published several book chapters. He is a fellow of IET. He served as an Associate Editor of the IEEE TRANSACTIONS ON VEHICULAR TECHNOLOGY and the *Journal of Communications and Networks*. He is an Associate Editor of the IEEE ACCESS and the *Security and Communication Networks Journal*.

H. VINCENT POOR (S'72–M'77–SM'82–F'87) received the Ph.D. degree in electrical engineering and computer sciences from Princeton University, in 1977. From 1977 to 1990, he was a Faculty Member with the University of Illinois at Urbana–Champaign. Since 1990, he has been a Faculty Member with Princeton University, where he is currently the Michael Henry Strater University Professor and Dean of the School of Engineering and Applied Science. He has held visiting appointments with several universities, including most recently with Stanford University and Imperial College. Among his publications in his research areas, he has authored a recent book entitled *Mechanisms and Games for Dynamic Spectrum Allocation* (Cambridge University Press, 2014). His research interests are in the area of wireless networks and related fields.

Dr. Poor is a member of the U.S. National Academy of Engineering and the U.S. National Academy of Sciences, and is a Foreign Member of Academia Europaea and the Royal Society. He is also a fellow of the American Academy of Arts and Sciences, the Royal Academy of Engineering (U.K.), and the Royal Society of Edinburgh. He received the Marconi and Armstrong Awards of the IEEE Communications Society in 2007 and 2009, respectively. Recent recognition of his work includes the 2014 URSI Booker Gold Medal, and honorary doctorates from several universities in Asia and Europe.

LAJOS HANZO (M'91–SM'92–F'03) received the degree in electronics in 1976, the Ph.D. degree in 1983, the Doctor Honoris Causa degree from the Technical University of Budapest, in 2009, and the D.Sc. degree. During his 35-year career in telecommunications, he has held various research and academic positions in Hungary, Germany, and U.K. Since 1986, he has been with the School of Electronics and Computer Science, University of Southampton, U.K., as the Chair in Telecommunications. He has successfully supervised 80 Ph.D. students, co-authored 20 *Mobile Radio Communications* (John Wiley/IEEE Press) books totaling in excess of 10 000 pages, authored over 1500 research entries at the IEEE Xplore, acted as the TPC Chair and General Chair of the IEEE conferences, presented keynote lectures, and received a number of distinctions. He is directing 60 strong academic research teams, working on a range of research projects in the field of wireless multimedia communications sponsored by the industry, the Engineering and Physical Sciences Research Council, U.K., the European IST Program, and the Mobile Virtual Centre of Excellence, U.K. He is an enthusiastic supporter of industrial and academic liaison. He offers a range of industrial courses. He is also a Governor of the IEEE VTS. From 2008 to 2012, he was the Editor-in-Chief of the *IEEE Press* and a Chaired Professor with Tsinghua University, Beijing. His research is funded by the European Research Council's Senior Research Fellow Grant. He is a fellow of REng, IET, and EURASIP.